US009675461B2

(12) **United States Patent**
Mahfouz

(10) **Patent No.: US 9,675,461 B2**
(45) **Date of Patent: Jun. 13, 2017**

(54) **DEFORMABLE ARTICULATING TEMPLATES**

(71) Applicant: **ZIMMER, INC.**, Warsaw, IN (US)

(72) Inventor: **Mohamed Rashwan Mahfouz**, Knoxville, TN (US)

(73) Assignee: **ZIMMER INC.**, Warzaw, IN (US)

(*) Notice: Subject to any disclaimer, the term of this patent is extended or adjusted under 35 U.S.C. 154(b) by 49 days.

(21) Appl. No.: **14/640,082**

(22) Filed: **Mar. 6, 2015**

(65) **Prior Publication Data**

US 2015/0342739 A1 Dec. 3, 2015

Related U.S. Application Data

(62) Division of application No. 13/203,012, filed as application No. PCT/US2010/025466 on Feb. 25, 2010, now Pat. No. 8,989,460.

(Continued)

(51) **Int. Cl.**
A61F 2/38 (2006.01)
A61F 2/30 (2006.01)

(Continued)

(52) **U.S. Cl.**
CPC ***A61F 2/30942*** (2013.01); ***A61B 8/4245*** (2013.01); ***A61B 34/10*** (2016.02);

(Continued)

(58) **Field of Classification Search**
CPC A61F 2/0077; A61F 2002/30112; A61F 2002/30125; A61F 2002/30133;

(Continued)

(56) **References Cited**

U.S. PATENT DOCUMENTS

4,841,975 A 6/1989 Woolson 128/653
5,098,383 A 3/1992 Hemmy et al. 604/116

(Continued)

FOREIGN PATENT DOCUMENTS

AU 2004293091 A1 6/2005 ..... A61F 2/08
AU 2004293104 A1 6/2005 ..... A61F 2/08

(Continued)

OTHER PUBLICATIONS

Extended European Search Report, Application No. EP 12837887.4, Apr. 20, 2016.

(Continued)

Primary Examiner — Andrew W Johns
(74) *Attorney, Agent, or Firm* — Norton Rose Fulbright Canada LLP

(57) **ABSTRACT**

A method of designing a prosthetic implant. Exemplary methods may include developing a three-dimensional model of an anatomic feature from one or more two-dimensional images. The three-dimensional model may include a plurality of radii of curvature representing the shape of respective portions of a contact surface. In some exemplary embodiments, three-dimensional models associated with a large number members of a population may be utilized to create templates for prosthetic implants. A three-dimensional model of an anatomic feature of a patient may be compared to the available templates, and a suitable template may be tested by virtually implanting the template on the three-dimensional model of the patient's anatomical feature. In some embodiments, a patient's three-dimensional model for which a suitable pre-made template is not available may be used to customize a pre-made template to design a suitable implant.

12 Claims, 56 Drawing Sheets

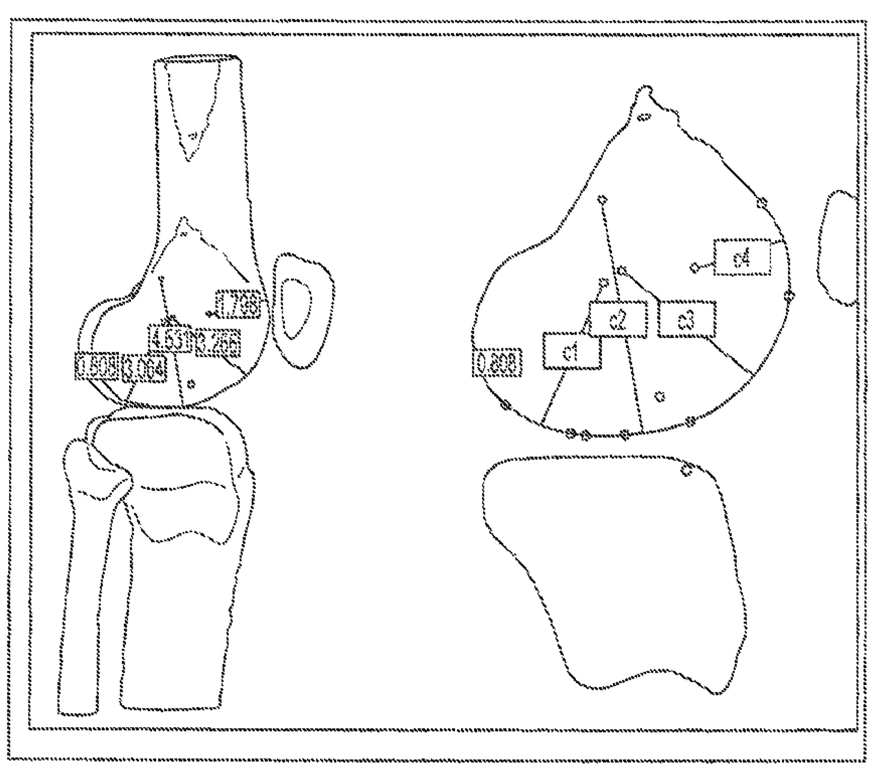

Related U.S. Application Data

(60) Provisional application No. 61/208,509, filed on Feb. 25, 2009, provisional application No. 61/222,560, filed on Jul. 2, 2009.

(51) **Int. Cl.**

G06F 17/18	(2006.01)
G06F 19/00	(2011.01)
A61B 8/00	(2006.01)
G06T 19/00	(2011.01)
A61F 2/36	(2006.01)
A61F 2/40	(2006.01)
A61B 34/10	(2016.01)

(52) **U.S. Cl.**
CPC ***A61F 2/3094*** (2013.01); ***A61F 2/3601*** (2013.01); ***A61F 2/389*** (2013.01); ***A61F 2/3859*** (2013.01); ***A61F 2/4003*** (2013.01); ***G06F 17/18*** (2013.01); ***G06F 19/3437*** (2013.01); ***G06T 19/00*** (2013.01); *A61B 2034/102* (2016.02); *A61B 2034/108* (2016.02); *A61F 2/38* (2013.01); *A61F 2002/30943* (2013.01); *A61F 2002/30948* (2013.01); *A61F 2002/3863* (2013.01); *A61F 2002/3895* (2013.01); *G06T 2210/41* (2013.01)

(58) **Field of Classification Search**
CPC A61F 2002/30327; A61F 2/38; A61F 2/3859; A61F 2002/3863
See application file for complete search history.

(56) **References Cited**

U.S. PATENT DOCUMENTS

5,490,854	A	2/1996	Fisher et al.	606/88
5,609,643	A	3/1997	Colleran et al.	623/20
5,768,134	A	6/1998	Swaelens et al.	364/468.28
5,871,018	A	2/1999	Delp et al.	128/898
5,916,219	A	6/1999	Matsuno et al.	606/88
6,893,467	B1 *	5/2005	Bercovy	623/20.14
7,239,908	B1	7/2007	Alexander et al.	600/427
7,269,241	B2	9/2007	Siltanen et al.	378/4
7,357,057	B2	4/2008	Chiang	83/614
7,468,075	B2	12/2008	Lang et al.	623/16.11
7,510,557	B1	3/2009	Bonutti	606/86 R
7,534,263	B2	5/2009	Burdulis, Jr. et al.	623/14.12
7,618,451	B2	11/2009	Berez et al.	623/14.12
7,634,119	B2	12/2009	Tsougarakis et al.	382/128
7,717,956	B2	5/2010	Lang	623/14.12
7,796,791	B2	9/2010	Tsougarakis et al.	382/128
7,799,077	B2	9/2010	Lang et al.	623/14.12
7,806,896	B1	10/2010	Bonutti	606/86 R
7,806,897	B1	10/2010	Bonutti	606/86 R
7,967,868	B2	6/2011	White et al.	623/20.35
7,981,158	B2	7/2011	Fitz et al.	623/17.16
8,062,302	B2	11/2011	Lang et al.	606/87
8,066,708	B2	11/2011	Lang et al.	606/88
8,070,752	B2	12/2011	Metzger et al.	606/88
8,077,950	B2	12/2011	Tsougarakis et al.	382/128
8,083,745	B2	12/2011	Lang et al.	606/87
8,092,465	B2	1/2012	Metzger et al.	606/96
8,094,900	B2	1/2012	Steines et al.	382/128
8,105,330	B2	1/2012	Fitz et al.	606/88
8,122,582	B2	2/2012	Burdulis, Jr. et al.	29/527.1
8,133,234	B2	3/2012	Meridew et al.	606/91
8,160,345	B2	4/2012	Pavlovskaia et al.	382/131
8,175,683	B2	5/2012	Roose	600/427
8,221,430	B2	7/2012	Park et al.	606/88
8,234,097	B2	7/2012	Steines et al.	703/1
8,241,293	B2	8/2012	Stone et al.	606/87
8,282,646	B2	10/2012	Schoenefeld et al.	606/88
8,298,237	B2	10/2012	Schoenefeld et al.	606/87
8,337,501	B2	12/2012	Fitz et al.	606/868 R
8,337,507	B2	12/2012	Lang et al.	606/102
8,343,218	B2	1/2013	Lang et al.	623/16.11
8,366,771	B2	2/2013	Burdulis, Jr. et al.	623/14.12
8,377,129	B2	2/2013	Fitz et al.	623/14.12
8,439,926	B2	5/2013	Bojarski et al.	606/88
8,460,304	B2	6/2013	Fitz et al.	606/88
8,480,754	B2	7/2013	Bojarski et al.	623/20.35
8,500,740	B2	8/2013	Bojarski et al.	606/868
8,529,568	B2	9/2013	Bouadi	606/84
8,529,630	B2	9/2013	Bojarski et al.	623/20.14
8,545,569	B2	10/2013	Fitz et al.	623/20.14
8,551,099	B2	10/2013	Lang et al.	606/86 R
8,551,102	B2	10/2013	Fitz et al.	606/88
8,551,103	B2	10/2013	Fitz et al.	606/88
8,551,169	B2	10/2013	Fitz et al.	623/14.12
8,556,906	B2	10/2013	Fitz et al.	606/87
8,556,907	B2	10/2013	Fitz et al.	606/87
8,556,971	B2	10/2013	Lang	623/14.12
8,556,983	B2	10/2013	Bojarski et al.	623/20.35
8,561,278	B2	10/2013	Fitz et al.	29/407.09
8,562,611	B2	10/2013	Fitz et al.	606/80
8,562,618	B2	10/2013	Fitz et al.	606/88
8,568,479	B2	10/2013	Fitz et al.	623/14.12
8,568,480	B2	10/2013	Fitz et al.	623/14.12
8,585,708	B2	11/2013	Fitz et al.	606/88
8,617,172	B2	12/2013	Fitz et al.	606/88
8,617,242	B2	12/2013	Philipp	623/16.11
8,623,026	B2	1/2014	Wong et al.	606/96
8,634,617	B2	1/2014	Tsougarakis et al.	382/128
8,638,998	B2	1/2014	Steines et al.	382/128
8,641,716	B2	2/2014	Fitz et al.	606/80
8,657,827	B2	2/2014	Fitz et al.	606/87
8,682,052	B2	3/2014	Fitz et al.	382/131
2002/0055692	A1	5/2002	Tanaka et al.	600/587
2003/0040806	A1	2/2003	MacDonald	623/23.49
2003/0055502	A1	3/2003	Lang et al.	623/16.11
2003/0181831	A1	9/2003	Tanaka et al.	600/587
2003/0216669	A1	11/2003	Lang et al.	600/587
2004/0039259	A1	2/2004	Krause et al.	600/300
2004/0068187	A1	4/2004	Krause et al.	600/443
2004/0098132	A1	5/2004	Andriacchi et al.	623/20.35
2004/0133276	A1	7/2004	Lang et al.	623/14.12
2004/0138754	A1	7/2004	Lang et al.	623/20.14
2004/0147927	A1	7/2004	Tsougarakis et al.	606/53
2004/0153079	A1	8/2004	Tsougarakis et al.	606/77
2004/0204644	A1	10/2004	Tsougarakis et al.	600/410
2004/0204760	A1	10/2004	Fitz et al.	623/14.12
2004/0236424	A1	11/2004	Berez et al.	623/14.12
2005/0010444	A1	1/2005	Iliff	705/2
2005/0197709	A1	9/2005	Schaefer et al.	623/20.3
2005/0234461	A1	10/2005	Burdulis, Jr. et al.	606/79
2005/0267584	A1	12/2005	Burdulis, Jr. et al.	623/20.19
2006/0111722	A1	5/2006	Bouadi	606/79
2006/0195198	A1	8/2006	James	700/1
2007/0081706	A1	4/2007	Zhou et al.	382/128
2007/0083266	A1	4/2007	Lang	623/17.11
2007/0100462	A1	5/2007	Lang et al.	623/20.29
2007/0118243	A1	5/2007	Schroeder et al.	700/118
2007/0156171	A1	7/2007	Lang et al.	606/205
2007/0157783	A1	7/2007	Chiang	83/485
2007/0168225	A1	7/2007	Haider et al.	705/2
2007/0179626	A1	8/2007	de la Barrera et al.	623/20.14
2007/0198022	A1	8/2007	Lang et al.	606/88
2007/0226986	A1	10/2007	Park et al.	29/592
2007/0233141	A1	10/2007	Park et al.	606/88
2007/0233269	A1	10/2007	Steines et al.	623/20.21
2007/0250169	A1	10/2007	Lang	623/17.12
2007/0255288	A1	11/2007	Mahfouz et al.	606/102
2007/0276214	A1	11/2007	Dachille et al.	600/407
2008/0058945	A1	3/2008	Hajaj et al.	623/20.14
2008/0097187	A1	4/2008	Gielen et al.	600/409
2008/0114370	A1	5/2008	Schoenefeld	606/96
2008/0147072	A1	6/2008	Park et al.	606/87
2008/0161815	A1	7/2008	Schoenefeld et al.	606/87
2008/0172125	A1	7/2008	Ek	623/14.12
2008/0195216	A1	8/2008	Philipp	623/18.11
2008/0243127	A1	10/2008	Lang et al.	606/87
2008/0275452	A1	11/2008	Lang et al.	606/88
2008/0281328	A1	11/2008	Lang et al.	606/87

(56) **References Cited**

U.S. PATENT DOCUMENTS

2008/0281329 A1 11/2008 Fitz et al. 606/88
2008/0281426 A1 11/2008 Fitz et al. 623/17.16
2008/0287954 A1 11/2008 Kunz et al. 606/87
2009/0024131 A1 1/2009 Metzger et al. 606/88
2009/0043556 A1 2/2009 Axelson et al. 703/11
2009/0088753 A1 4/2009 Aram et al. 606/79
2009/0088754 A1 4/2009 Aker et al. 606/79
2009/0088755 A1 4/2009 Aker et al. 606/79
2009/0088758 A1 4/2009 Bennett 606/82
2009/0088759 A1 4/2009 Aram et al. 606/87
2009/0088760 A1 4/2009 Aram et al. 606/87
2009/0088761 A1 4/2009 Roose et al. 606/87
2009/0088763 A1 4/2009 Aram et al. 606/88
2009/0093816 A1 4/2009 Roose et al. 606/87
2009/0099567 A1 4/2009 Zajac 606/79
2009/0110498 A1 4/2009 Park ..... 408/1 R
2009/0131941 A1 5/2009 Park et al. 606/87
2009/0131942 A1 5/2009 Aker et al. 606/88
2009/0138020 A1 5/2009 Park et al. 606/88
2009/0157083 A1 6/2009 Park et al. 606/88
2009/0222014 A1 9/2009 Bojarski et al. 606/88
2009/0222016 A1 9/2009 Park et al. 606/89
2009/0222103 A1 9/2009 Fitz et al. 623/18.11
2009/0226068 A1 9/2009 Fitz et al. 382/131
2009/0228113 A1 9/2009 Lang et al. 623/20.32
2009/0254093 A1 10/2009 White et al. 606/89
2009/0270868 A1 10/2009 Park et al. 606/87
2009/0276045 A1 11/2009 Lang 623/14.12
2009/0306676 A1 12/2009 Lang et al. 606/102
2009/0307893 A1 12/2009 Burdulis, Jr. et al. 29/527.1
2009/0312805 A1 12/2009 Lang et al. ..... 606/86 R
2010/0023015 A1 1/2010 Park 606/87
2010/0042105 A1 2/2010 Park et al. 606/87
2010/0049195 A1 2/2010 Park et al. 606/87
2010/0054572 A1 3/2010 Tsougarakis et al. 382/131
2010/0082035 A1 4/2010 Keefer 606/91
2010/0087829 A1 4/2010 Metzger et al. 606/96
2010/0152741 A1 6/2010 Park et al. 606/89
2010/0152782 A1 6/2010 Stone et al. 606/280
2010/0160917 A1 6/2010 Fitz et al. 606/88
2010/0168754 A1 7/2010 Fitz et al. 606/88
2010/0174376 A1 7/2010 Lang 623/18.11
2010/0185202 A1 7/2010 Lester et al. 606/88
2010/0191244 A1 7/2010 White et al. 606/88
2010/0212138 A1 8/2010 Carroll et al. 29/446
2010/0217270 A1 8/2010 Polinski et al. 606/87
2010/0217338 A1 8/2010 Carroll et al. ..... 606/86 R
2010/0228257 A1 9/2010 Bonutti 606/87
2010/0234849 A1 9/2010 Bouadi 606/84
2010/0256479 A1 10/2010 Park et al. 600/410
2010/0262150 A1 10/2010 Lian 606/87
2010/0274534 A1 10/2010 Steines et al. 703/1
2010/0281678 A1 11/2010 Burdulis, Jr. et al. 29/592
2010/0286700 A1 11/2010 Snider et al. 606/89
2010/0298894 A1 11/2010 Bojarski et al. ..... 606/86 R
2010/0298946 A1* 11/2010 Sun et al. 623/20.24
2010/0303313 A1 12/2010 Lang et al. 382/128
2010/0303317 A1 12/2010 Tsougarakis et al. 382/128
2010/0303324 A1 12/2010 Lang et al. 382/131
2010/0305573 A1 12/2010 Fitz et al. 606/87
2010/0305574 A1 12/2010 Fitz et al. 606/88
2010/0305708 A1 12/2010 Lang et al. 623/20.18
2010/0305907 A1 12/2010 Fitz et al. 703/1
2010/0329530 A1 12/2010 Lang et al. 382/131
2011/0015636 A1 1/2011 Katrana et al. 606/87
2011/0015637 A1 1/2011 De Smedt et al. 606/89
2011/0015639 A1 1/2011 Metzger et al. 606/91
2011/0022179 A1 1/2011 Andriacchi et al. 623/20.18
2011/0029091 A1 2/2011 Bojarski et al. 623/20.32
2011/0029093 A1 2/2011 Bojarski et al. 62/20.35
2011/0040168 A1 2/2011 Arnaud et al. 600/407
2011/0054478 A1 3/2011 Vanasse et al. 606/87
2011/0060341 A1 3/2011 Angibaud et al. 606/89
2011/0066193 A1 3/2011 Lang et al. ..... 606/86 R
2011/0066245 A1 3/2011 Lang et al. 623/18.11
2011/0071533 A1 3/2011 Metzger et al. 606/88
2011/0071581 A1 3/2011 Lang et al. ..... 606/86 R
2011/0071645 A1 3/2011 Bojarski et al. 623/20.35
2011/0071802 A1 3/2011 Bojarski et al. 703/1
2011/0087332 A1 4/2011 Bojarski et al. 623/20.32
2011/0092977 A1 4/2011 Salehi et al. 606/88
2011/0093108 A1 4/2011 Ashby et al. 700/103
2011/0106093 A1 5/2011 Romano et al. 606/88
2011/0125275 A1 5/2011 Lipman et al. 623/20.11
2011/0144760 A1* 6/2011 Wong et al. 623/20.14
2011/0153026 A1* 6/2011 Heggendorn et al. 623/20.35
2011/0160736 A1 6/2011 Meridew et al. 606/89
2011/0160867 A1 6/2011 Meridew et al. 623/20.36
2011/0166578 A1 7/2011 Stone et al. 606/88
2011/0172672 A1 7/2011 Dubeau et al. 606/87
2011/0184419 A1 7/2011 Meridew et al. 606/80
2011/0196377 A1 8/2011 Hodorek et al. 606/87
2011/0213368 A1 9/2011 Fitz et al. 606/80
2011/0213373 A1 9/2011 Fitz et al. 606/87
2011/0213374 A1 9/2011 Fitz et al. 606/87
2011/0213376 A1 9/2011 Maxson et al. 606/88
2011/0213377 A1 9/2011 Lang et al. 606/89
2011/0213427 A1 9/2011 Fitz et al. ..... 606/86 R
2011/0213428 A1 9/2011 Fitz et al. ..... 606/86 R
2011/0213429 A1 9/2011 Lang et al. ..... 606/86 R
2011/0213430 A1 9/2011 Lang et al. ..... 606/86 R
2011/0213431 A1 9/2011 Fitz et al. ..... 606/86 R
2011/0214279 A1 9/2011 Park et al. 29/592
2011/0218539 A1 9/2011 Fitz et al. 606/87
2011/0218545 A1 9/2011 Catanzarite et al. 606/96
2011/0218584 A1 9/2011 Fitz et al. ..... 606/86 R
2011/0224674 A1 9/2011 White et al. 606/91
2011/0230888 A1 9/2011 Lang et al. 606/87
2011/0238073 A1 9/2011 Lang et al. 606/89
2011/0245835 A1 10/2011 Dodds et al. 606/87
2011/0266265 A1 11/2011 Lang 219/121.72
2011/0295329 A1 12/2011 Fitz et al. ..... 606/86 R
2011/0295378 A1 12/2011 Bojarski et al. 623/20.35
2011/0313423 A1 12/2011 Lang et al. 606/87
2011/0313424 A1 12/2011 Bono et al. 606/91
2011/0319897 A1 12/2011 Lang et al. 606/79
2011/0319900 A1 12/2011 Lang et al. 606/87
2012/0010711 A1 1/2012 Antonyshyn et al. 623/16.11
2012/0029520 A1 2/2012 Lang et al. 606/89
2012/0041445 A1 2/2012 Roose et al. 606/96
2012/0041446 A1 2/2012 Wong et al. 606/96
2012/0065640 A1 3/2012 Metzger et al. 606/88
2012/0066892 A1 3/2012 Lang et al. 29/592
2012/0071881 A1 3/2012 Lang et al. 606/87
2012/0071882 A1 3/2012 Lang et al. 606/88
2012/0071883 A1 3/2012 Lang et al. 606/88
2012/0072185 A1 3/2012 Lang et al. 703/1
2012/0078254 A1 3/2012 Ashby et al. 606/79
2012/0078258 A1 3/2012 Lo et al. 606/87
2012/0078259 A1 3/2012 Meridew 606/87
2012/0093377 A1 4/2012 Tsougarakis et al. 382/128
2012/0101503 A1 4/2012 Lang et al. 606/87
2012/0109138 A1 5/2012 Meridew et al. 606/91
2012/0116203 A1 5/2012 Vancraen et al. 600/407
2012/0116562 A1 5/2012 Agnihotri et al. 700/98
2012/0123422 A1 5/2012 Agnihotri et al. 606/89
2012/0123423 A1 5/2012 Fryman 606/89
2012/0130382 A1 5/2012 Iannotti et al. 606/87
2012/0130687 A1 5/2012 Otto et al. 703/1
2012/0141034 A1 6/2012 Iannotti et al. 382/199
2012/0143197 A1 6/2012 Lang et al. 606/87
2012/0151730 A1 6/2012 Fitz et al. 29/407.01
2012/0158001 A1 6/2012 Burdulis, Jr. et al. 606/88
2012/0165820 A1 6/2012 De Smedt et al. 606/87
2012/0172884 A1 7/2012 Zheng et al. 606/91
2012/0191205 A1 7/2012 Bojarski et al. 623/20.32
2012/0191420 A1 7/2012 Bojarski et al. 703/1
2012/0192401 A1 8/2012 Pavlovskaia et al. 29/428
2012/0197260 A1 8/2012 Fitz et al. 606/88
2012/0197408 A1 8/2012 Lang et al. 623/18.11
2012/0201440 A1 8/2012 Steines et al. 382/131
2012/0209276 A1 8/2012 Schuster 606/88
2012/0209394 A1 8/2012 Bojarski et al. 623/20.32
2012/0215226 A1 8/2012 Bonutti 606/87

(56) **References Cited**

U.S. PATENT DOCUMENTS

2012/0221008	A1	8/2012	Carroll et al.	606/87
2012/0226283	A1	9/2012	Meridew et al.	606/81
2012/0232669	A1	9/2012	Bojarski et al.	623/20.3
2012/0232670	A1	9/2012	Bojarski et al.	623/20.35
2012/0232671	A1	9/2012	Bojarski	623/20.35
2012/0239045	A1	9/2012	Li	606/88
2012/0245647	A1	9/2012	Kunz et al.	606/86 R
2012/0245699	A1	9/2012	Lang et al.	623/20.3
2012/0265208	A1	10/2012	Smith	606/87
2012/0271366	A1	10/2012	Katrana et al.	606/86 R
2012/0276509	A1	11/2012	Iannotti et al.	434/267
2012/0277751	A1	11/2012	Catanzarite et al.	606/88
2012/0289966	A1	11/2012	Fitz et al.	606/88
2012/0296337	A1	11/2012	Fitz et al.	606/80
2013/0018379	A1	1/2013	Fitz et al.	606/87
2013/0018380	A1	1/2013	Fitz et al.	606/88
2013/0018464	A1	1/2013	Fitz et al.	623/14.12
2013/0023884	A1	1/2013	Fitz et al.	606/88
2013/0024000	A1	1/2013	Bojarski et al.	623/20.14
2013/0030419	A1	1/2013	Fitz et al.	606/1
2013/0030441	A1	1/2013	Fitz et al.	606/87
2013/0079781	A1	3/2013	Fitz et al.	A61B 17/1675
2013/0079876	A1	3/2013	Fitz et al.	A61F 2/30756
2013/0081247	A1	4/2013	Fitz et al.	B23Q 17/00
2013/0096562	A1	4/2013	Fitz et al.	A61B 17/1764
2013/0103363	A1	4/2013	Lang et al.	G06F 17/50
2013/0110471	A1	5/2013	Lang et al.	G06F 17/50
2013/0123792	A1	5/2013	Fitz et al.	A61B 17/1739
2013/0184713	A1	7/2013	Bojarski et al.	A61B 17/154
2013/0197870	A1	8/2013	Steines et al.	G06F 17/50
2013/0211409	A1	8/2013	Burdulis, Jr. et al.	A61B 17/158
2013/0211410	A1	8/2013	Landes et al.	A61B 17/1767
2013/0211531	A1	8/2013	Steines et al.	A16F 2/3859
2013/0245803	A1	9/2013	Lang	G06F 17/50
2013/0253522	A1	9/2013	Bojarski et al.	A61B 317/1764
2013/0289570	A1	10/2013	Chao	A61B 17/157
2013/0296874	A1	11/2013	Chao	A61B 17/157
2013/0297031	A1	11/2013	Hafez	A61F 2/30942
2013/0317511	A1	11/2013	Bojarski et al.	A16B 19/50
2013/0331850	A1	12/2013	Bojarski et al.	A61F 2/4657
2014/0005792	A1	1/2014	Lang et al.	A61F 2/30942
2014/0029814	A1	1/2014	Fitz et al.	G06T 7/0014
2014/0031826	A1	1/2014	Bojarski et al.	A61B 17/17
2014/0039631	A1	2/2014	Bojarski et al.	A61F 2/30
2014/0058396	A1	2/2014	Fitz et al.	A61B 17/1739
2014/0058397	A1	2/2014	Fitz et al.	A61B 17/1764
2014/0066935	A1	3/2014	Fitz et al.	A61B 17/1739
2014/0066936	A1	3/2014	Fitz et al.	A61B 17/1682
2014/0074441	A1	3/2014	Fitz et al.	A61B 17/1739
2014/0086780	A1	3/2014	Miller et al.	A61F 5/01

FOREIGN PATENT DOCUMENTS

AU	2005309692	A1	6/2006	A61F 2/38
AU	2005311558	A1	6/2006	A61B 17/17
AU	2002310193	B2	3/2007	A61L 27/00
AU	2006297137	A1	4/2007	A61F 2/38
AU	2002310193	B8	5/2007	A61L 27/00
AU	2007202573	A1	6/2007	A61L 27/00
AU	2007212033	A1	8/2007	A61B 17/15
AU	2007226924	A1	9/2007	A61F 2/30
AU	2009221773	A1	9/2009	A61F 2/38
AU	2009246474	A1	11/2009	A61F 2/30
AU	2010201200	A1	4/2010	A61F 2/30
AU	2011203237	A1	7/2011	A61F 2/38
AU	2010217903	A1	9/2011	A61F 2/30
AU	2010236263	A1	11/2011	A61B 17/90
AU	2010264466	A1	2/2012	A61F 2/38
AU	2010289706	A1	3/2012	A61F 2/38
AU	2010315099	A1	5/2012	A61B 5/103
AU	2010327987	A1	6/2012	A61B 17/68
AU	2011203237	B2	6/2012	A61F 2/08
AU	2012216829	A1	10/2012	A61F 2/08
AU	2012217654	A1	10/2013	A61F 2/28
AU	2007212033	B2	1/2014	A61B 17/15
AU	2014200073	A1	1/2014	A61B 17/15
AU	2012289973	A1	3/2014	A61F 2/30
AU	2012296556	A1	3/2014	A61F 2/38
CA	2501041	A1	4/2004	A61F 2/30
CA	2505371	A1	5/2004	A61F 2/30
CA	2505419	A1	6/2004	G06T 7/00
CA	2506849	A1	6/2004	G06T 7/00
CA	2546958	A1	6/2005	A61F 2/08
CA	2546965	A1	6/2005	A61F 2/08
CA	2804883	A1	6/2005	A61F 2/30
CA	2588907	A1	6/2006	A61B 17/15
CA	2590534	A1	6/2006	A61F 2/38
CA	2623834	A1	4/2007	A61F 2/38
CA	2641241	A1	8/2007	A61B 17/15
CA	2646288	A1	9/2007	A61F 2/30
CA	2717760	A1	9/2009	A61F 2/38
CA	2765499	A1	12/2010	A61F 2/38
CA	2771573	A1	3/2011	A61F 2/38
CA	2779283	A1	5/2011	A61F 2/38
CA	2782137	A1	6/2011	A61F 2/38
CA	2546965	C	3/2013	A61F 2/08
CN	1728976	A	2/2006	A61F 2/30
CN	1729483	A	2/2006	G06T 7/00
CN	1729484	A	2/2006	G06T 7/00
CN	1913844	A	2/2007	A61F 2/08
CN	101111197	A	1/2008	A61B 17/17
CN	101384230	A	3/2009	A61F 2/30
CN	101442960	A	5/2009	A61F 2/38
CN	100502808	C	6/2009	A61F 2/30
CN	102006841	A	4/2011	A61F 2/38
CN	102125448	A	7/2011	A61B 17/00
CN	102405032	A	4/2012	A61F 2/30
CN	102448394	A	5/2012	A61B 17/90
CN	101420911	B	7/2012	A61B 17/15
CN	102599960	A	7/2012	A16B 17/16
CN	1913844	B	9/2012	A61B 17/15
CN	102711670	A	10/2012	A61F 2/38
CN	102724934	A	10/2012	A61F 2/38
CN	102805677	A	12/2012	A61F 2/38
CN	1729483	B	10/2013	G06T 7/00
CN	103476363	A	12/2013	A61F 2/30
DE	60336002	D1	3/2011	A61F 21/30
DE	60239674	D1	5/2011	A61F 2/38
DE	602004032166	D1	5/2011	A61F 2/44
DE	602005027391	D1	5/2011	A61B 17/17
EP	1555962		4/2004	A61F 2/30
EP	1558181		5/2004	A61F 2/30
EP	1567985		6/2004	G01R 33/56
EP	1575460		6/2004	A61F 2/46
EP	1686930		6/2005	A61F 2/08
EP	1814491		6/2006	A61F 2/38
EP	1833387		6/2006	A61B 17/17
EP	1686931	A1	8/2006	A61F 2/08
EP	1951136		5/2007	A61B 17/88
EP	1996121		9/2007	A61F 2/30
EP	1928359	A2	6/2008	A61F 2/38
EP	2114312		8/2008	A61F 2/38
EP	2124764		9/2008	A61B 17/15
EP	2259753		9/2009	A61F 2/38
EP	2259753	A0	9/2009	A61F 2/38
EP	2265199		9/2009	A61B 17/58
EP	2303193		11/2009	A61F 2/30
EP	2403434		9/2010	A61F 2/30
EP	2405865		9/2010	A61F 2/38
EP	2419035		10/2010	A61B 17/90
EP	2445451		12/2010	A61F 2/38
EP	1555962	B1	2/2011	A61F 2/30
EP	2292188	A2	3/2011	A61F 2/46
EP	2292189	A2	3/2011	A61F 2/46
EP	2470126		3/2011	A61F 2/38
EP	1389980	B1	4/2011	A61F 2/30
EP	1686930	B1	4/2011	A61F 2/08
EP	1833387	B1	4/2011	A61B 17/17
EP	2316357	A1	5/2011	A61B 17/17
EP	2324799	A2	5/2011	A61F 2/38
EP	2496183		5/2011	A61F 2/38
EP	2335654	A1	6/2011	A61F 2/38

(56) **References Cited**

FOREIGN PATENT DOCUMENTS

EP	2509539		6/2011	A61F 2/38
EP	2512381		6/2011	A61F 2/38
EP	2292188	A3	5/2012	A61F 2/46
EP	2292189	A3	5/2012	A61F 2/46
EP	2324799	A3	1/2013	A61F 2/38
EP	2419035	A4	1/2013	A61B 17/15
EP	2591756	A1	5/2013	A61F 2/38
EP	2649951	A2	10/2013	A61B 17/15
EP	2671520	A3	12/2013	A61B 17/15
EP	2671521	A3	12/2013	A61B 17/15
EP	2671522	A3	12/2013	A61B 17/15
EP	2114312	B1	1/2014	A61F 2/38
EP	2710967	A2	3/2014	A61B 17/15
EP	1686931	B1	2/2015	A61F 2/38
GB	2484042	A	3/2012	A61F 2/38
GB	2489884	A	10/2012	A61F 2/38
GB	2484042	B	3/2014	A61F 2/38
HK	1059882	A1	8/2011	A61F 2/30
HK	1072710	A1	8/2011	A61F 2/30
HK	1087324	A1	11/2011	A61B 17/15
HK	1104776	A1	11/2011	A61B 17/15
JP	2002085435	A	3/2002	A61F 2/28
JP	2004202126	A	7/2004	A61F 2/28
JP	2006510403	A	3/2006	A61F 2/46
JP	2006263241	A	10/2006	A61B 19/00
JP	2007511470	A	6/2007	A61F 2/38
JP	2007514470	A	6/2007	A61F 2/38
JP	2011519713	A	7/2011	A61F 2/44
JP	2011224384	A	11/2011	A61F 2/30
JP	2012091033	A	5/2012	A61F 2/30
JP	2012176318	A	9/2012	A61F 2/38
JP	5053515	B2	10/2012	A61F 2/30
JP	2012187415	A	10/2012	A61F 2/30
JP	2012523897	A	10/2012	A61F 2/08
JP	5074036	B2	11/2012	A61F 2/38
JP	2012531265	A	12/2012	A61F 2/30
JP	2013503007	A	1/2013	A61F 2/38
JP	5148284	B2	2/2013	A61B 17/56
JP	5198069	B2	5/2013	A61F 2/38
JP	2014000425	A	1/2014	A61F 2/30
KR	20050072500	A	7/2005	A61B 5/055
KR	20050084024	A	8/2005	A61F 2/46
KR	20120090997	A	8/2012	A61F 2/38
KR	20120102576		9/2012	A61F 2/38
MX	2012007140	A	1/2013	A61F 2/38
NZ	597261	A	11/2013	A61F 2/30
SG	173840	A1	9/2011	A61F 2/30
SG	175229	A1	11/2011	A61B 17/90
SG	176833	A1	1/2012	A61F 2/38
SG	178836	A1	4/2012	A61F 2/38
SG	193484	A1	10/2013	A61F 2/30
TW	200509870	A	3/2005	A61B 17/15
TW	1231755	B	5/2005	A61F 2/30
TW	200800123	A	1/2008	A61F 2/30
TW	1330075	B	9/2010	A61B 17/15
WO	2004051301	A3	12/2004	G06T 7/00
WO	2004049981	A3	4/2005	G06T 7/00
WO	2005051239	A1	6/2005	A61F 2/30
WO	2005051240	A1	6/2005	A61F 2/30
WO	2006058057	A2	6/2006	A61F 2/38
WO	2006060795	A1	6/2006	A61B 17/17
WO	2007041375	A2	4/2007	A61F 2/38
WO	2007062103	A1	5/2007	A61B 17/88
WO	2007092841	A2	8/2007	A61B 17/15
WO	2007092841	A3	8/2007	A61B 17/15
WO	2007109467	A1	9/2007	A61B 2/30
WO	2007109641	A2	9/2007	A61F 2/30
WO	2007109641	A3	9/2007	A61F 2/30
WO	2008101090	A2	8/2008	A61F 2/38
WO	2008112996	A1	9/2008	A61B 17/15
WO	2008101090	A3	11/2008	A61F 2/38
WO	2008157412	A2	12/2008	A61B 17/17
WO	2007041375	A3	4/2009	A61F 2/38
WO	2008157412	A3	4/2009	A61B 17/17
WO	2009111626	A2	9/2009	G06K 9/00
WO	2009111626	A3	9/2009	A61F 2/38
WO	2009111639	A1	9/2009	A61B 17/58
WO	2009111656	A1	9/2009	A61F 2/38
WO	2009140294	A1	11/2009	A61F 2/30
WO	2010099231	A2	9/2010	A61F 2/38
WO	2010099231	A3	9/2010	A61F 2/38
WO	2010099353	A1	9/2010	A61F 2/30
WO	2010099359	A1	9/2010	A61F 2/00
WO	2010121147	A1	10/2010	A61B 17/90
WO	2011028624	A1	3/2011	A61F 2/38
WO	2011056992	A2	5/2011	A61F 2/38
WO	2011/071979	A2	6/2011	A61F 2/38
WO	2011072235	A2	6/2011	A61F 2/38
WO	2011075697	A2	6/2011	A61F 2/38
WO	2011056995	A3	9/2011	A61F 2/38
WO	2011075697	A3	10/2011	A61F 2/38
WO	2011072235	A3	12/2011	A61F 2/38
WO	2012112694	A1	8/2012	A61B 6/00
WO	2012112694	A2	8/2012	A61B 6/00
WO	2012112698	A2	8/2012	A61F 2/30
WO	2012112701	A2	8/2012	A61F 2/30
WO	2012112702	A2	8/2012	A61F 2/30
WO	2012112694	A3	1/2013	A61B 6/00
WO	2012112701	A3	1/2013	A61F 2/30
WO	2012112702	A3	1/2013	A61F 2/30
WO	2013020026	A1	2/2013	A61F 2/30
WO	2013025814	A1	2/2013	A61F 2/38
WO	2012112698	A3	3/2013	A61F 2/30
WO	2013056036	A1	4/2013	A61F 2/38
WO	2013119790	A1	8/2013	A61F 2/38
WO	2013119865	A1	8/2013	A61B 17/90
WO	2013131066	A1	9/2013	A61F 2/38
WO	2013152341	A1	10/2013	A61F 2/38
WO	2013155500	A1	10/2013	A61F 2/38
WO	2013155501	A1	10/2013	A61F 2/30
WO	2014008444	A1	1/2014	A61B 17/92
WO	2014035991	A1	3/2014	A61B 17/56
WO	2014047514	A1	3/2014	A61F 2/76

OTHER PUBLICATIONS

International Search Report and Written Opinion dated Jul. 1, 2010 for PCT/US2010/025466.

International Preliminary Report on Patentability dated Jun. 7, 2011 for PCT/US2010/025466.

International Search Report and Written Opinion dated Apr. 23, 2010 for PCT/US2010/025467.

International Preliminary Report on Patentability dated Oct. 11, 2011 for PCT/US2010/025467.

International Search Report and Written Opinion dated Jan. 5, 2009 for PCT/US2008/09837.

International Preliminary Report on Patentability dated Apr. 1, 2010 for PCT/US2008/09837.

Mahfouz et al., "Three-dimensional Morphology of the Knee Reveals Ethnic Differences," Clin. Orthop. Relat. Res., vol. 470, No. 1, Jan. 2012, pp. 172-185.

Dennis et al, Coventry Award Paper, Multicenter Determination of In Vivo Kinematics After Total Knee Arthroplasty, Clinical Orthopaedics and Related Research, No. 416, pp. 37-57, c 2003 Lippincott Williams & Wilkins, Inc., USA.

Mahfouz, et al, A Robust Method for Registration of Three-Dimensional Knee Implant Models to Two-Dimensional Fluoroscopy Images, IEEE Transactions on Medical Imaging, vol. 22, No. 12, Dec. 2003, c 2003 IEEE, USA.

Mahfouz et al, Automatic methods for characterization of sexual dimorphism of adult femora: distal femur, Computer Methods in Biomechanics and Biomedical Engineering, 2007, iFirst article, 1-10, c 2007 Taylor & Francis, GB.

Mahfouz et al, Patella sex determination by 3D statistical shape models and nonlinear classifiers, Forensic Science International, FSI-5154, pp. 1-10, c 2007 Elsevier Ireland Ltd., IE.

Merkl et al, Unsupervised Three-Dimensional Segmentation of Medical Images Using an Anatomical Bone Atlas, published in biomedical conference in Singapore, Dec. 2005, University of Tennessee/Department of Mechanical, Aerospace and Biomedical Engrg., Knoxville, TN, USA.

(56) **References Cited**

OTHER PUBLICATIONS

Taylor et al, "Computer-Integrated Surgery, Technology and Clinical Applications", The MIT Press, Cambridge, MA, London, UK, pp. 451-463.
Hofmann et al, "Natural-Knee II System", Intermedics Orthopedics, Austin, TX, 1995.

* cited by examiner

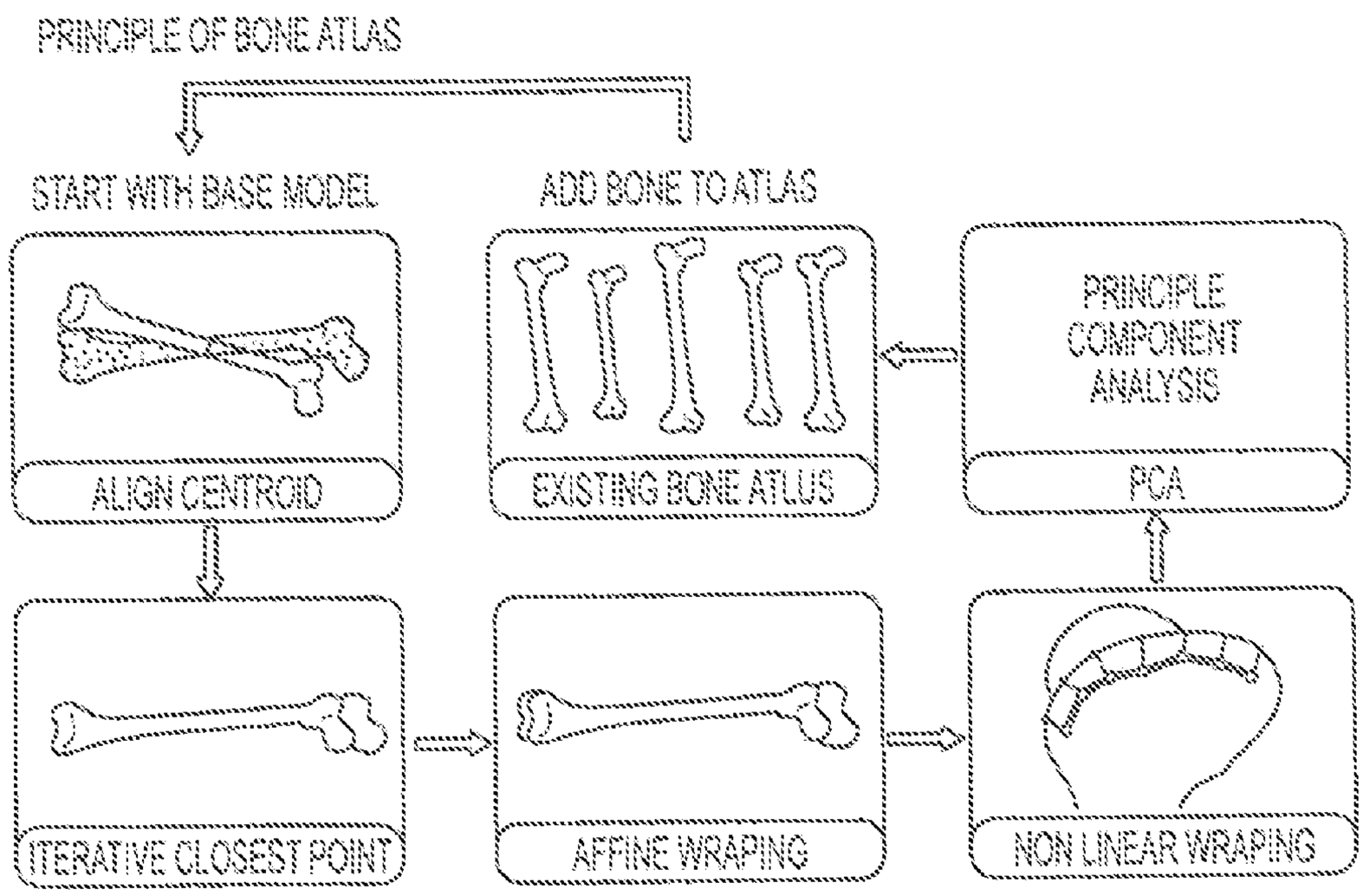
PRINCIPLE OF BONE ATLAS
START WITH BASE MODEL
ADD BONE TO ATLAS
ALIGN CENTROID
EXISTING BONE ATLUS
PRINCIPLE COMPONENT ANALYSIS
PCA
ITERATIVE CLOSEST POINT
AFFINE WRAPING
NON LINEAR WRAPING

FIG. 1

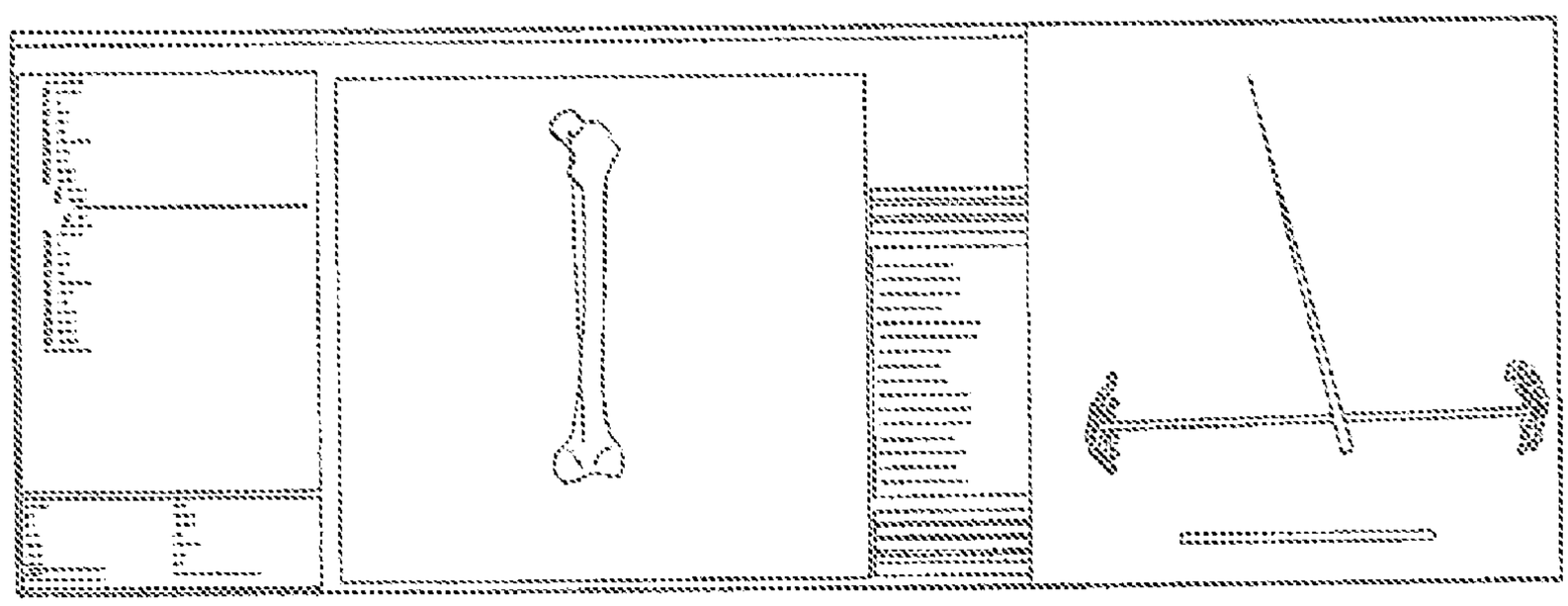

FIG. 2

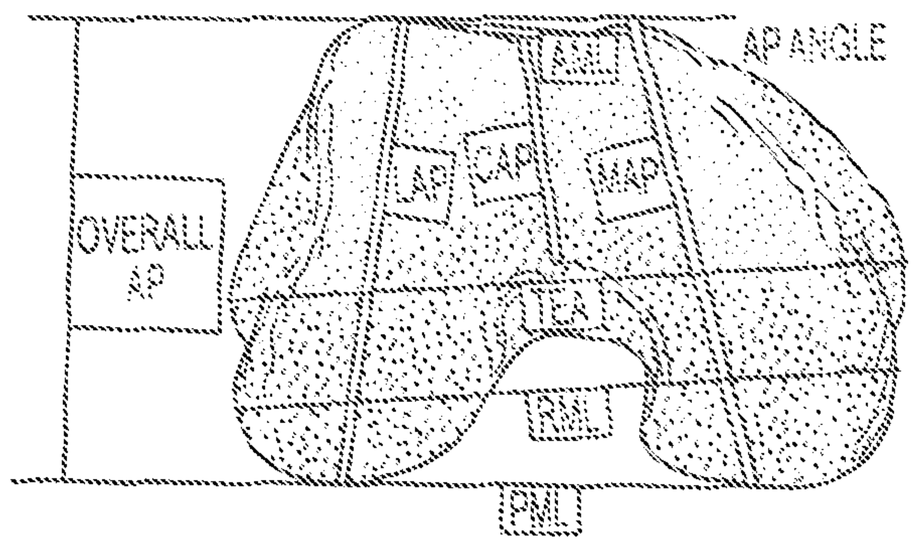

FIG. 3

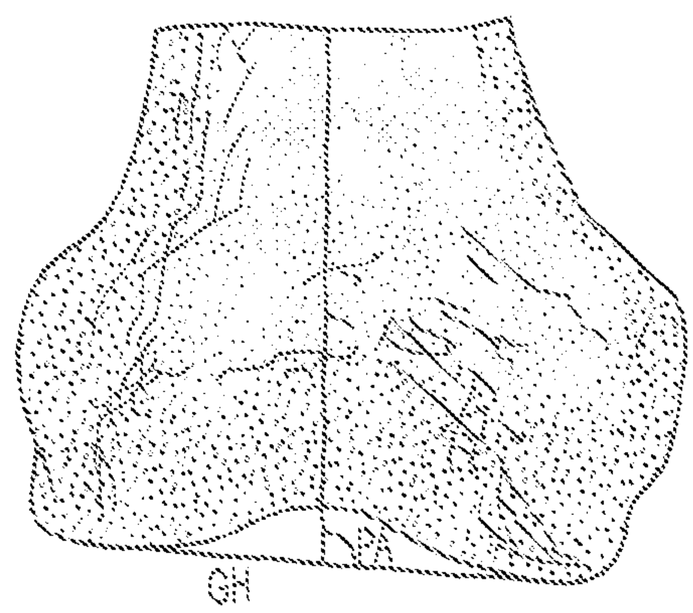

FIG. 4

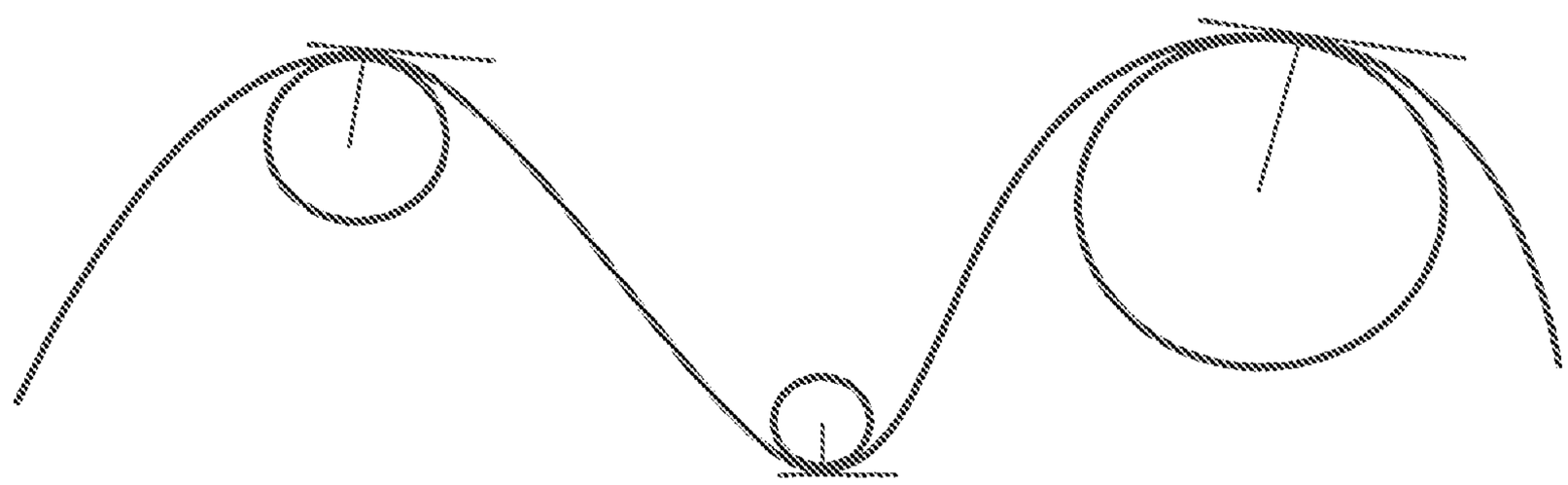

FIG. 5

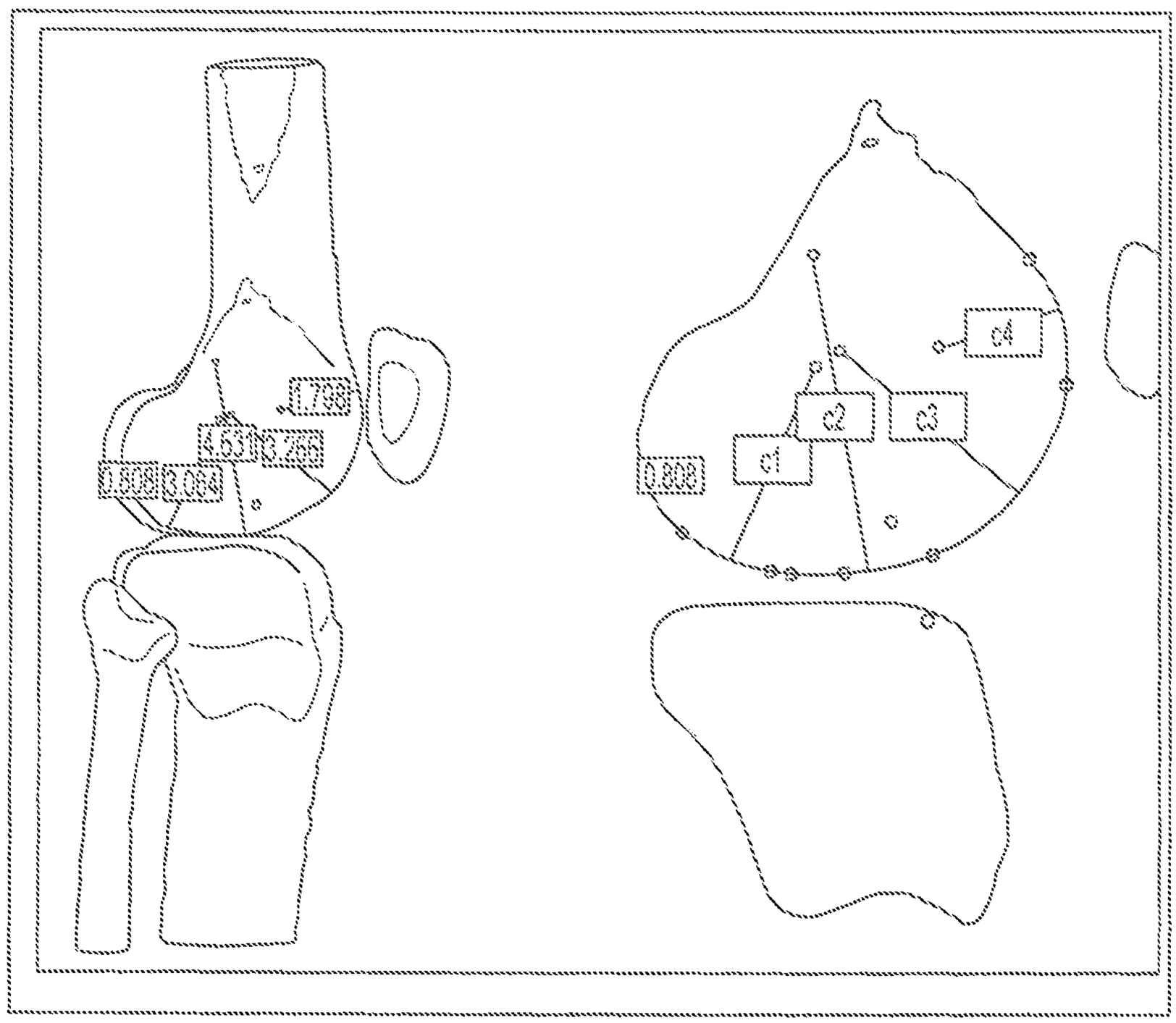

FIG. 6

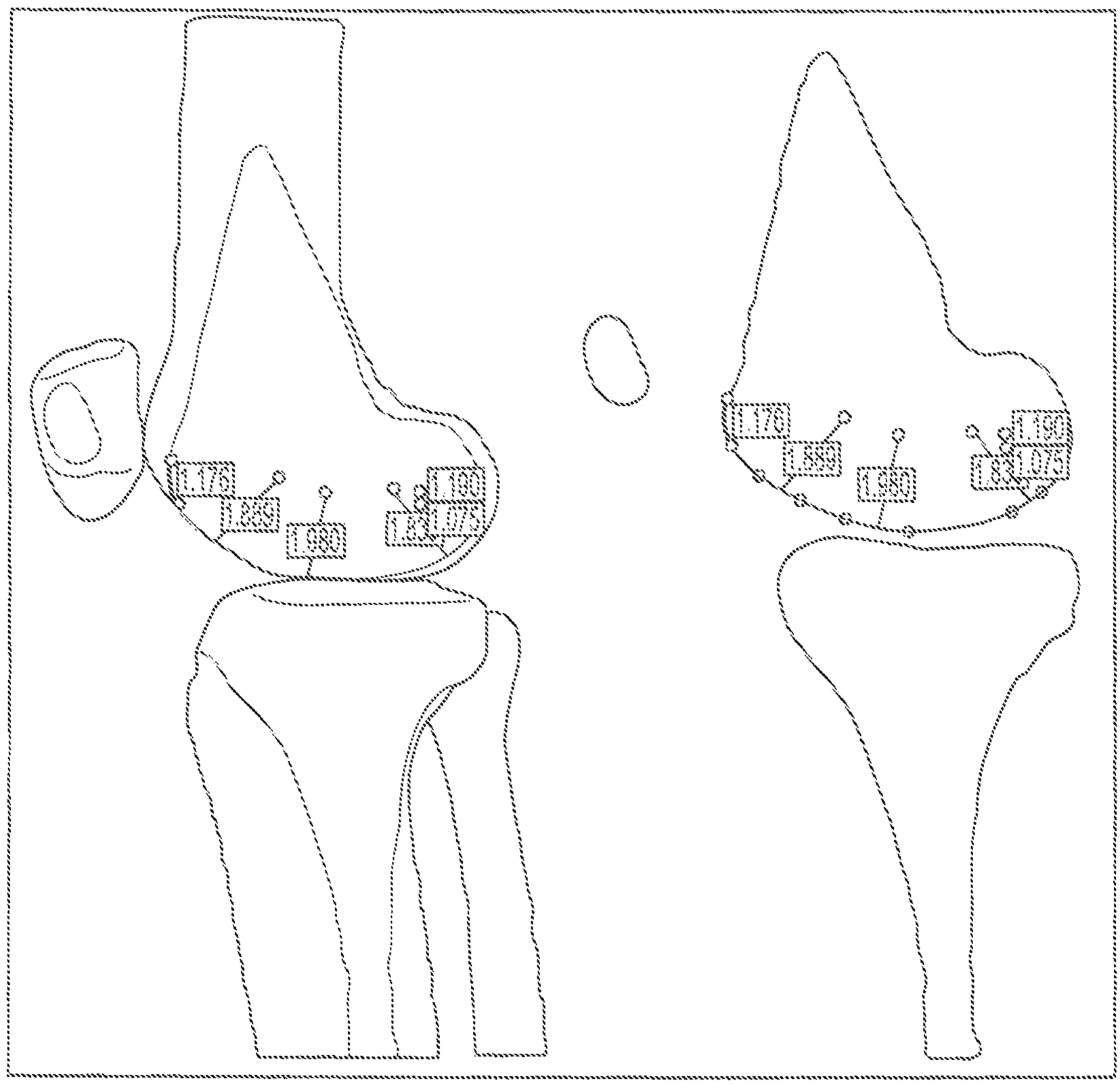

FIG. 7

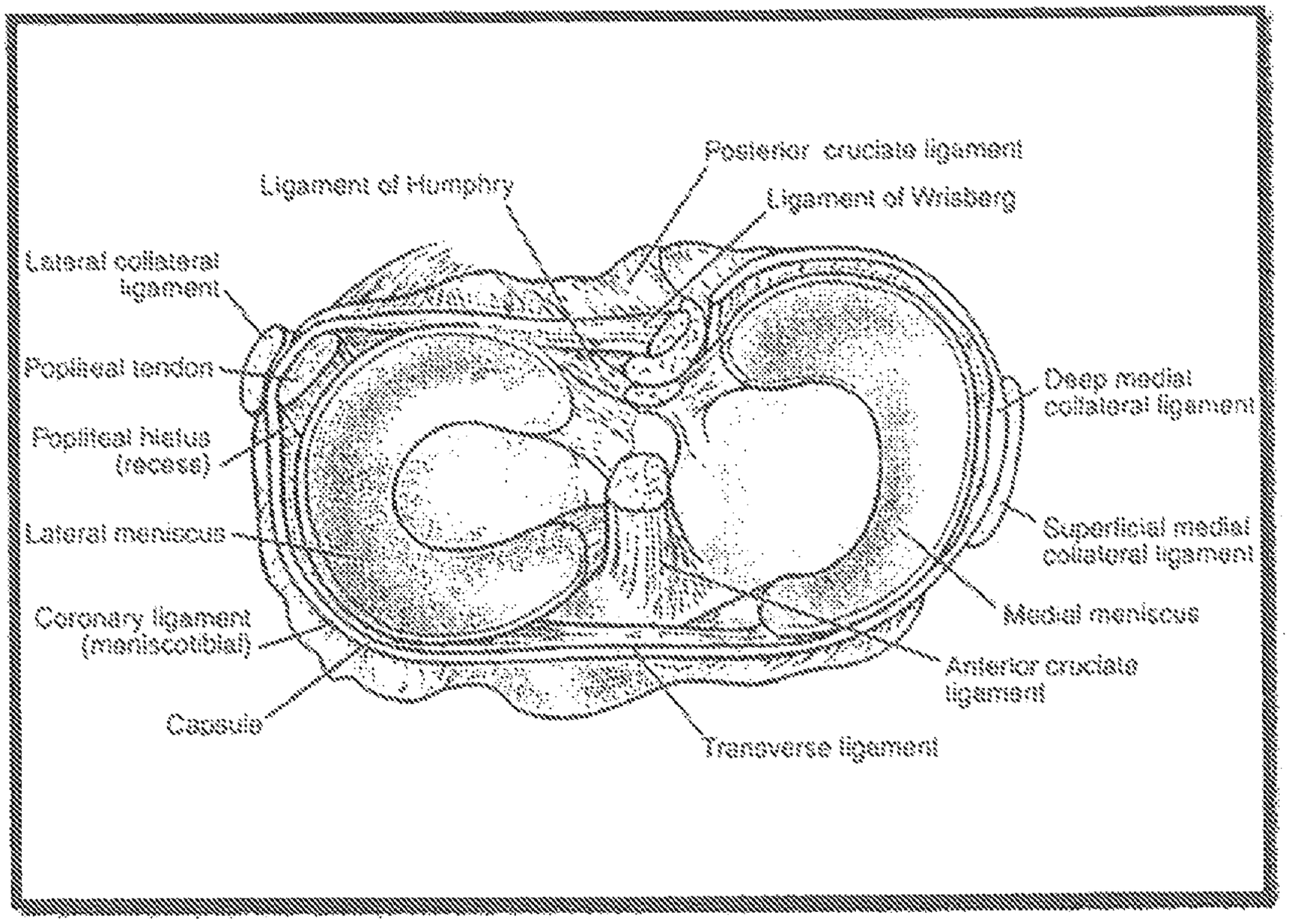
Posterior cruciate ligament
Ligament of Humphry
Ligament of Wrisberg
Lateral collateral ligament
Popliteal tendon
Popliteal hiatus (recess)
Lateral meniscus
Coronary ligament (meniscotibial)
Capsule
Deep medial collateral ligament
Superficial medial collateral ligament
Medial meniscus
Anterior cruciate ligament
Transverse ligament

FIG. 8

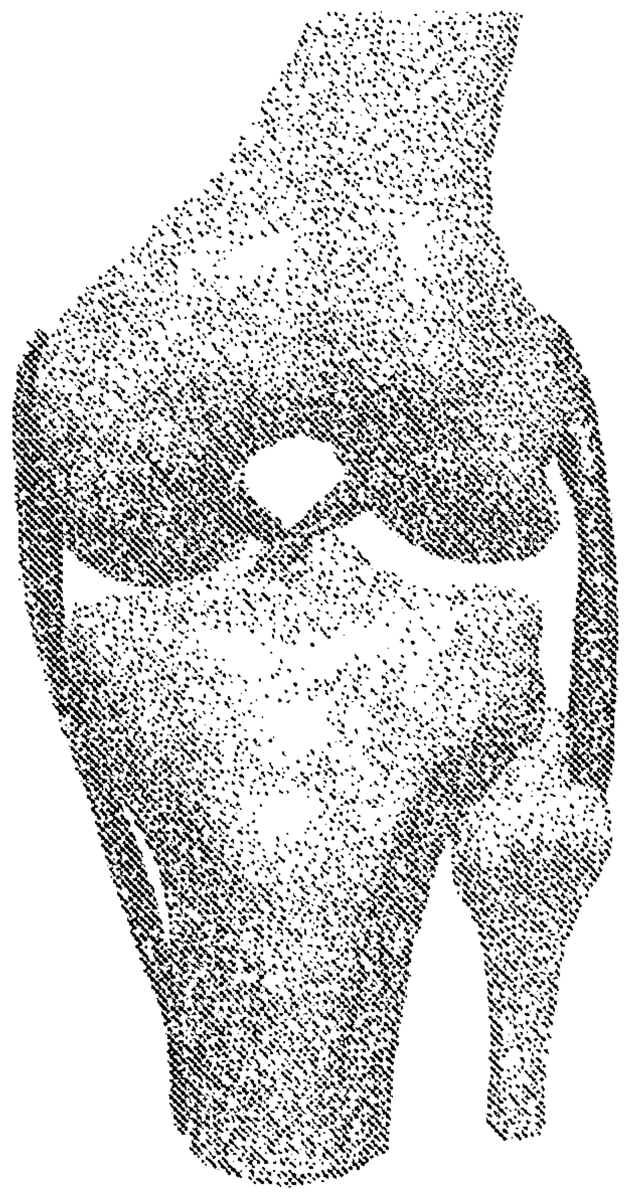

FIG. 9

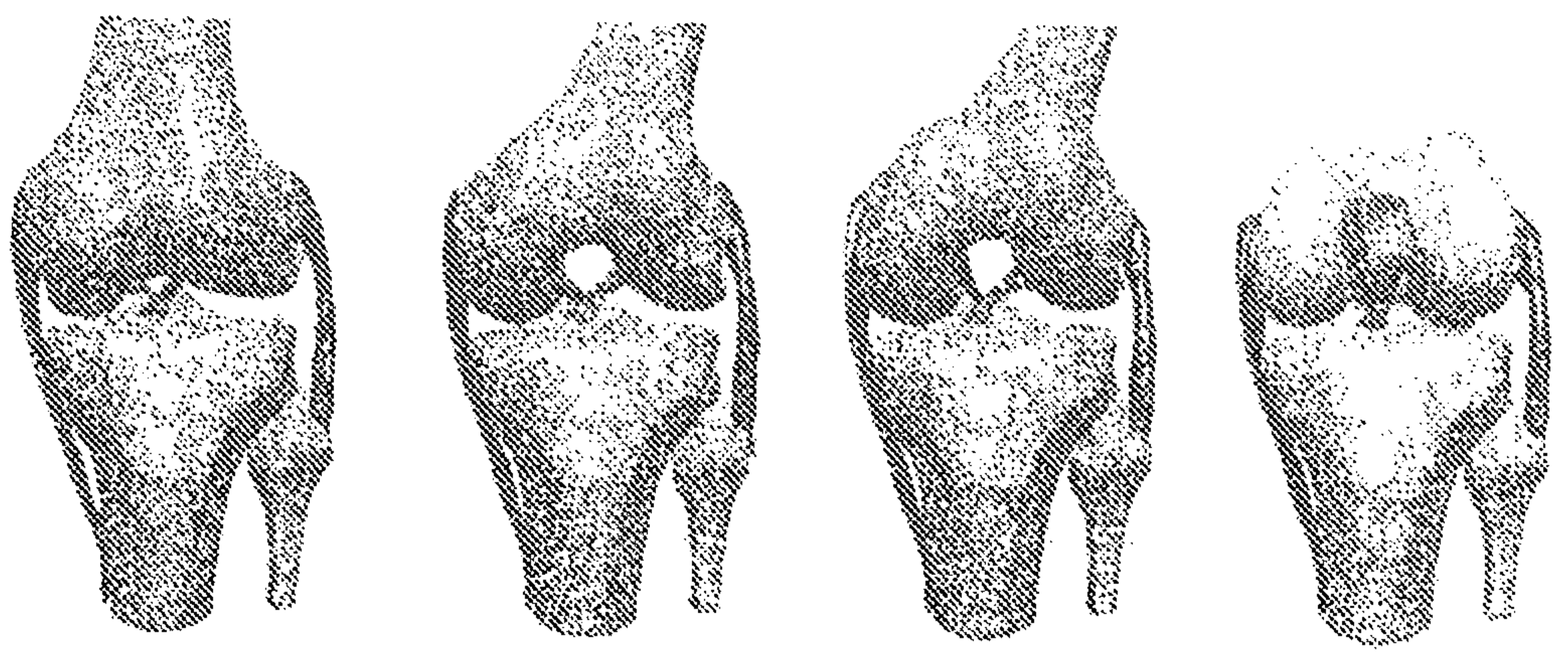

FIG. 10

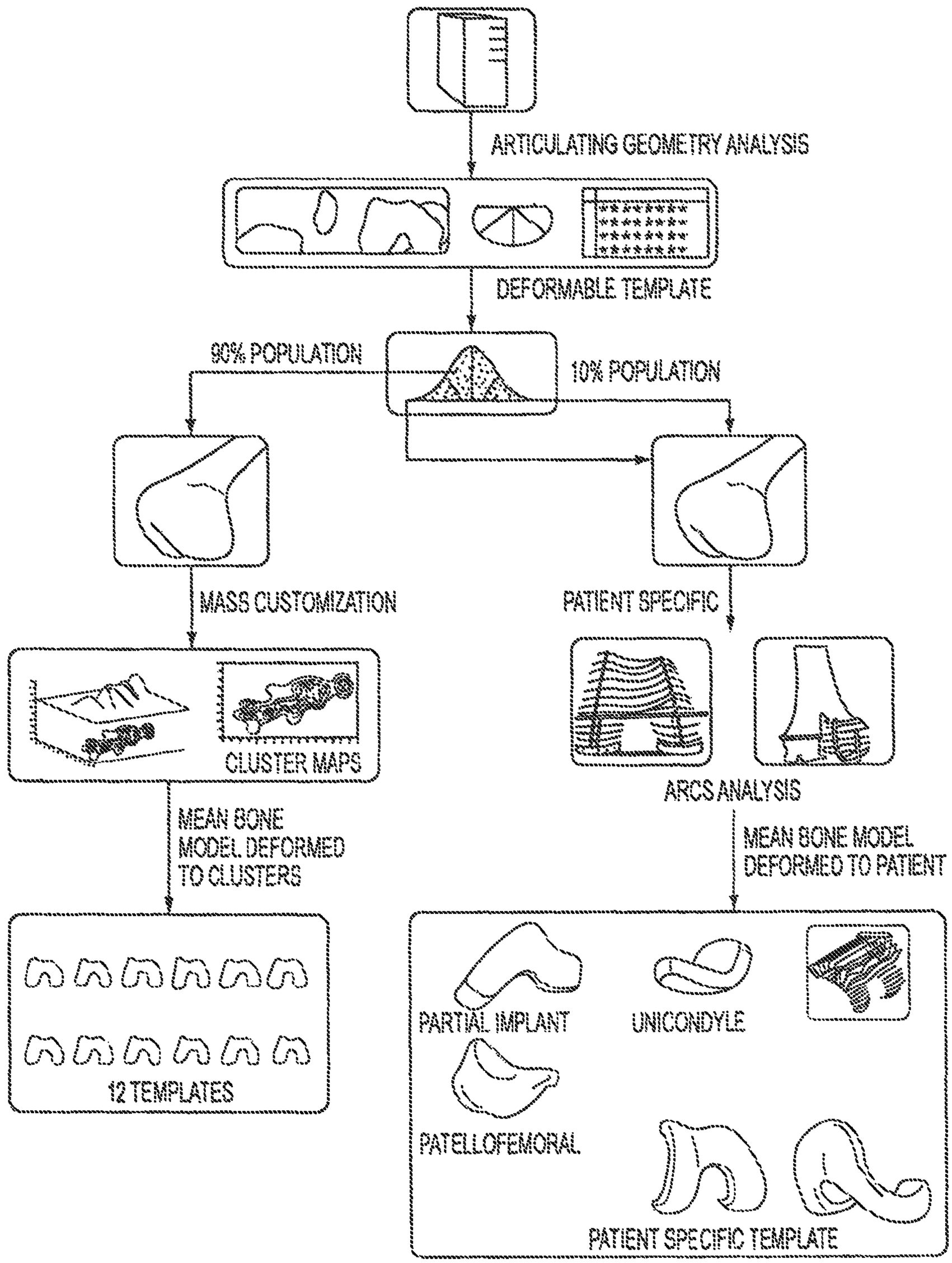
ARTICULATING GEOMETRY ANALYSIS
DEFORMABLE TEMPLATE
90% POPULATION
10% POPULATION
MASS CUSTOMIZATION
PATIENT SPECIFIC
CLUSTER MAPS
ARCS ANALYSIS
MEAN BONE MODEL DEFORMED TO CLUSTERS
MEAN BONE MODEL DEFORMED TO PATIENT
12 TEMPLATES
PARTIAL IMPLANT
UNICONDYLE
PATELLOFEMORAL
PATIENT SPECIFIC TEMPLATE

FIG. 11

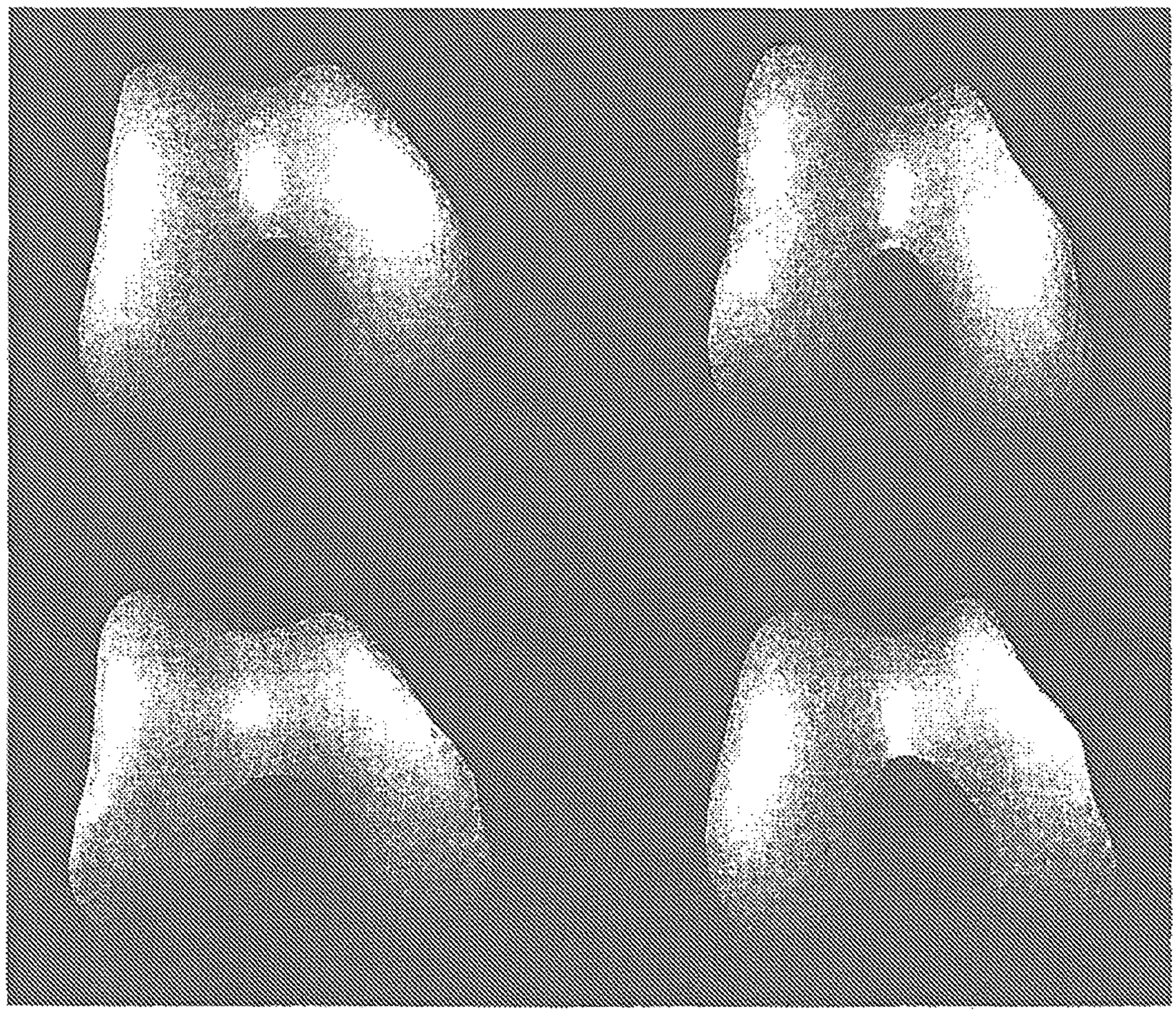

FIG. 12

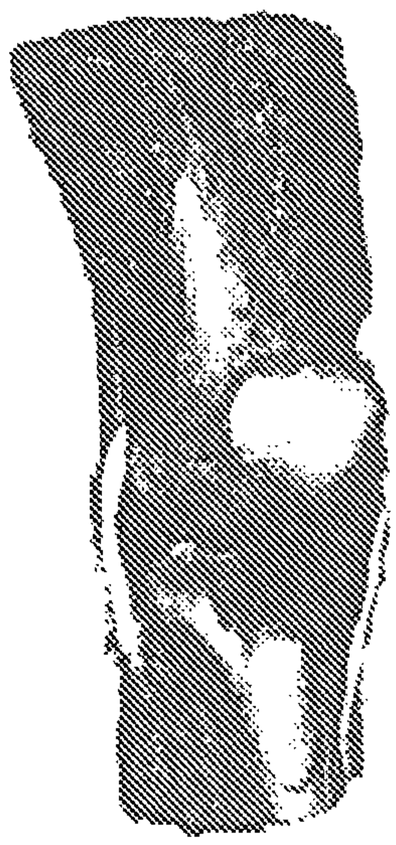

FIG. 13

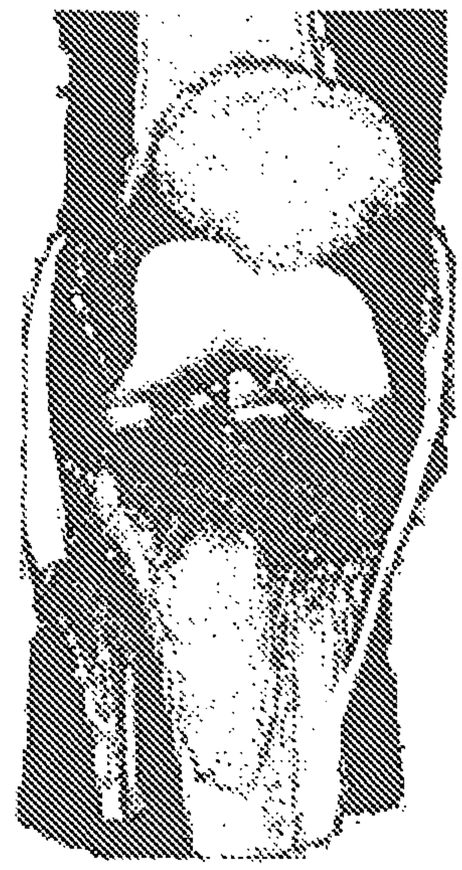

FIG. 14

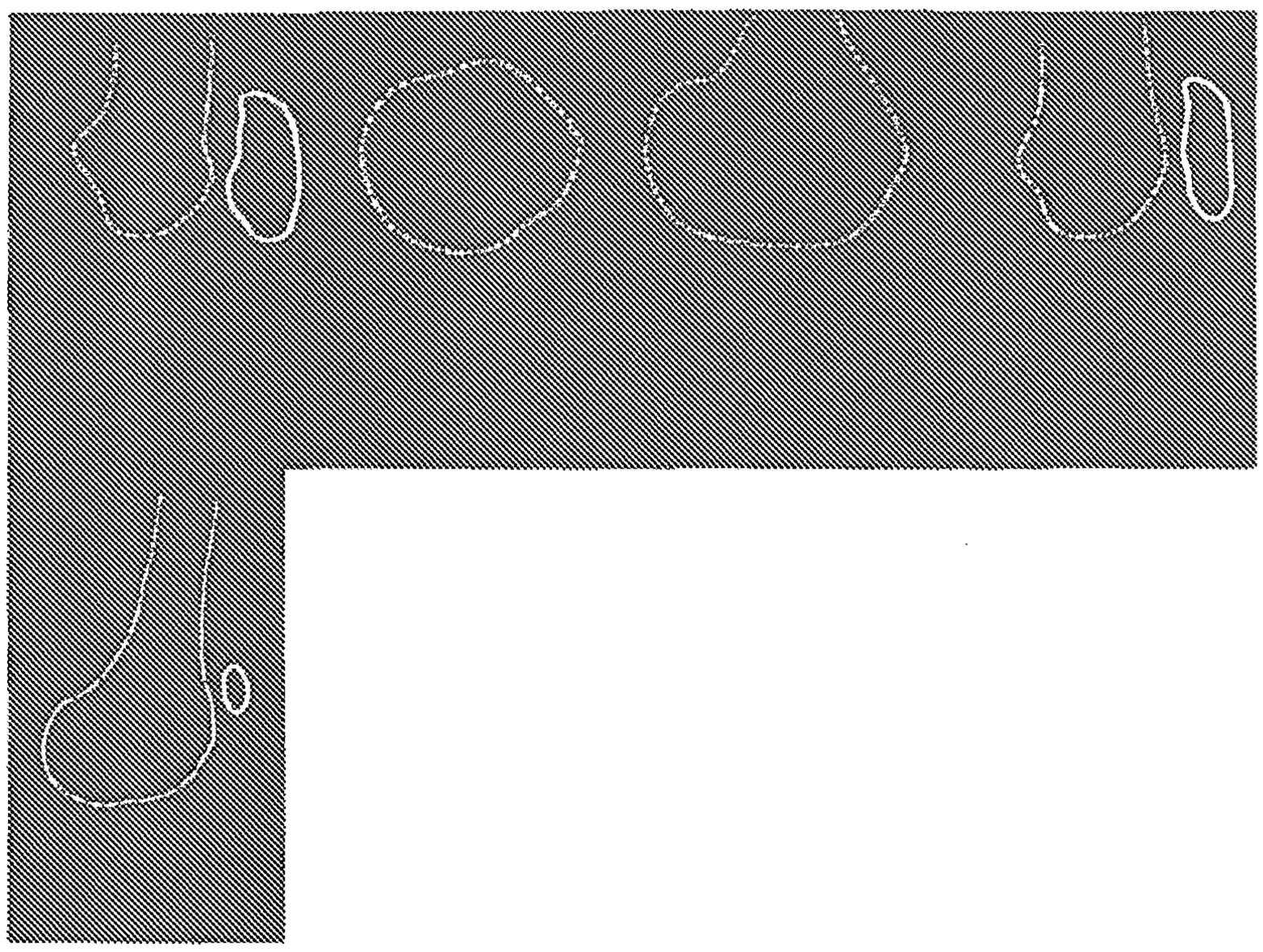

FIG. 15

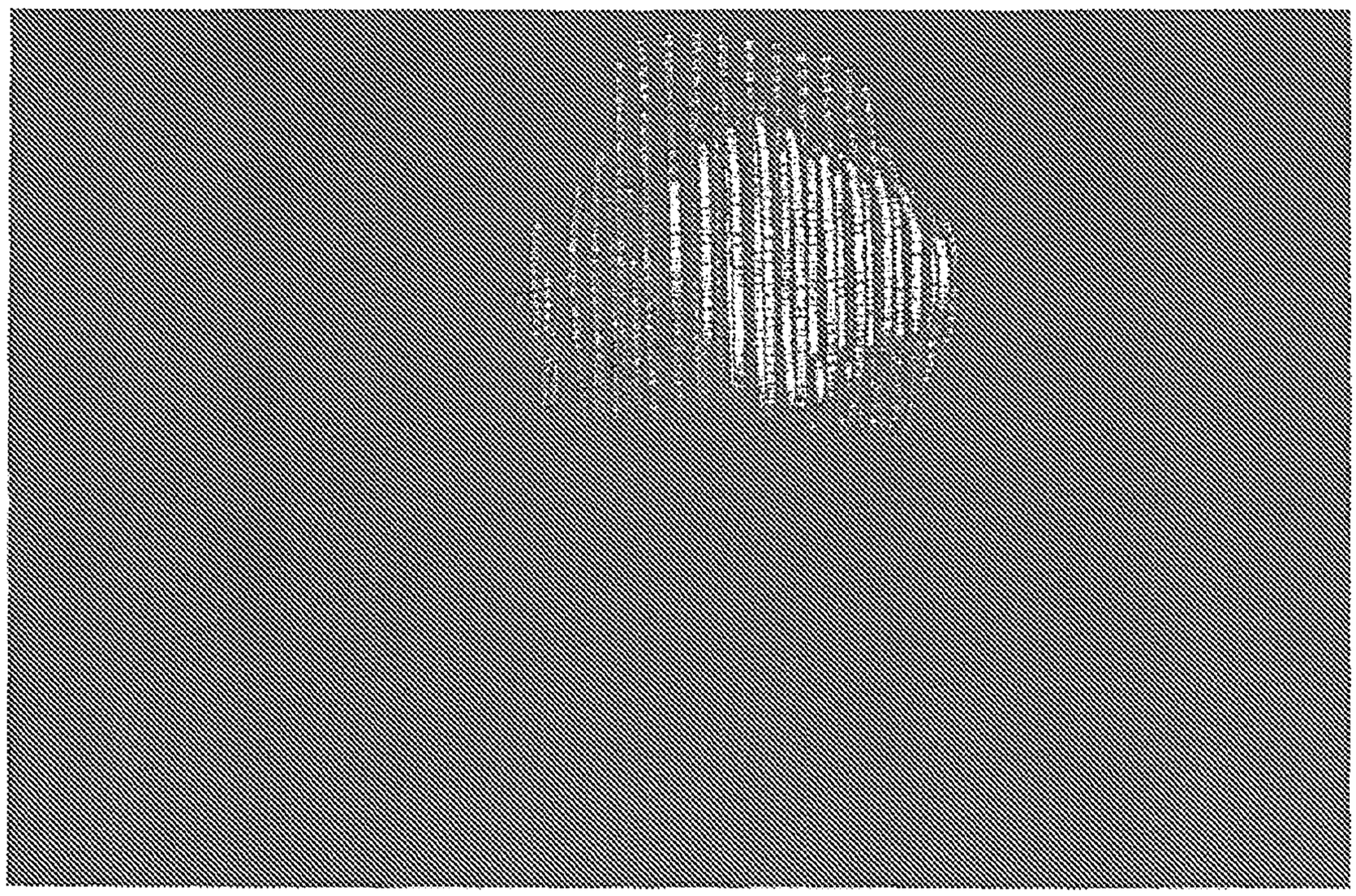

FIG. 16

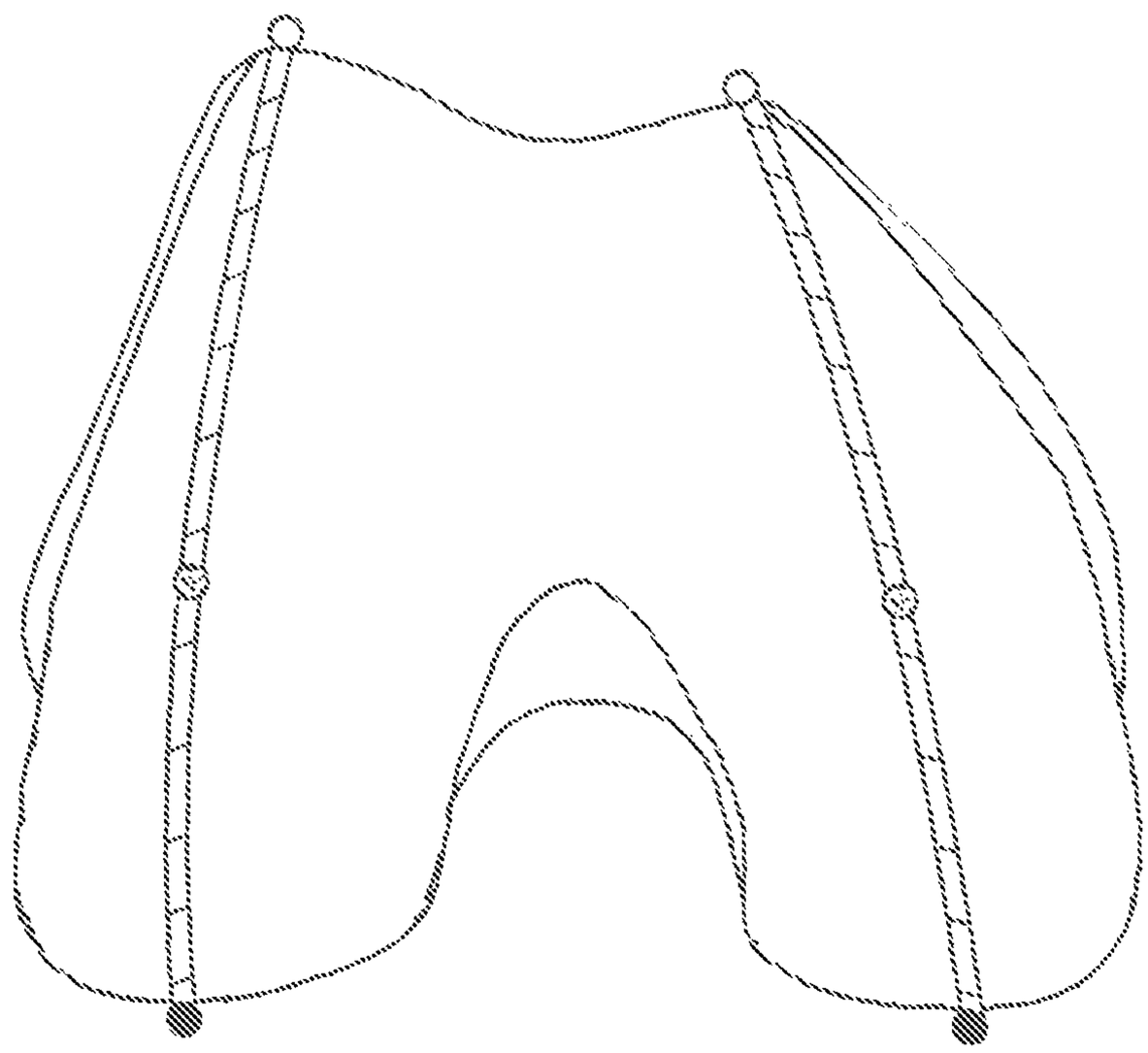

FIG. 17

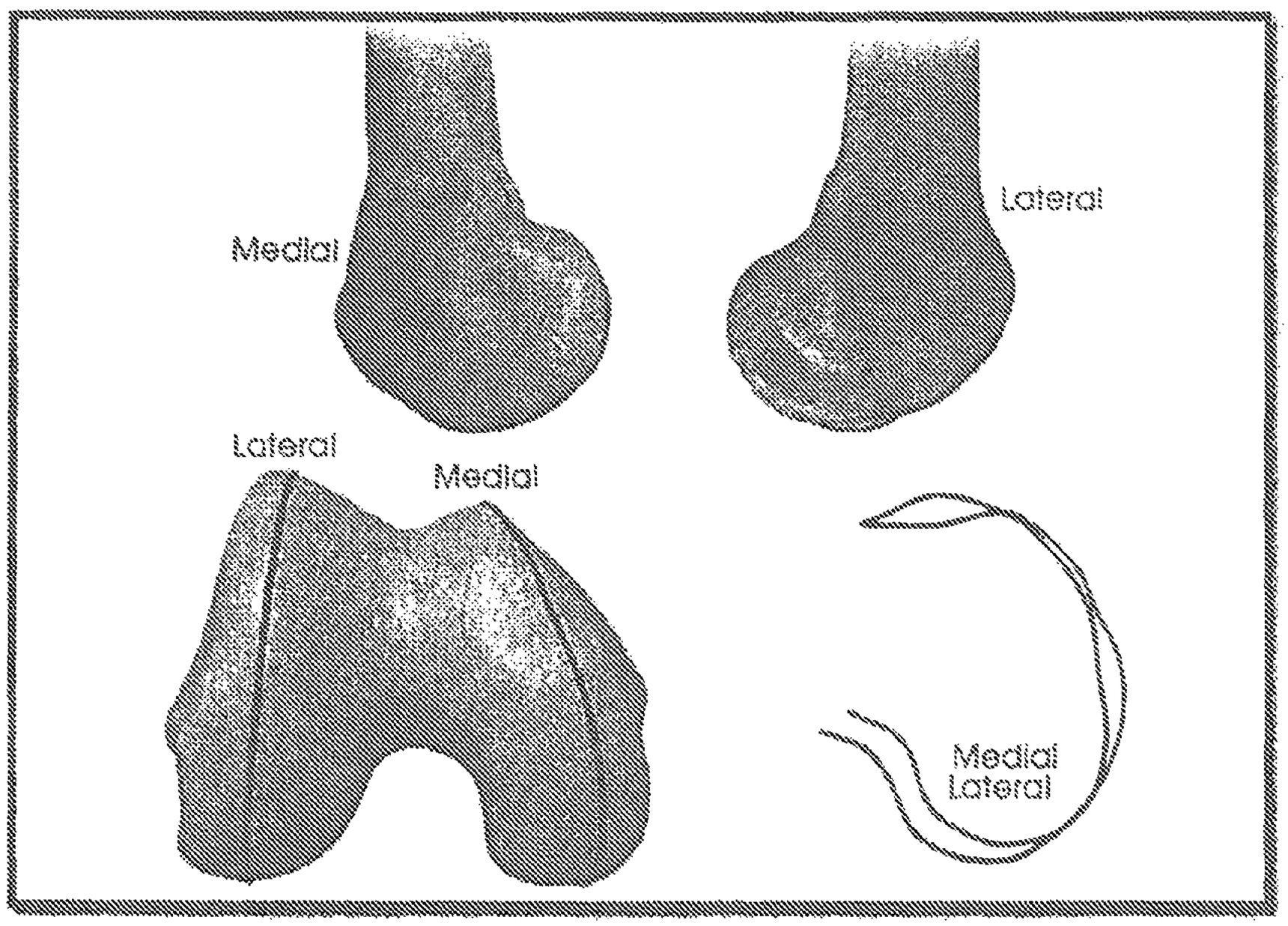

FIG. 18

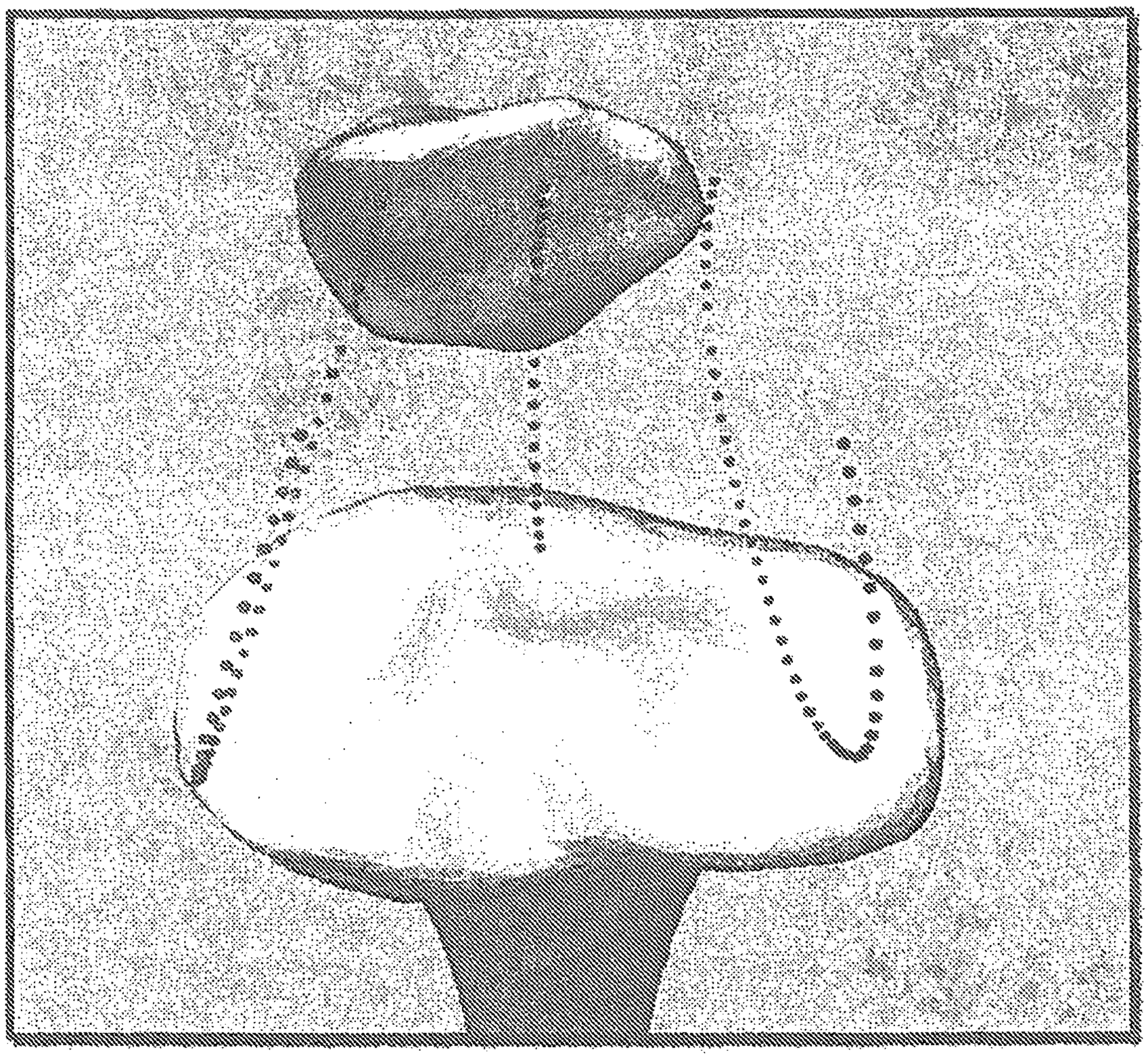

FIG. 19

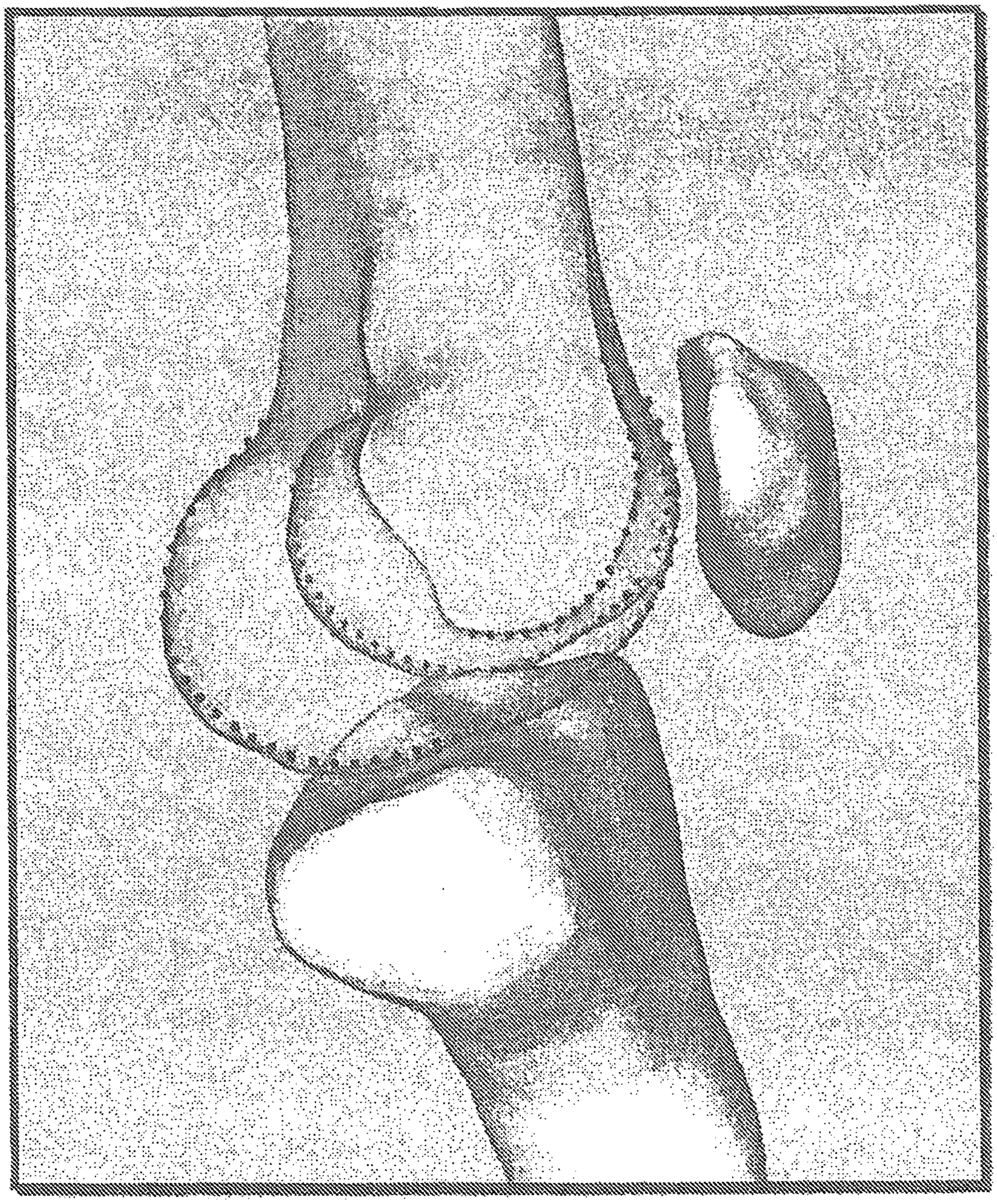

FIG. 20

MEDIAL	c1	c2	c3	c4
MEAN	2.15	1.94	3.38	2.80
STD	0.98	0.38	2.09	1.22
MEAN	2.73	2.46	3.96	3.34
STD	1.31	1.19	2.20	1.41
LATERAL	c1	c2	c3	c3
MEAN	5.13	2.12	4.92	2.43
STD	6.11	0.56	2.09	0.91
MEAN	6.20	2.44	5.89	2.79
STD	9.64	1.09	4.24	0.94

FIG. 21

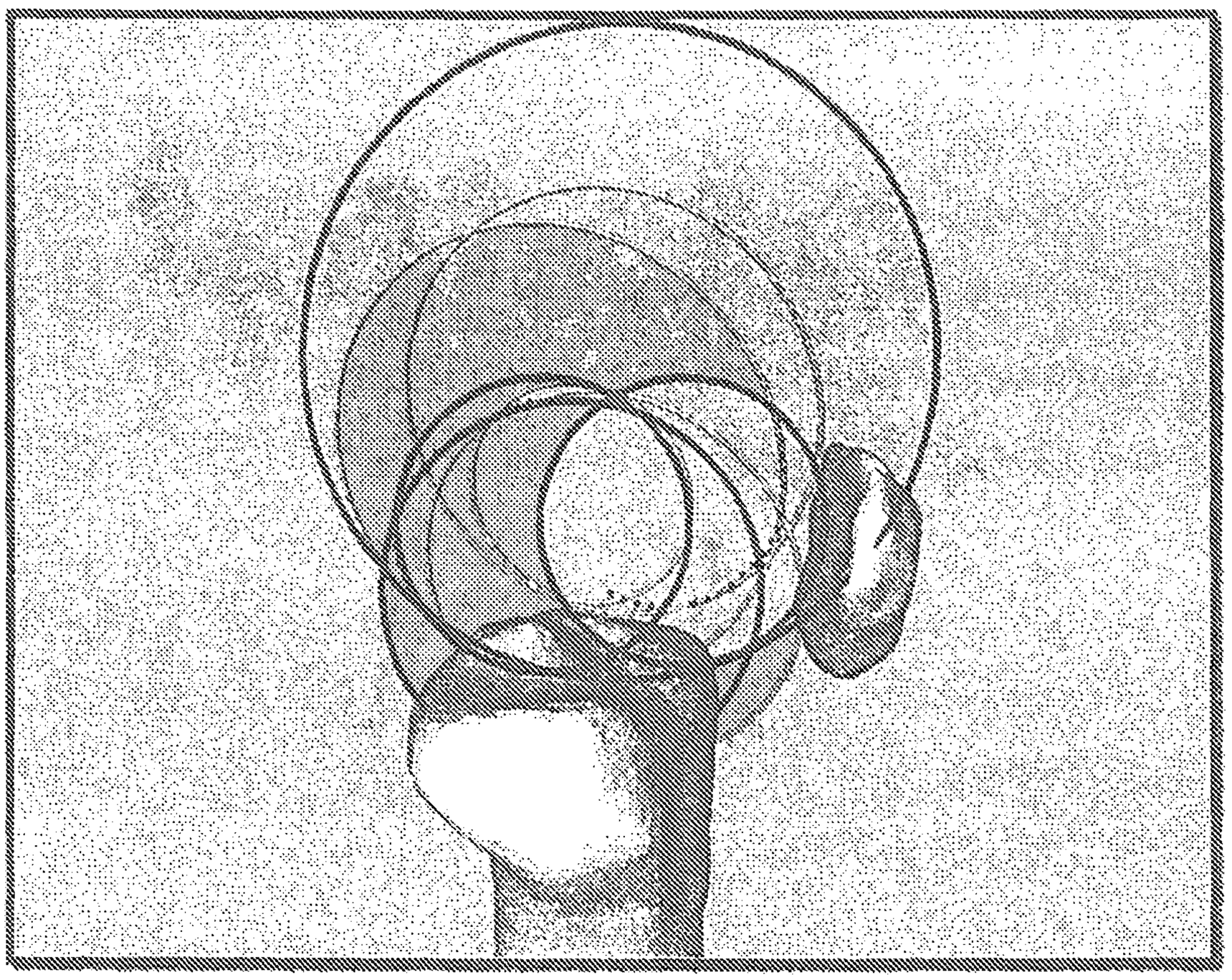

FIG. 22

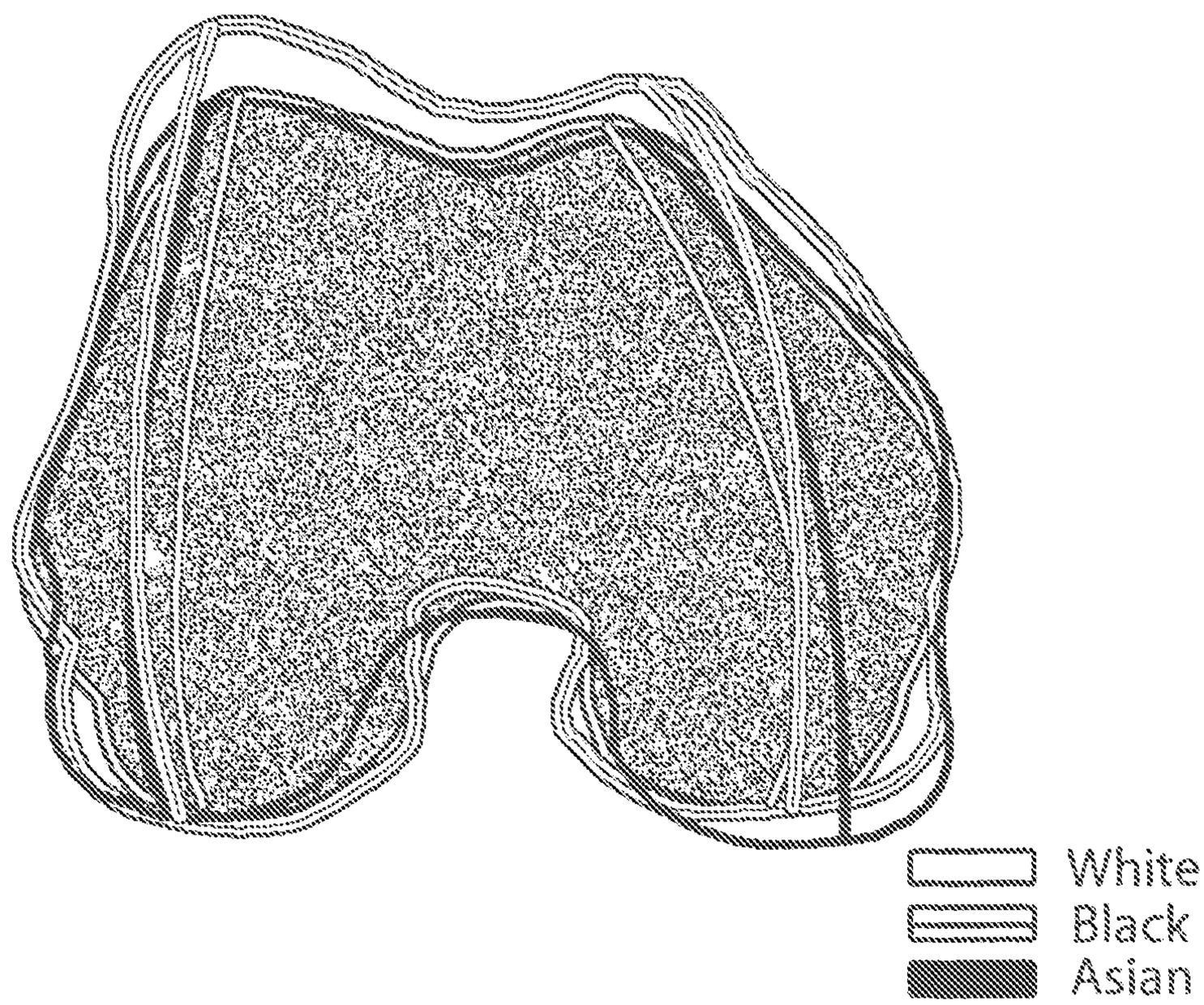

FIG. 23

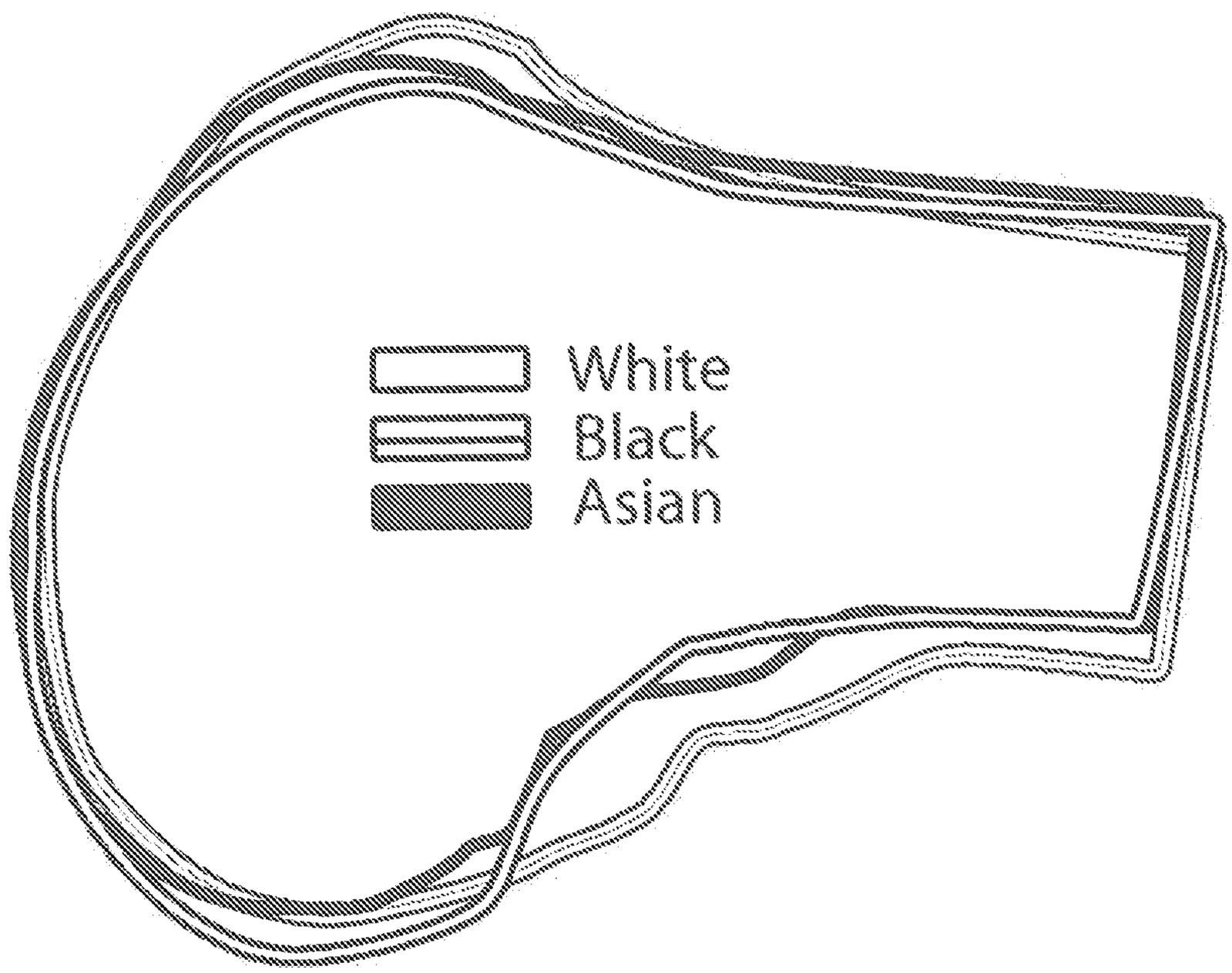

FIG. 24

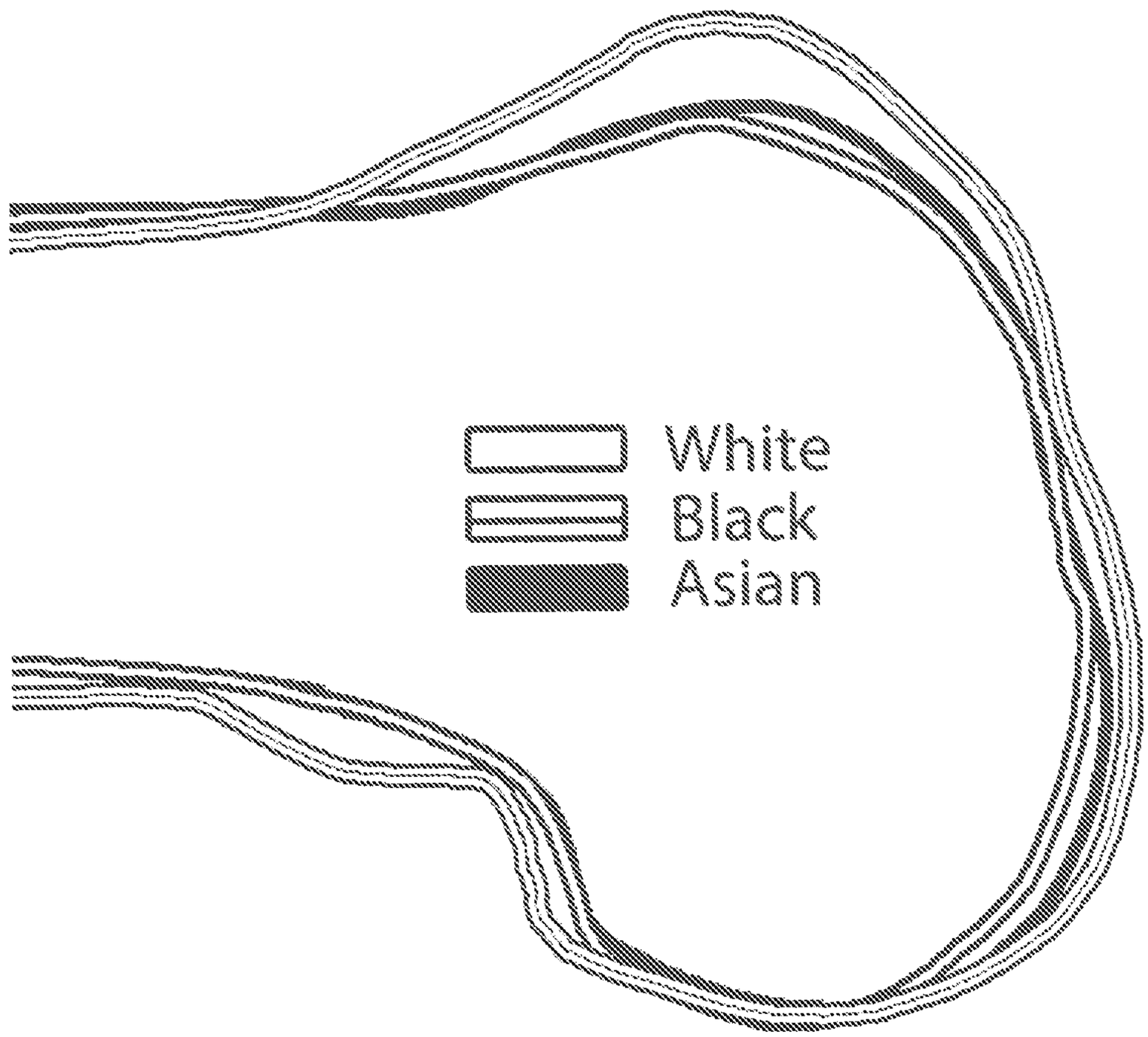

FIG. 25

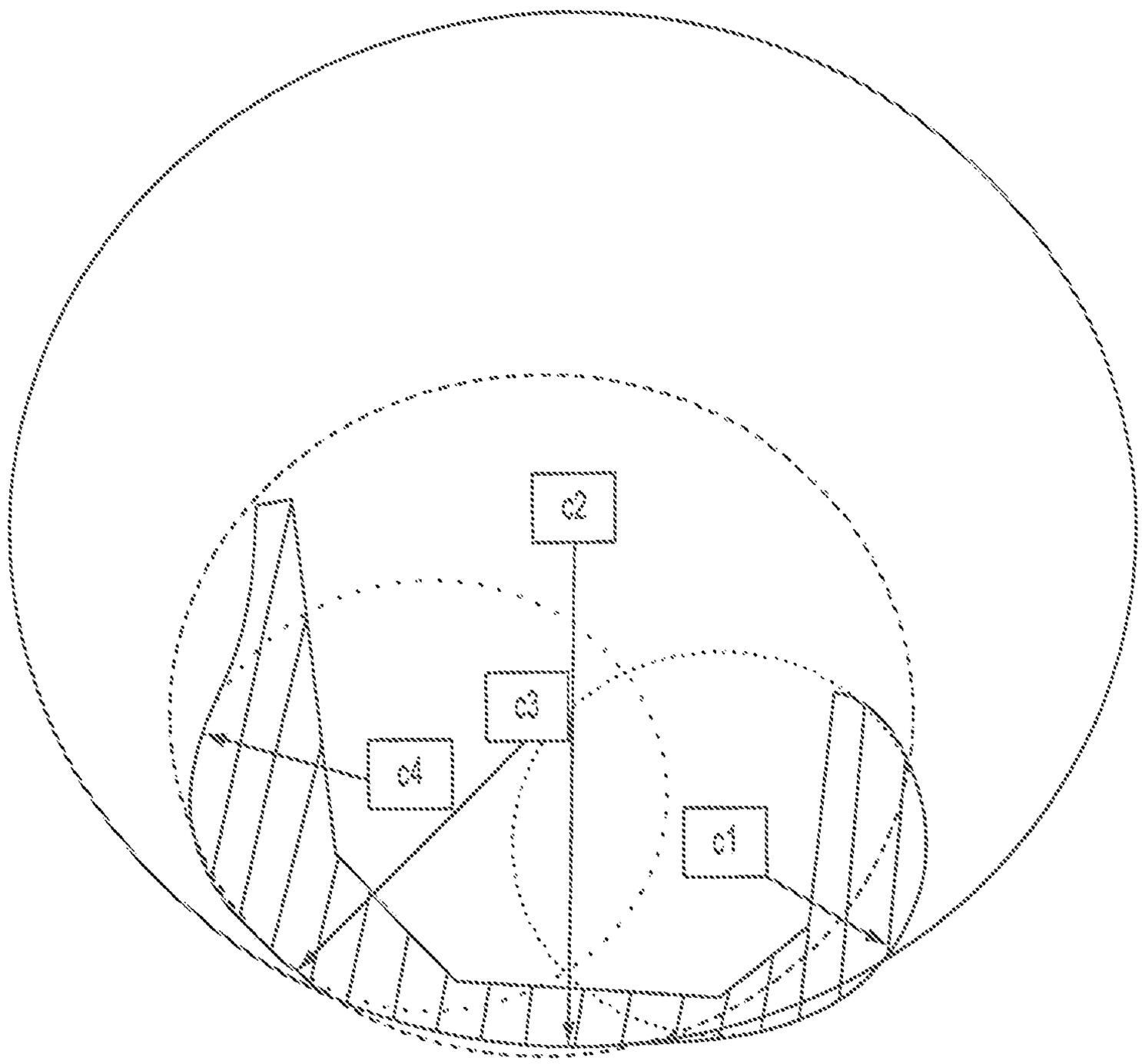

FIG. 26

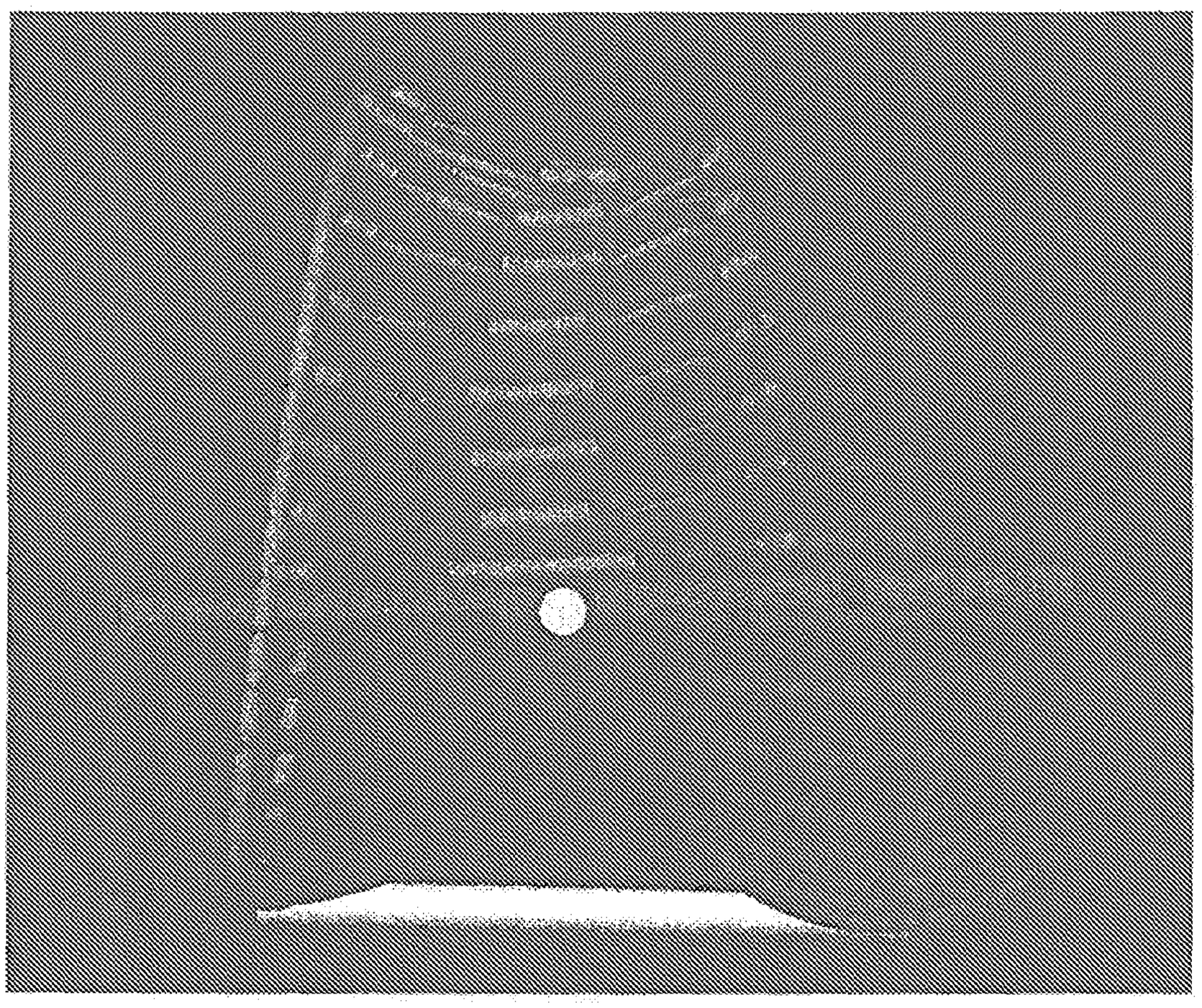

FIG. 27

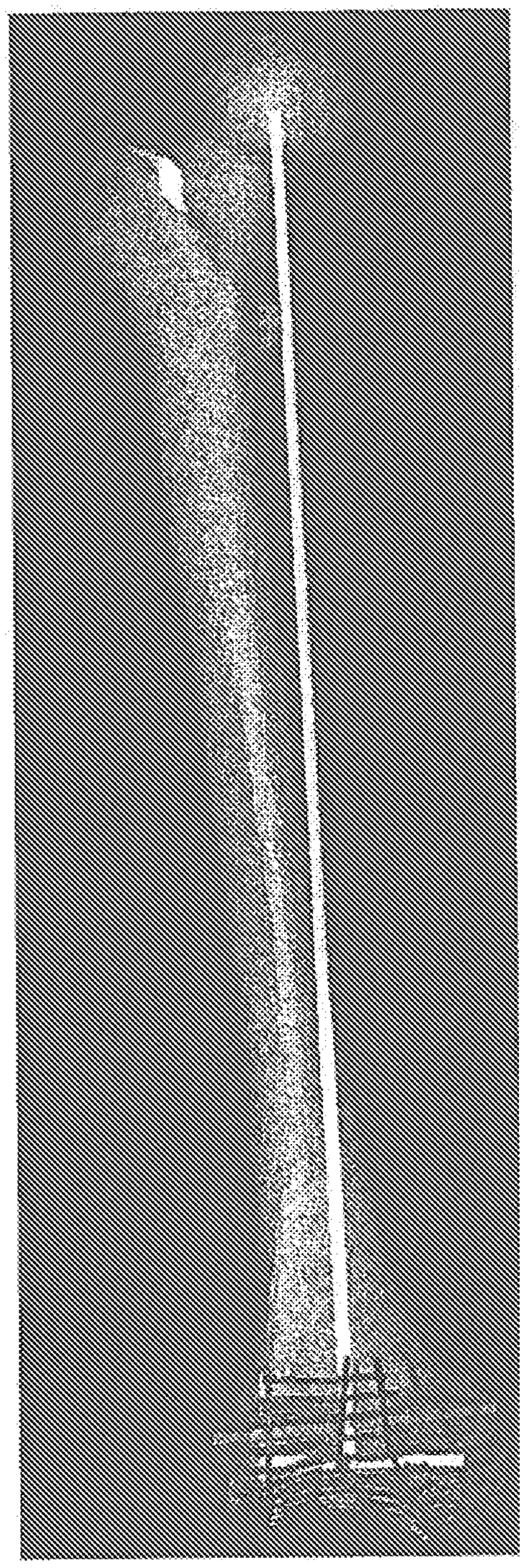

FIG. 28

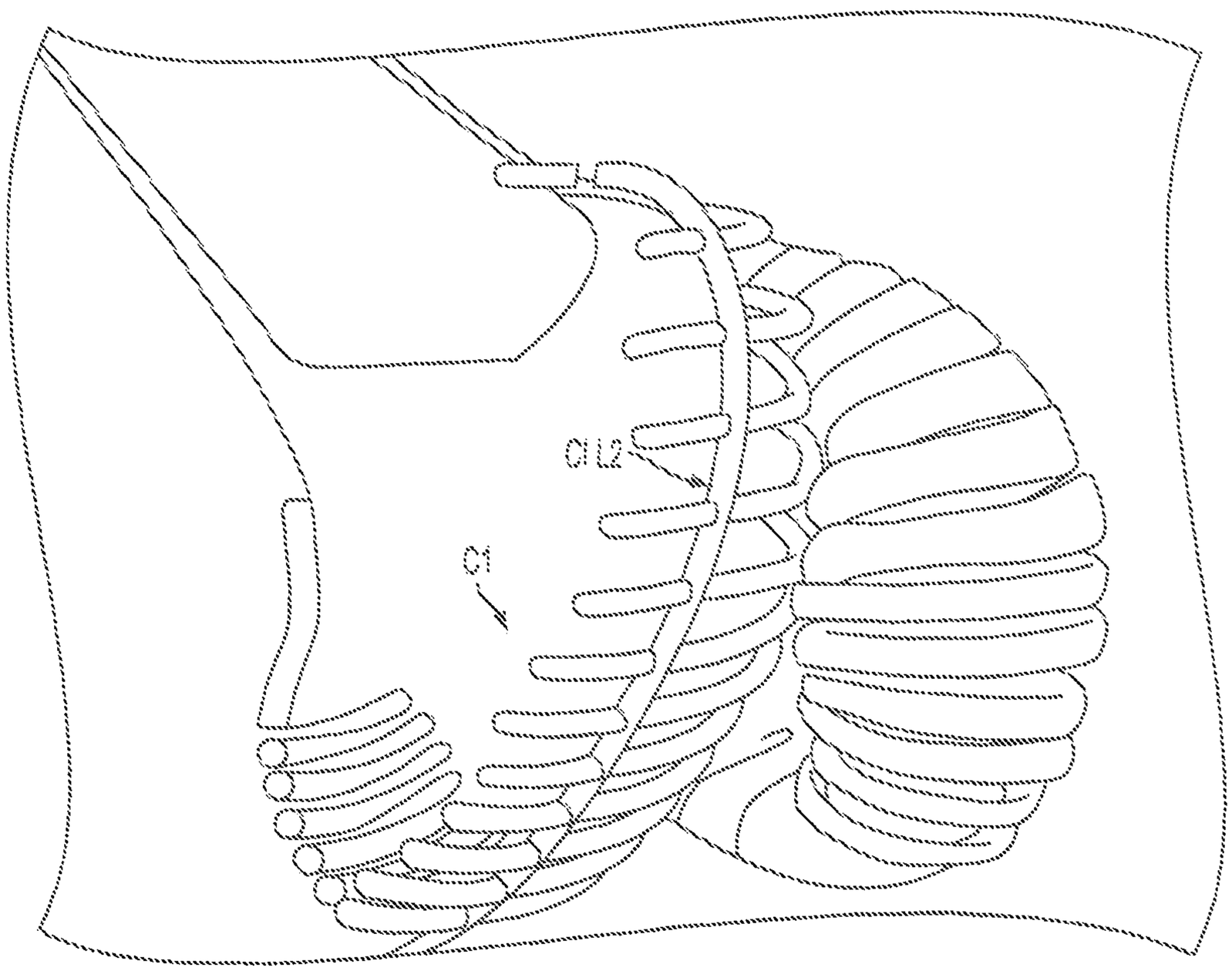

FIG. 29

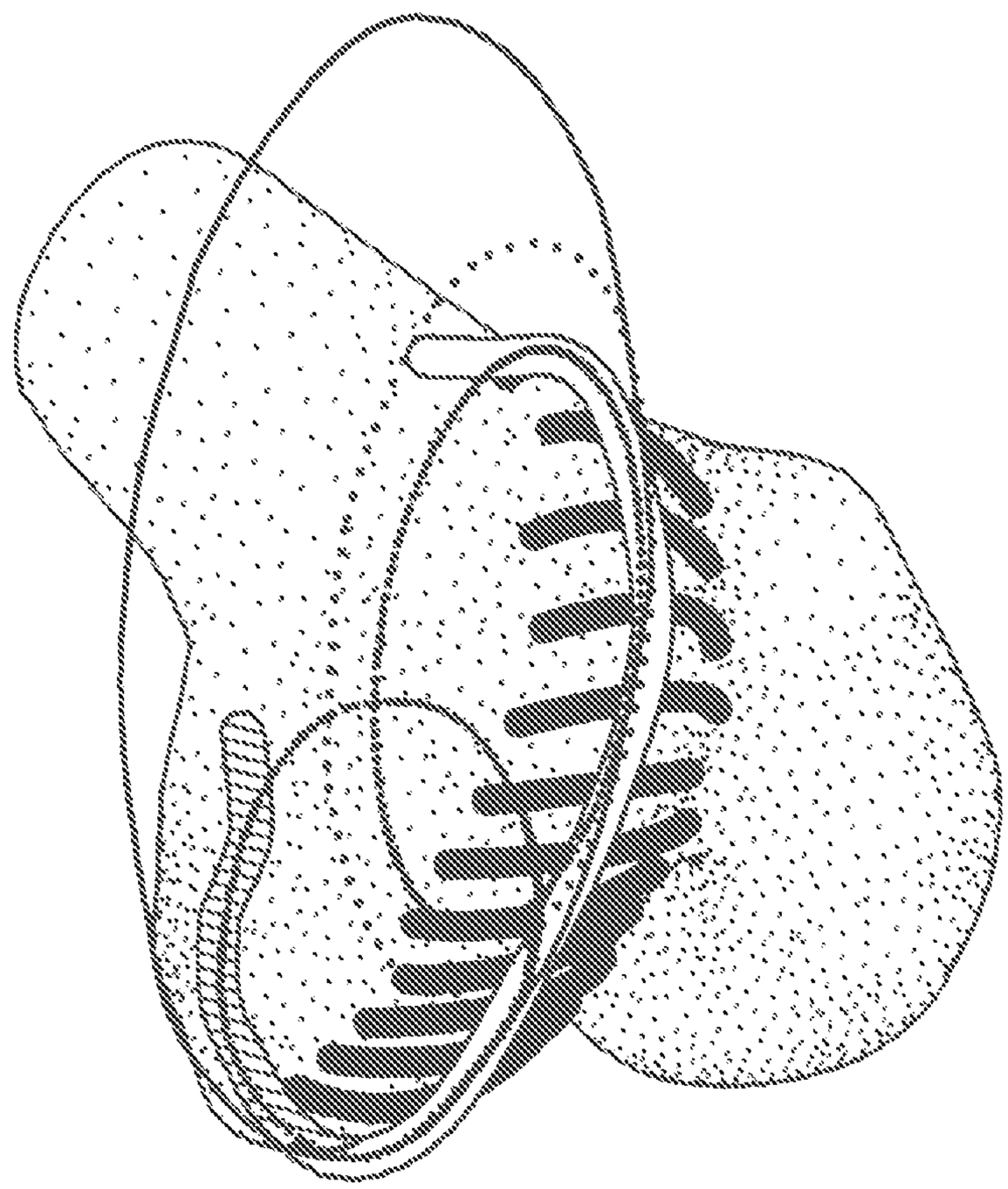

FIG. 30

	SAGITAL ARCS	M	L	PROFILE ARCS		M	L
0		2.45	1.95	3.08	11.41	0.79	0.17
10		2.66	1.77			0.86	0.16
20		2.53	1.84			0.82	0.16
30		2.42	2.03			0.78	0.18
40		2.01	1.88	3.73	2.02	0.54	0.93
50		1.96	1.96			0.53	0.97
60		2.21	2.12			0.59	1.05
70		2.30	2.38			0.62	1.18
80		2.54	2.70	2.09	2.18	1.22	1.24
90		2.15	2.31			1.03	1.06
100		1.95	2.09			0.93	0.96
110		1.71	2.18			0.82	1.00
120		1.46	2.31	2.29	2.91	0.64	0.79
130		1.27	2.56			0.56	0.88
140		2.62	2.54			1.14	1.01
150		2.62	2.94			1.14	1.01

FIG. 31

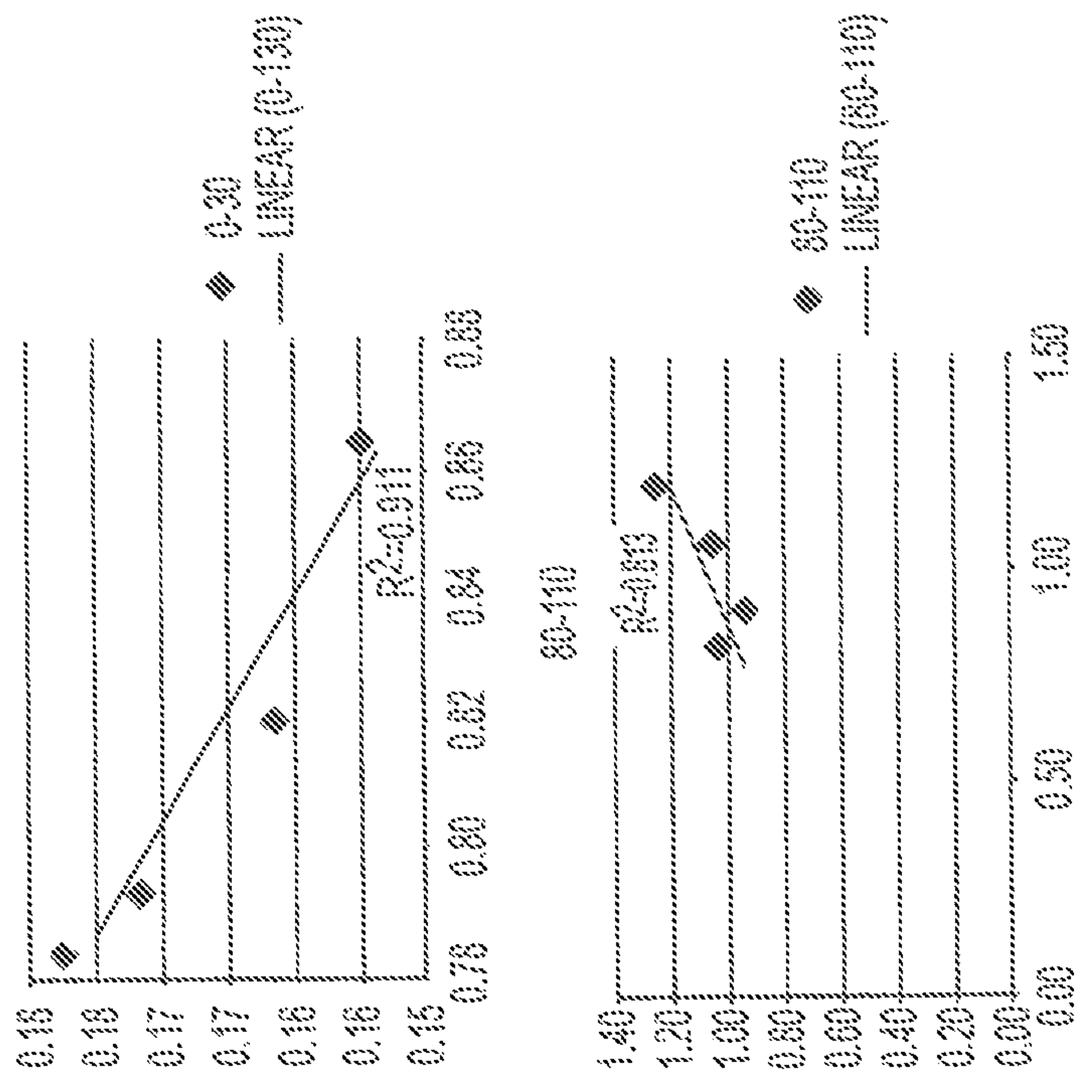

FIG. 32A

FIG. 32C

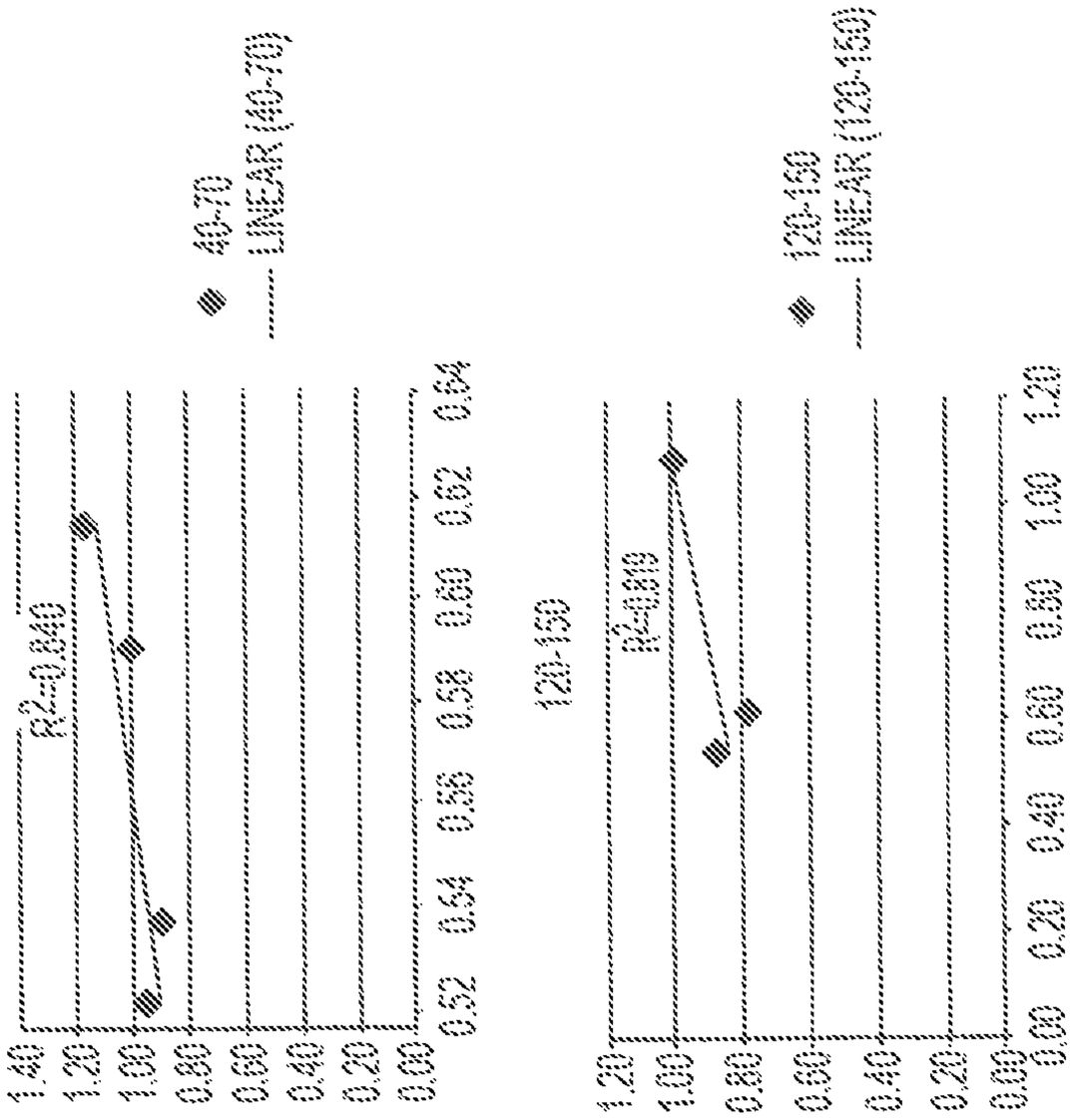

FIG. 32B

FIG. 32D

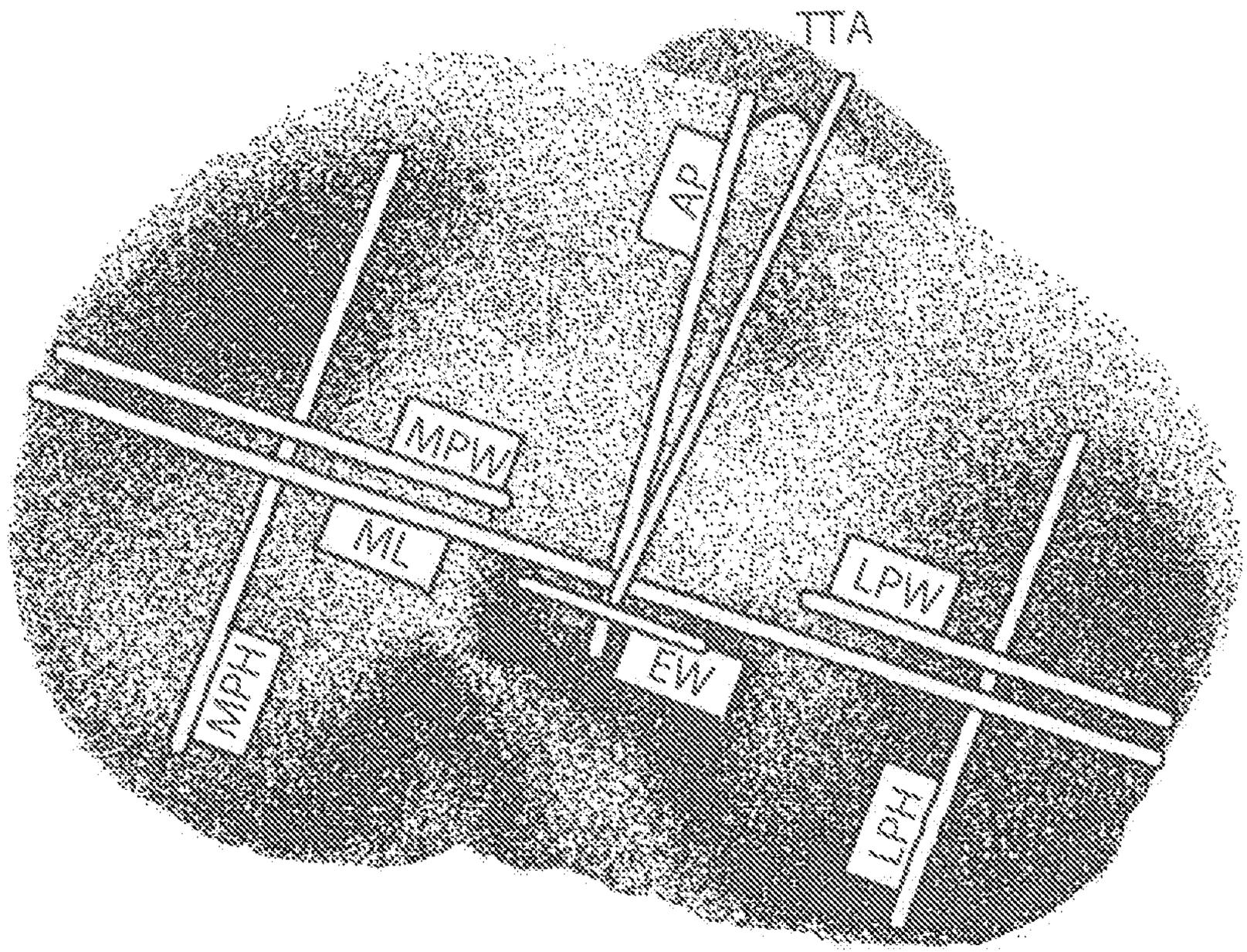

FIG. 33

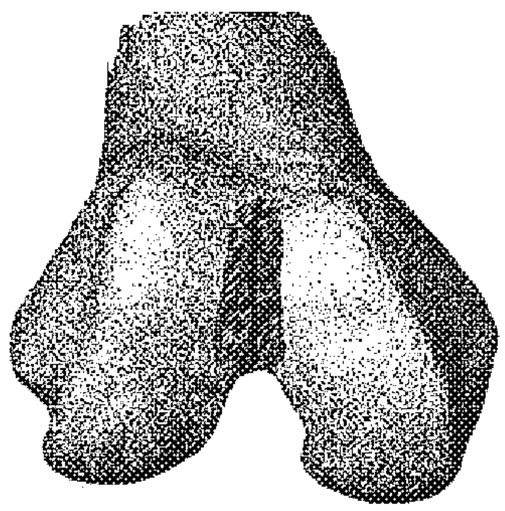

FIG. 34A

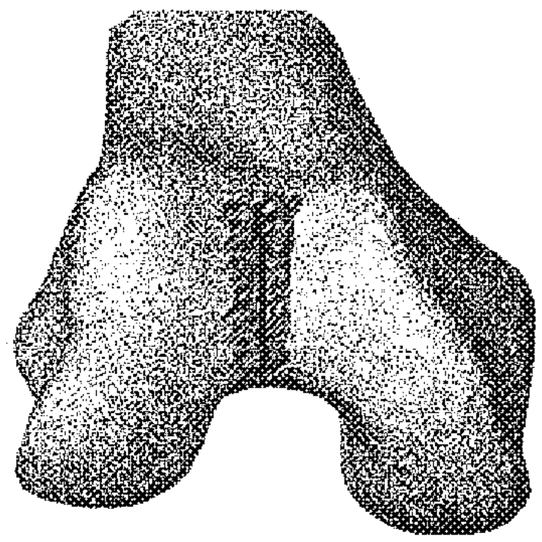

FIG. 34B

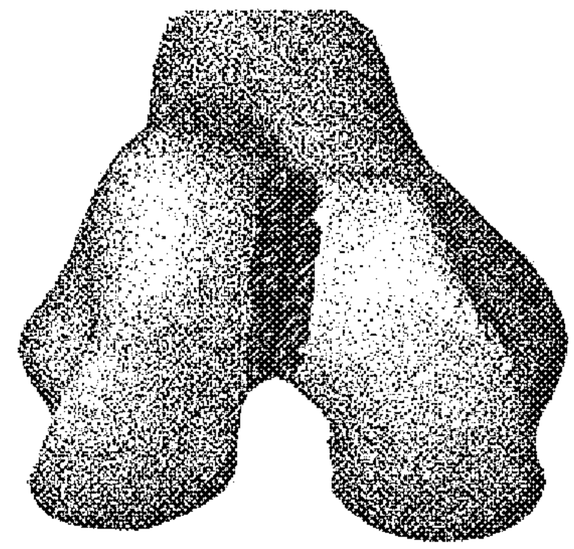

FIG. 34C

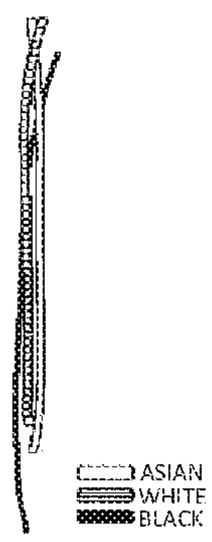

FIG. 35

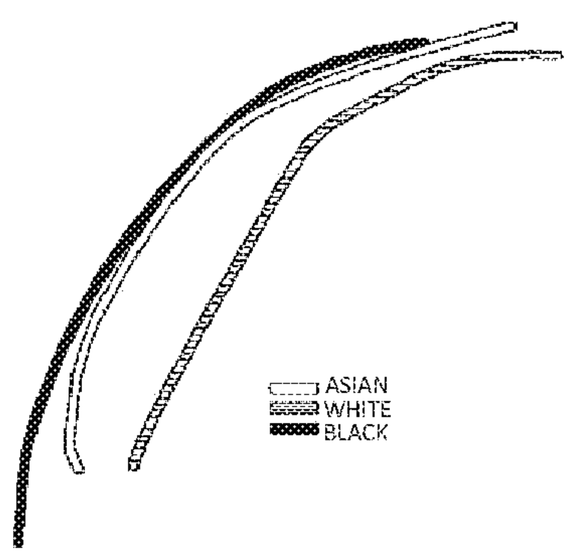

FIG. 36

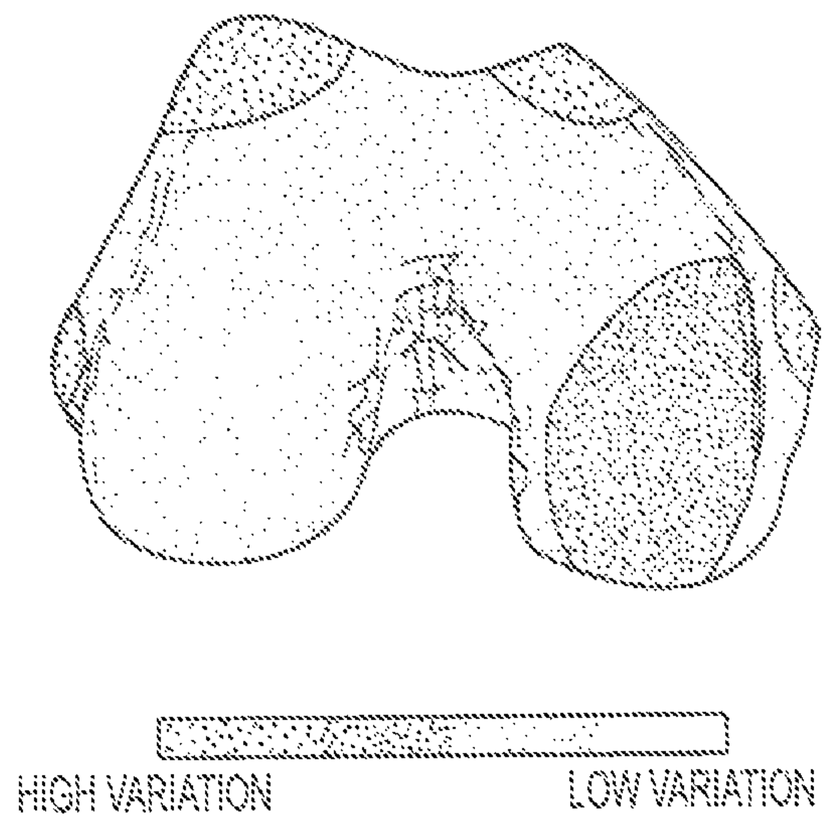
HIGH VARIATION
LOW VARIATION

FIG. 37

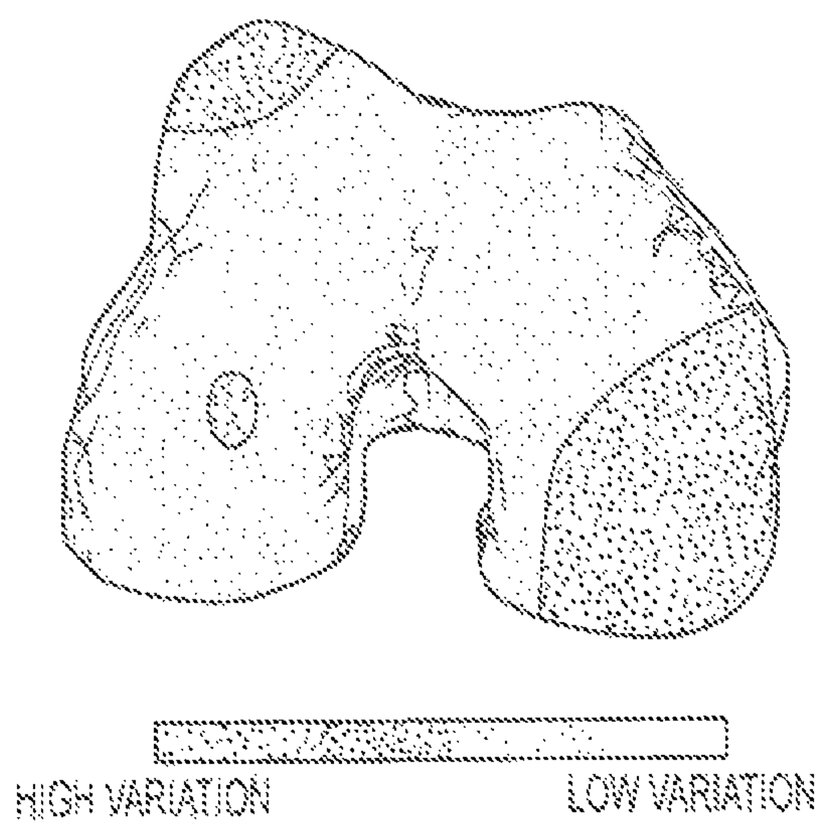
HIGH VARIATION
LOW VARIATION

FIG. 38

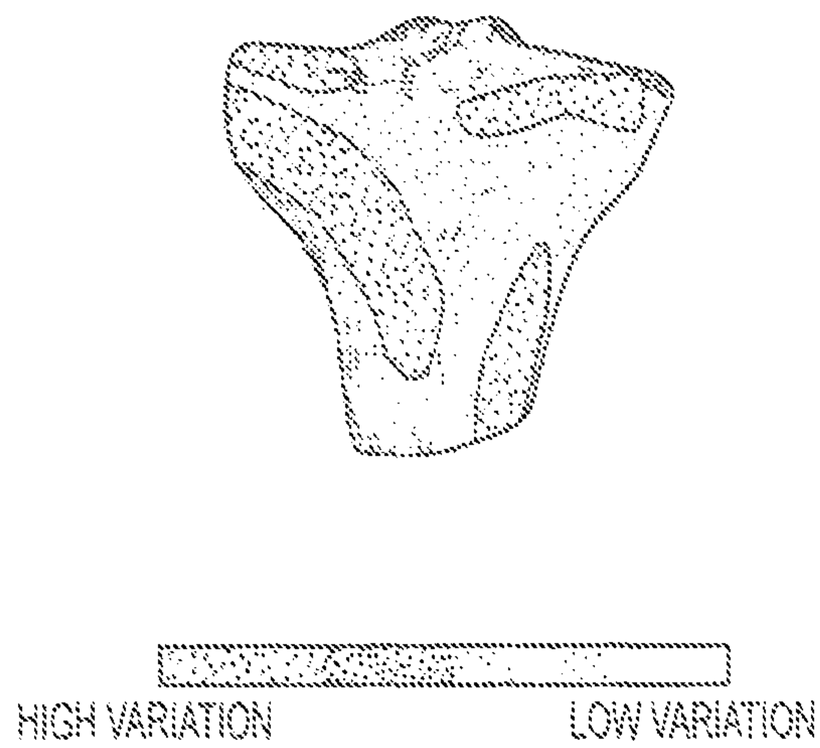
HIGH VARIATION
LOW VARIATION

FIG. 39

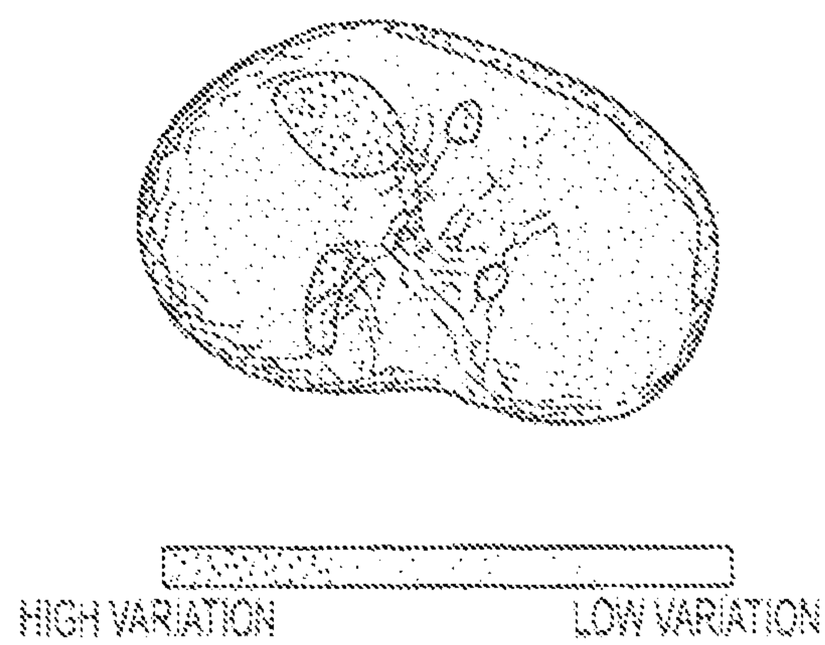
HIGH VARIATION
LOW VARIATION

FIG. 40

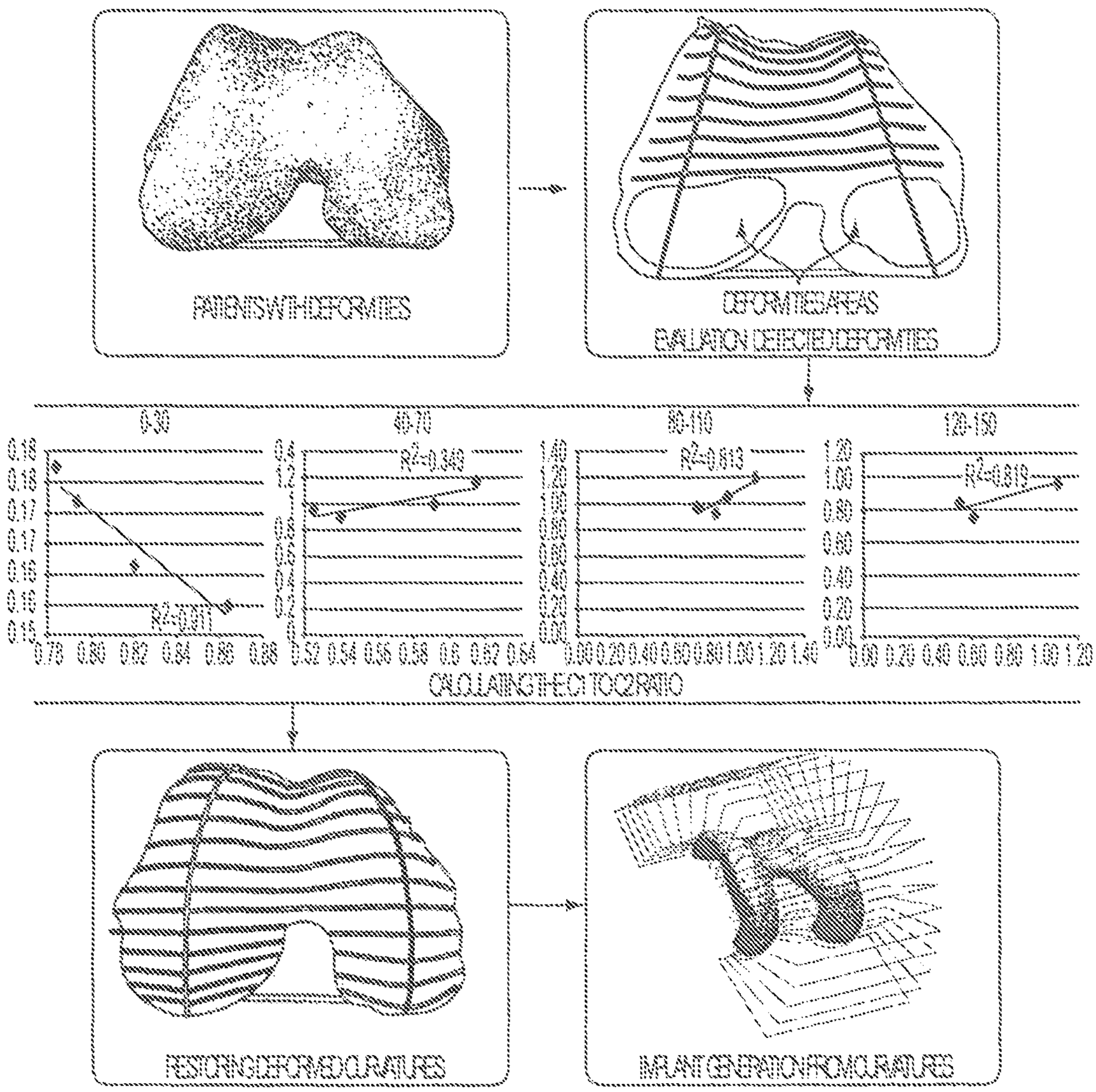
PATIENTS WITH DEFORMITIES
DEFORMITIES AREAS
EVALUATION DEFECTED DEFORMITIES
0-30
40-70
80-110
120-150
R²=0.349
R²=0.813
R²=0.319
R²=0.011
CALCULATING EFCT TO CZ RATIO
RESTORING DEFORMED CURVATURES
IMPLANT GENERATION FROM CURVATURES

FIG. 41

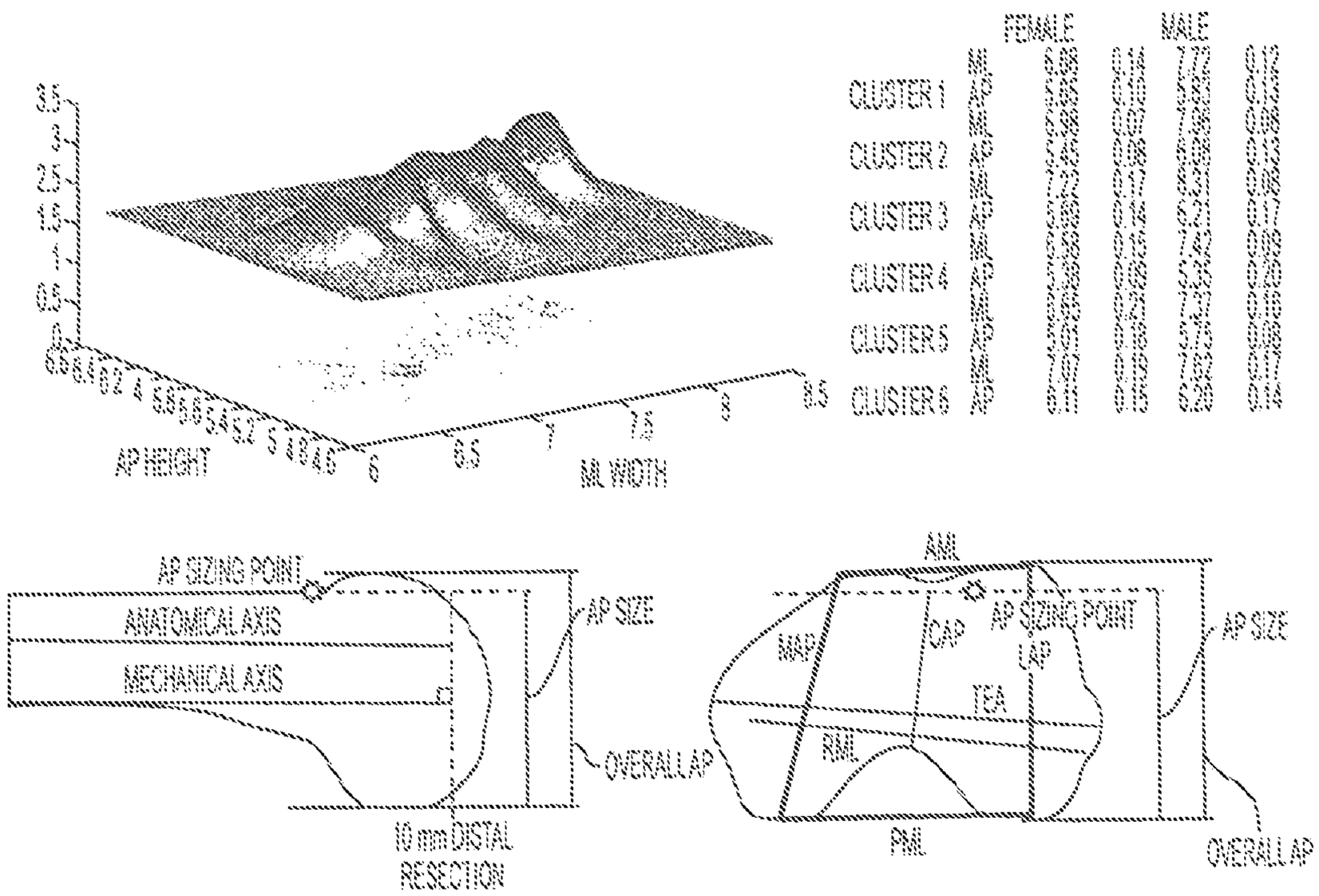
FEMALE
MALE
CLUSTER 1
CLUSTER 2
CLUSTER 3
CLUSTER 4
CLUSTER 5
CLUSTER 6
ML
AP
AP HEIGHT
ML WIDTH
AP SIZING POINT
ANATOMICAL AXIS
MECHANICAL AXIS
AP SIZE
OVERALL AP
10 mm DISTAL RESECTION
AML
MAP
CAP
LAP
TEA
RML
PML

FIG. 42

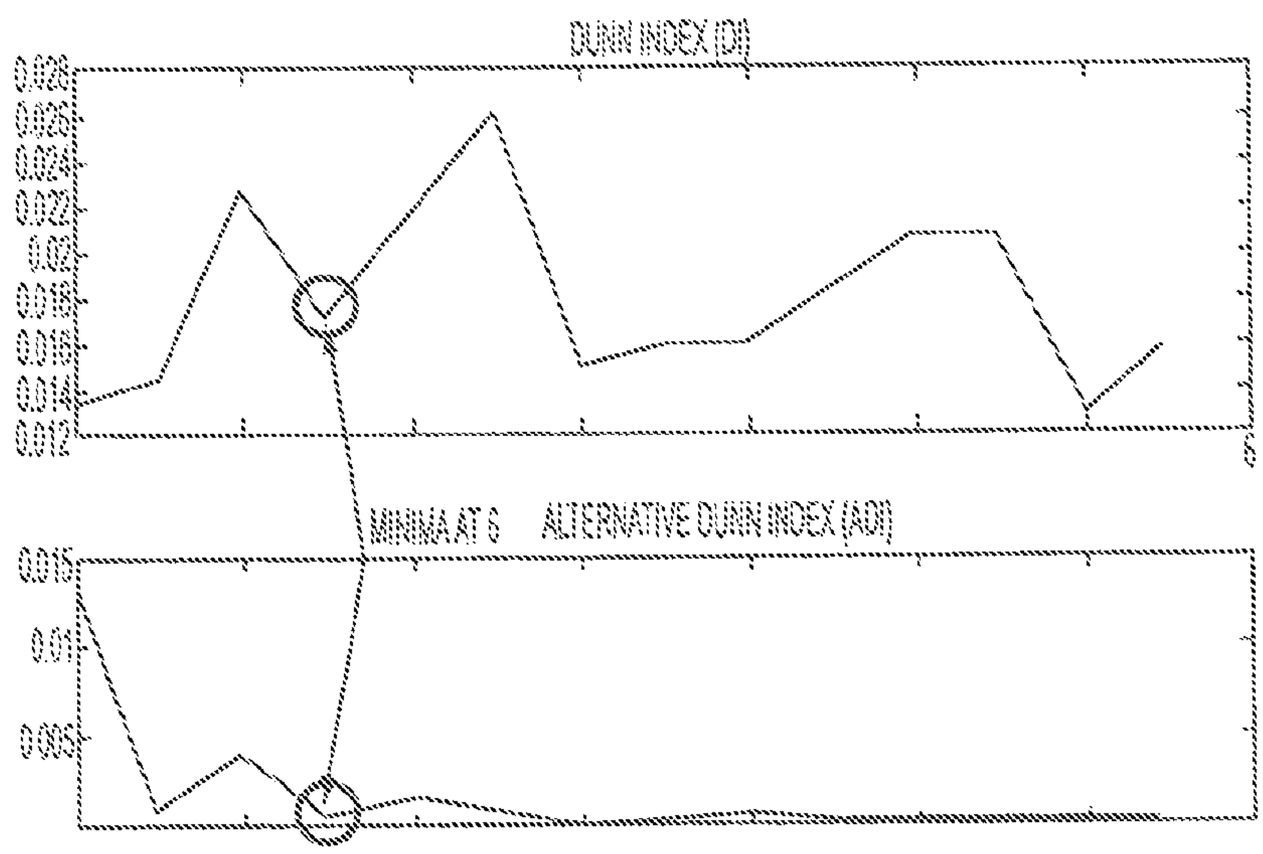
DUNN INDEX (DI)
MINIMA AT 6
ALTERNATIVE DUNN INDEX (ADI)

FIG. 43

$$ADI(c) = min_{i \in c}\{min_{j \in c, i \neq j}\{\frac{min_{x_i \in C_i, x_j \in C_j}|d(y, v_j) - d(x_i, v_j)|}{max_{k \in c}\{max_{x,y \in C} d(x, y)\}}\}\}$$

FIG. 44

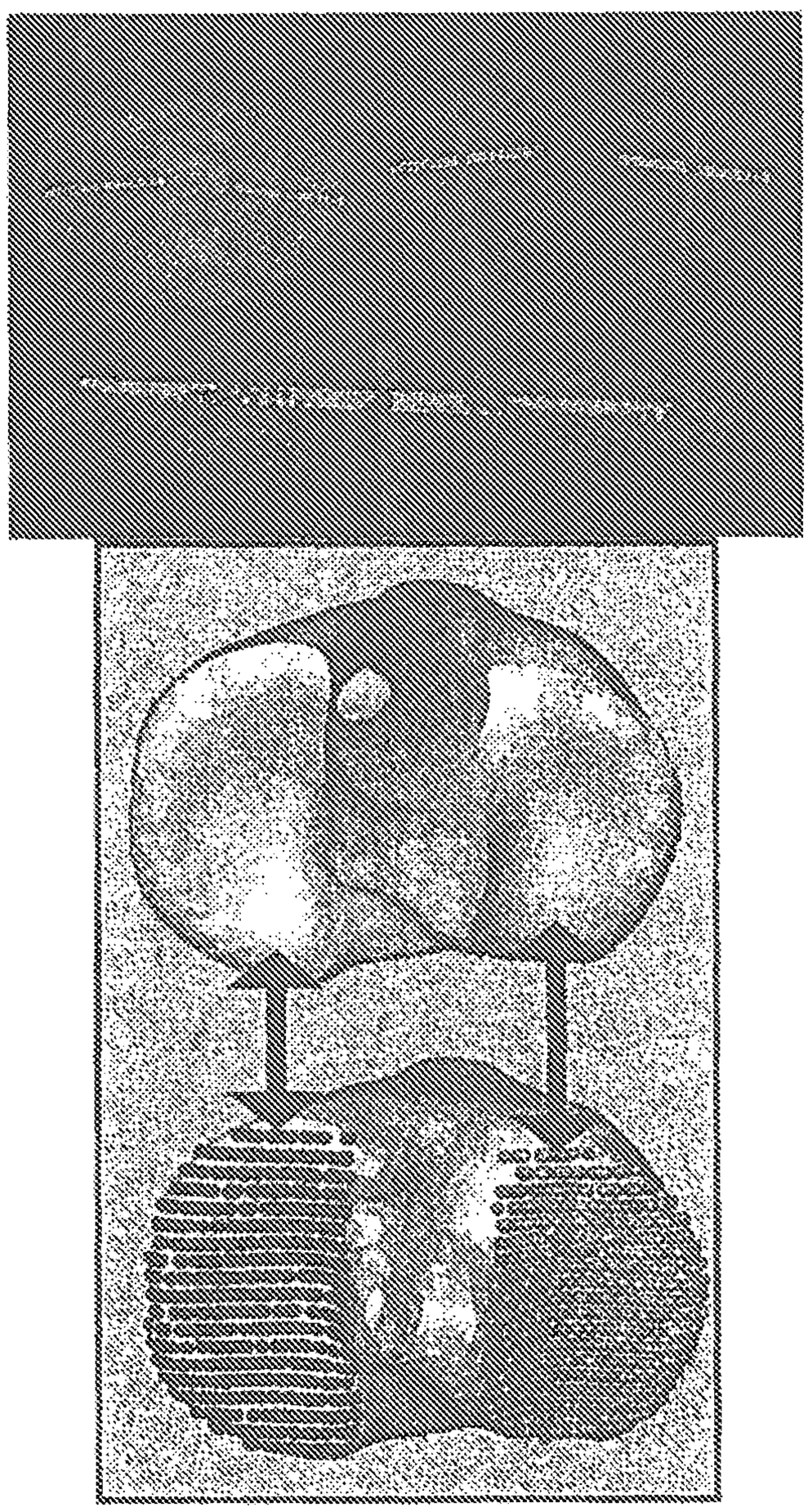

FIG. 45

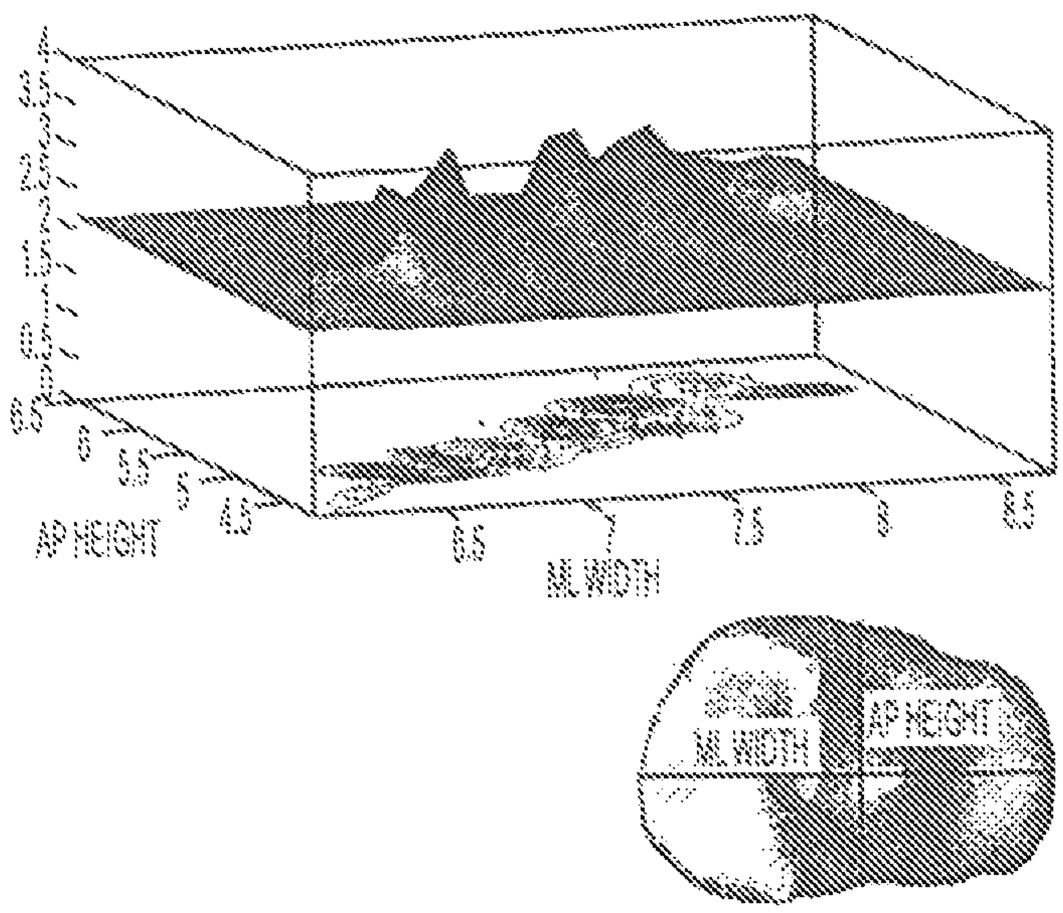

		FEMALE		MALE	
C1	ML	6.35	0.12	8.13	0.14
	AP	4.59	0.16	6.17	0.15
C2	ML	6.60	0.11	8.43	0.11
	AP	4.93	0.10	5.97	0.06
C3	ML	7.38	0.10	7.80	0.15
	AP	5.46	0.20	5.58	0.13
C4	ML	7.74	0.15	7.76	0.14
	AP	5.55	0.20	5.90	0.09
C5	ML	7.05	0.12	7.18	0.19
	AP	5.14	0.17	5.21	0.14
C6	ML	6.81	0.06	7.44	0.09
	AP	5.06	0.13	5.56	0.10

FIG. 46

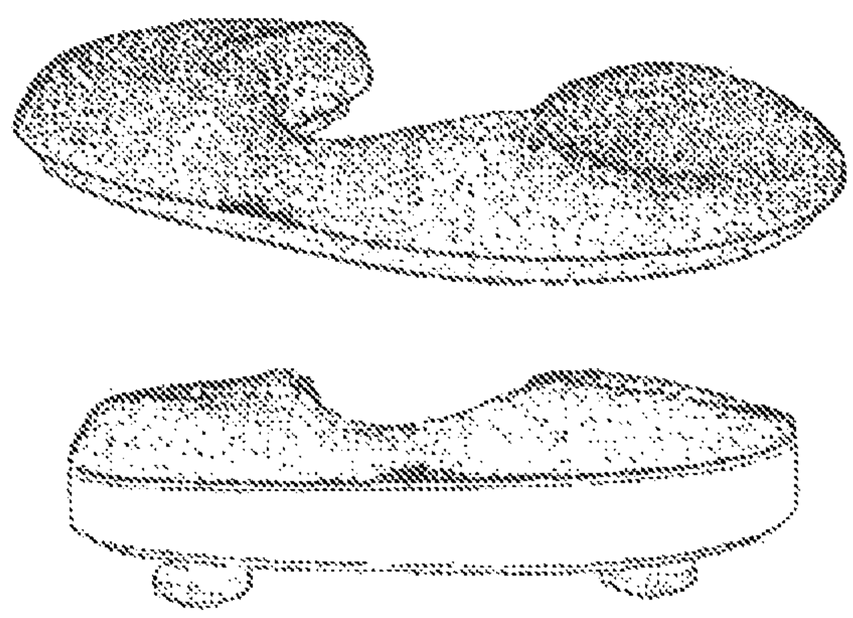

FIG. 47

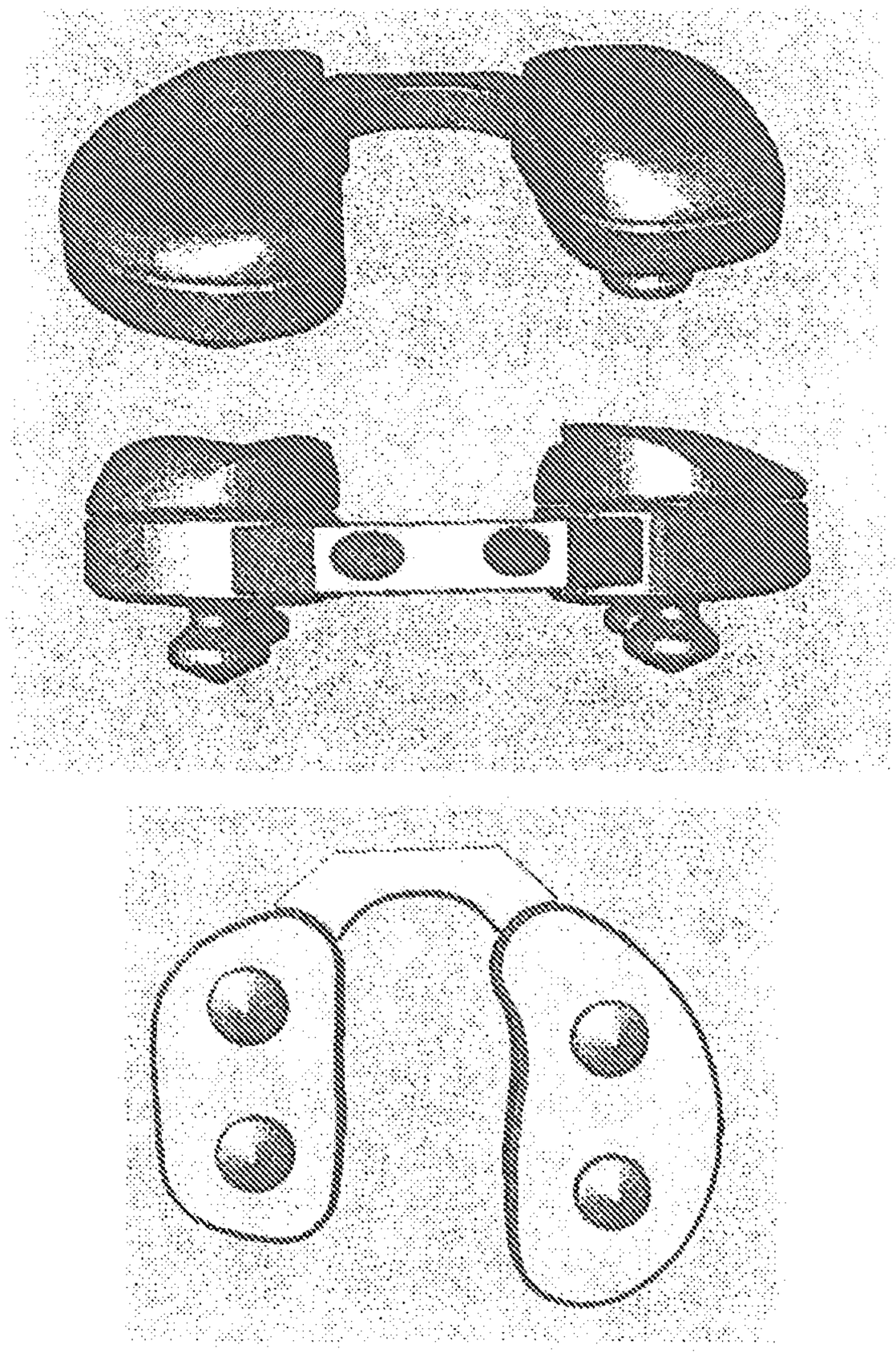

FIG. 48

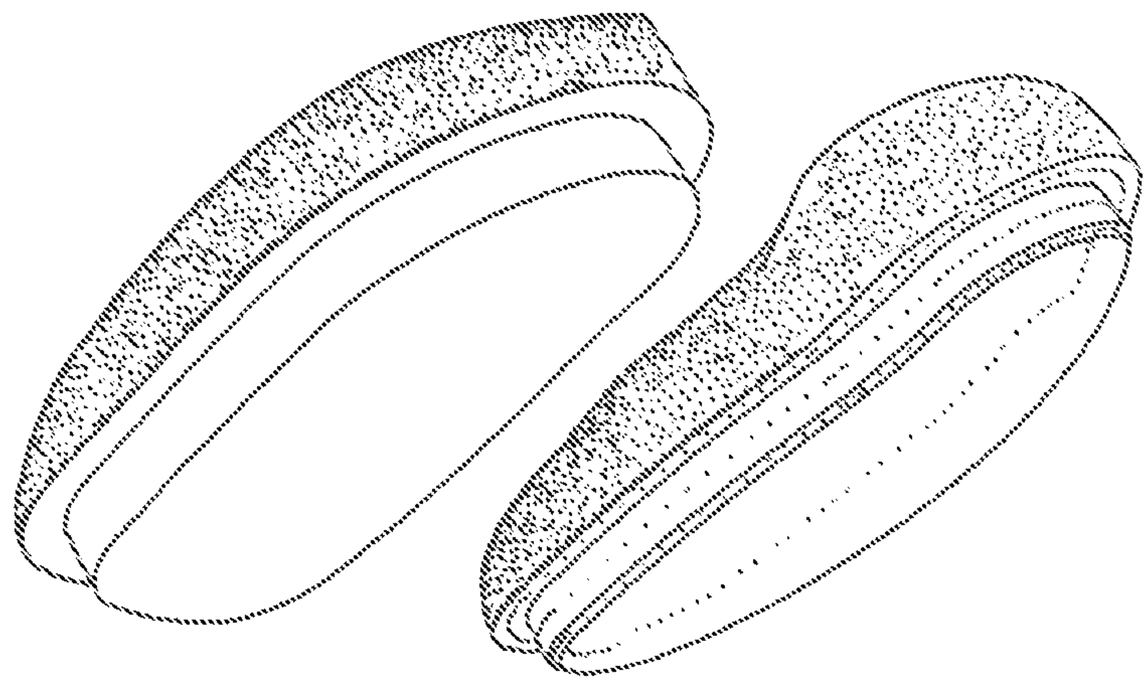

FIG. 49

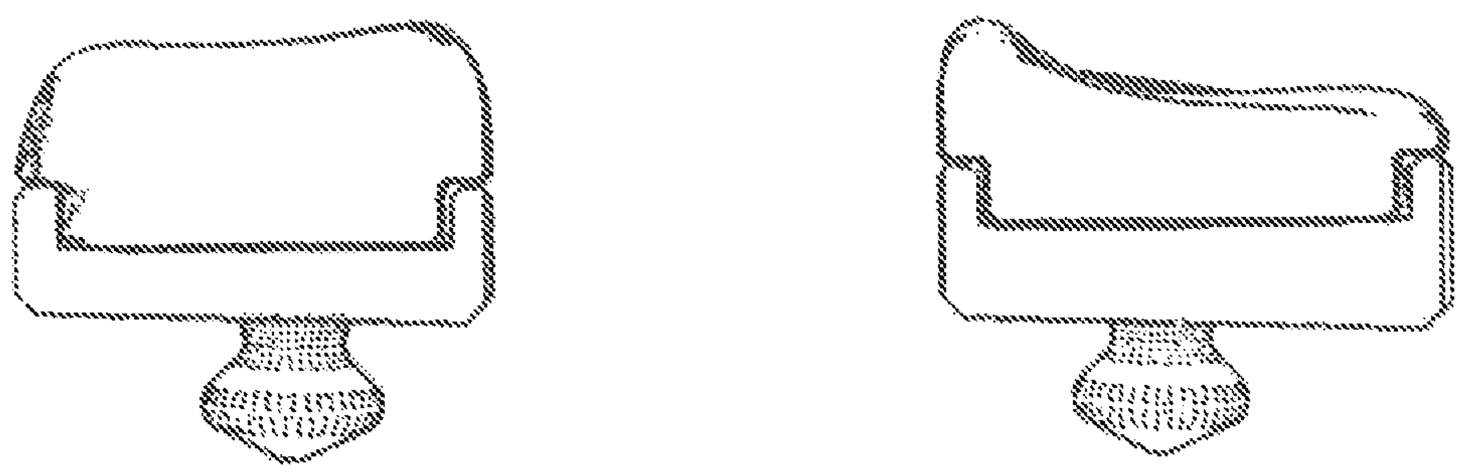

FIG. 50

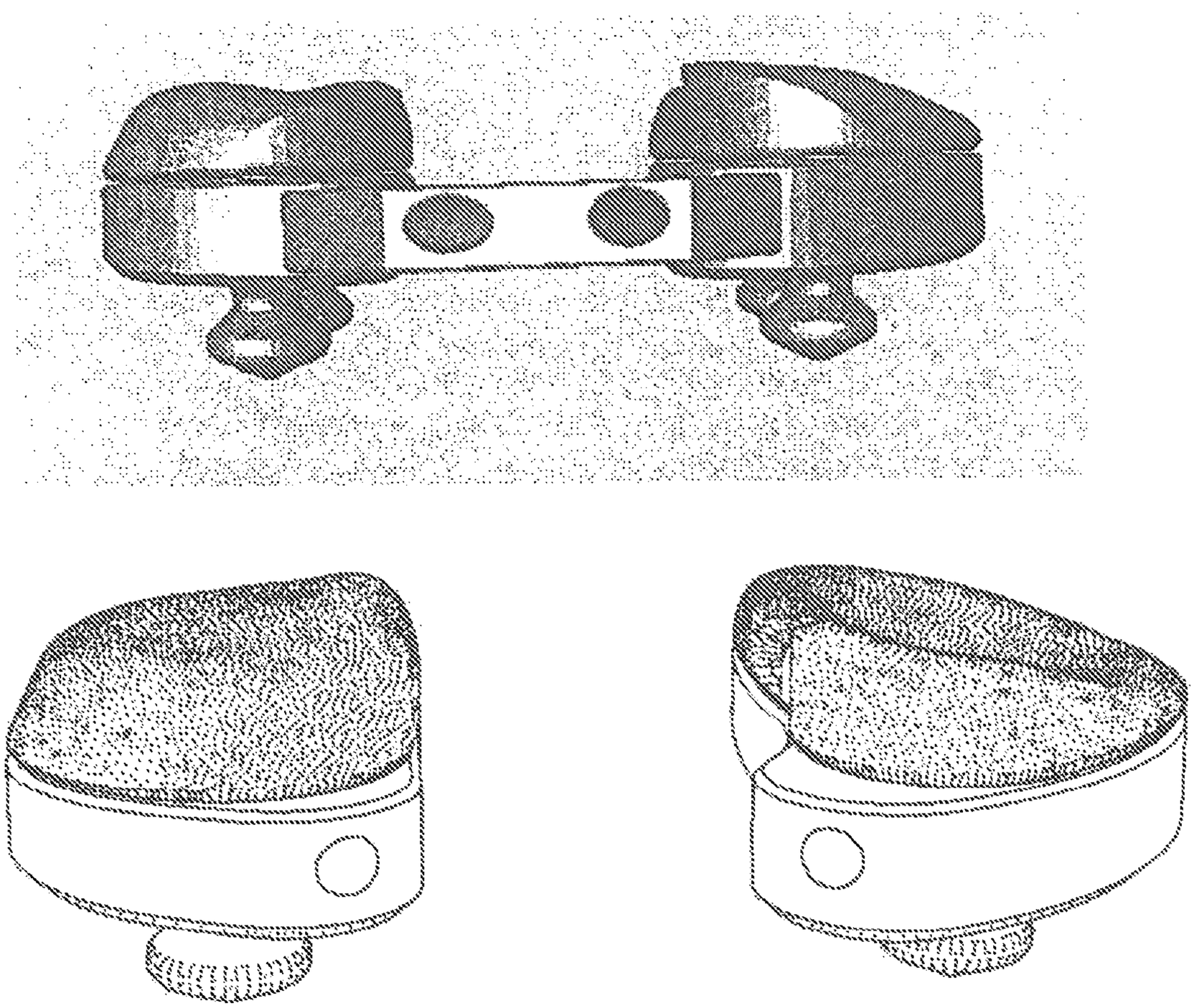

FIG. 51

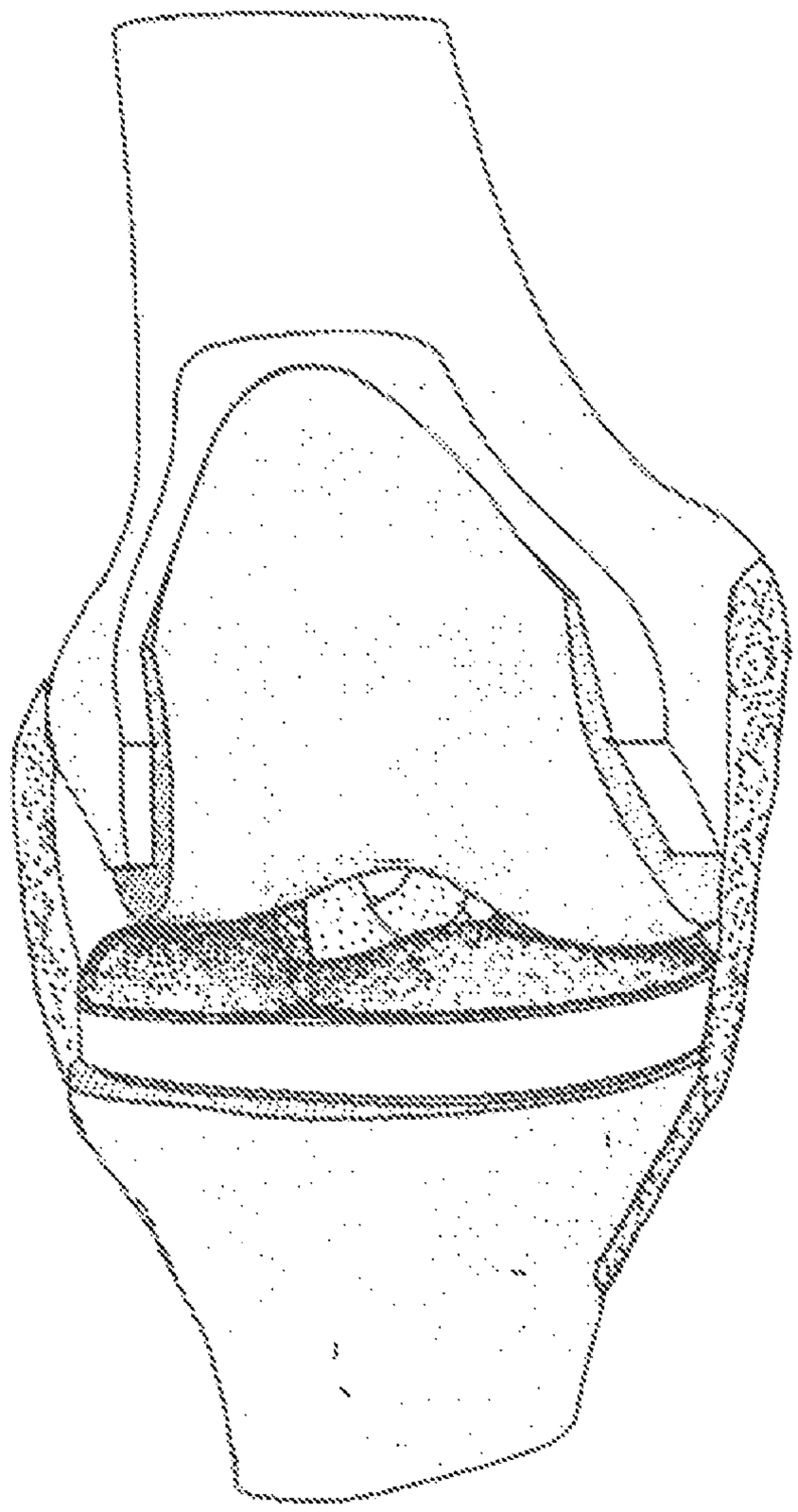

FIG. 52

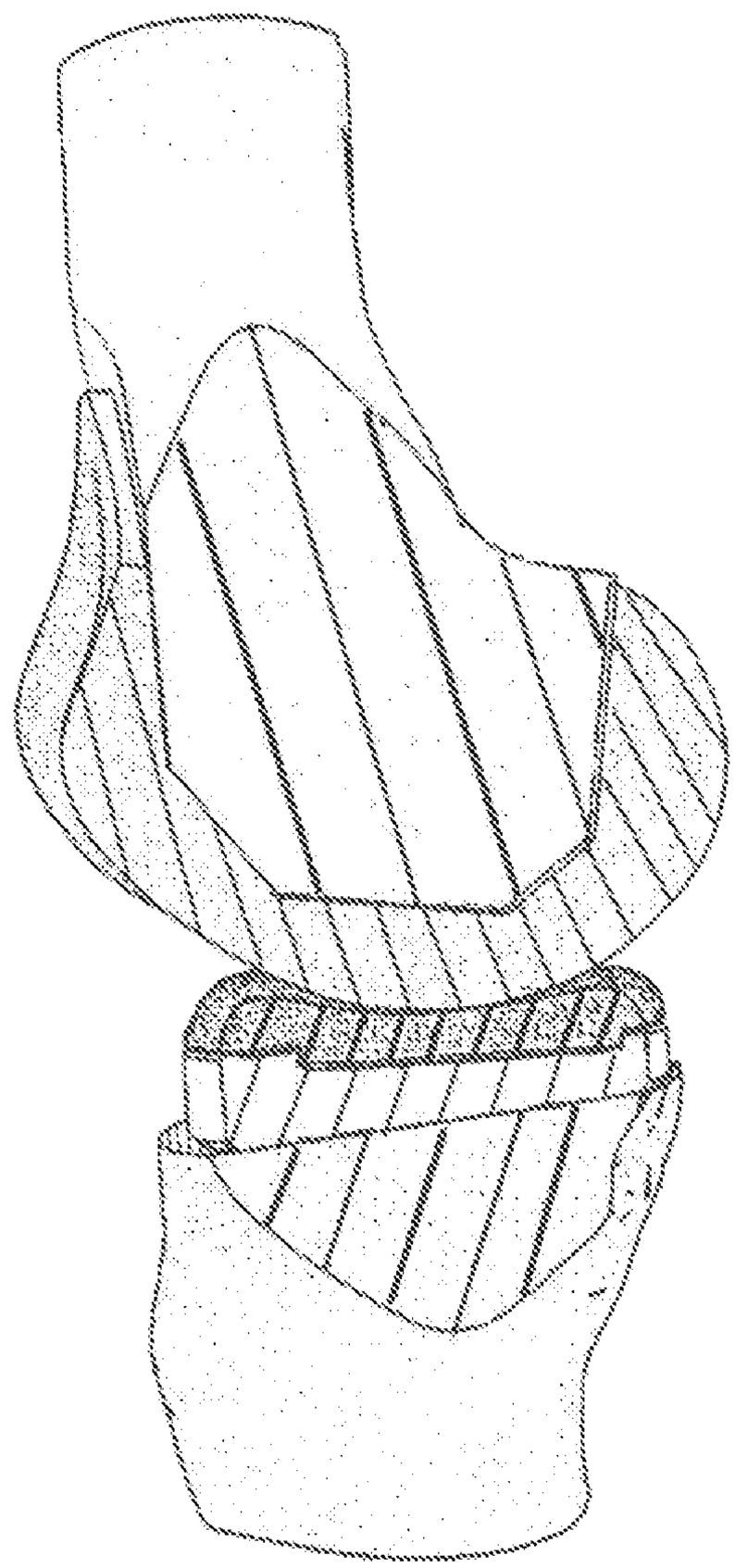

FIG. 53

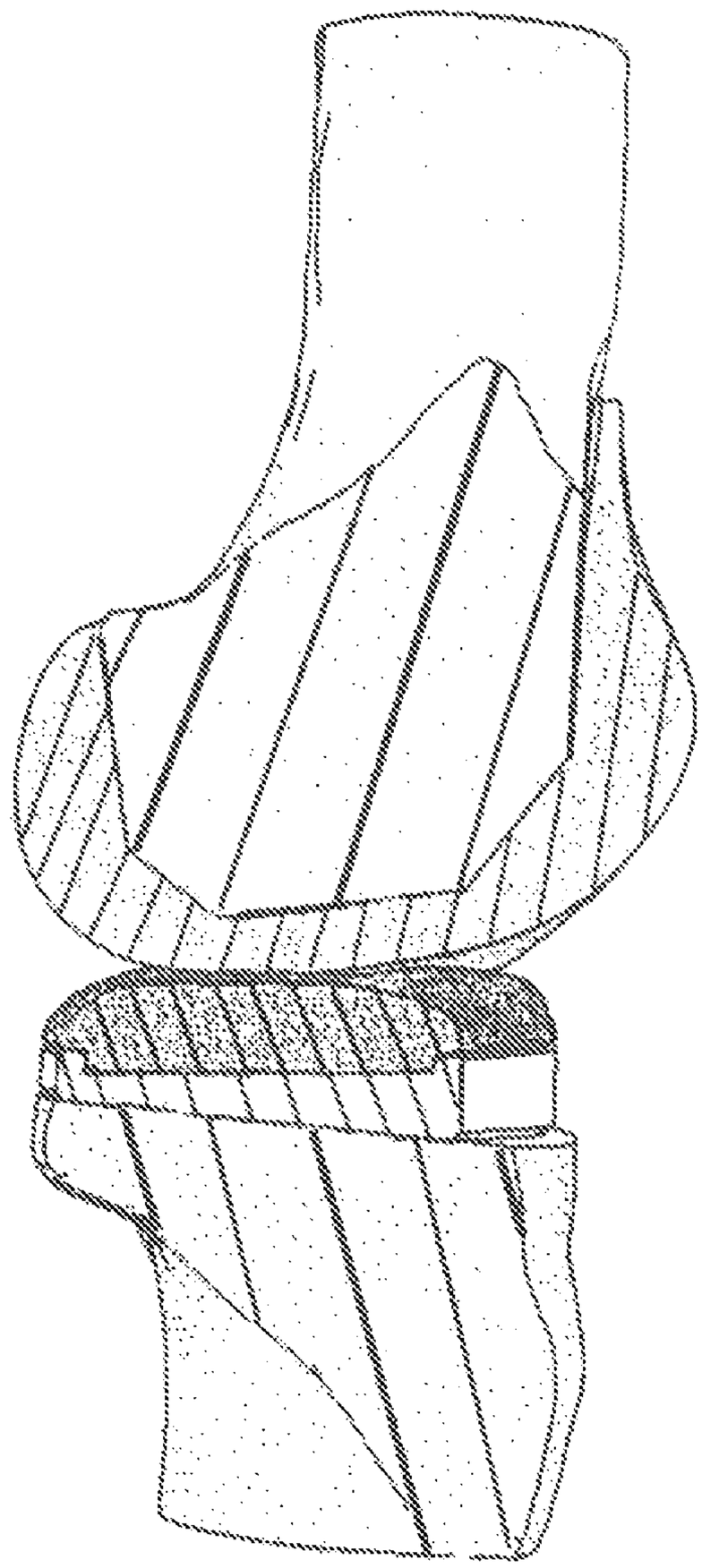

FIG. 54

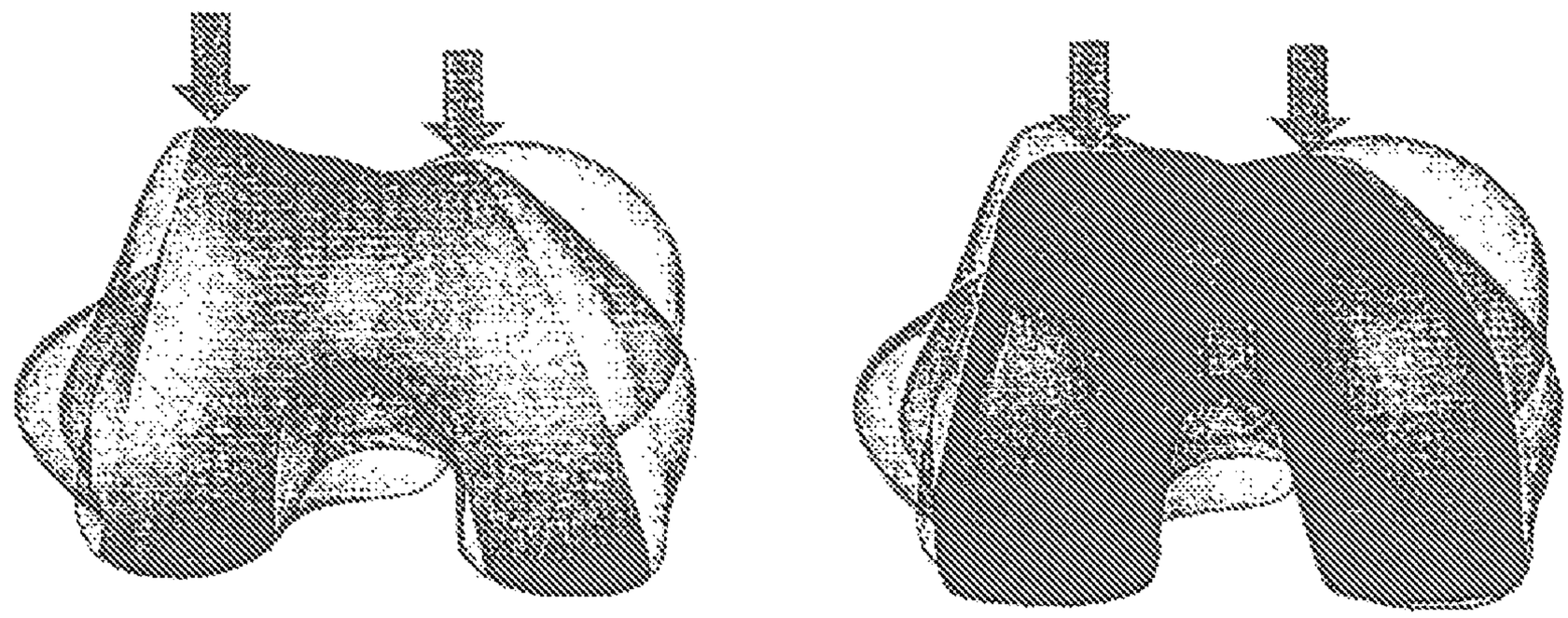

FIG. 55

FIG. 56

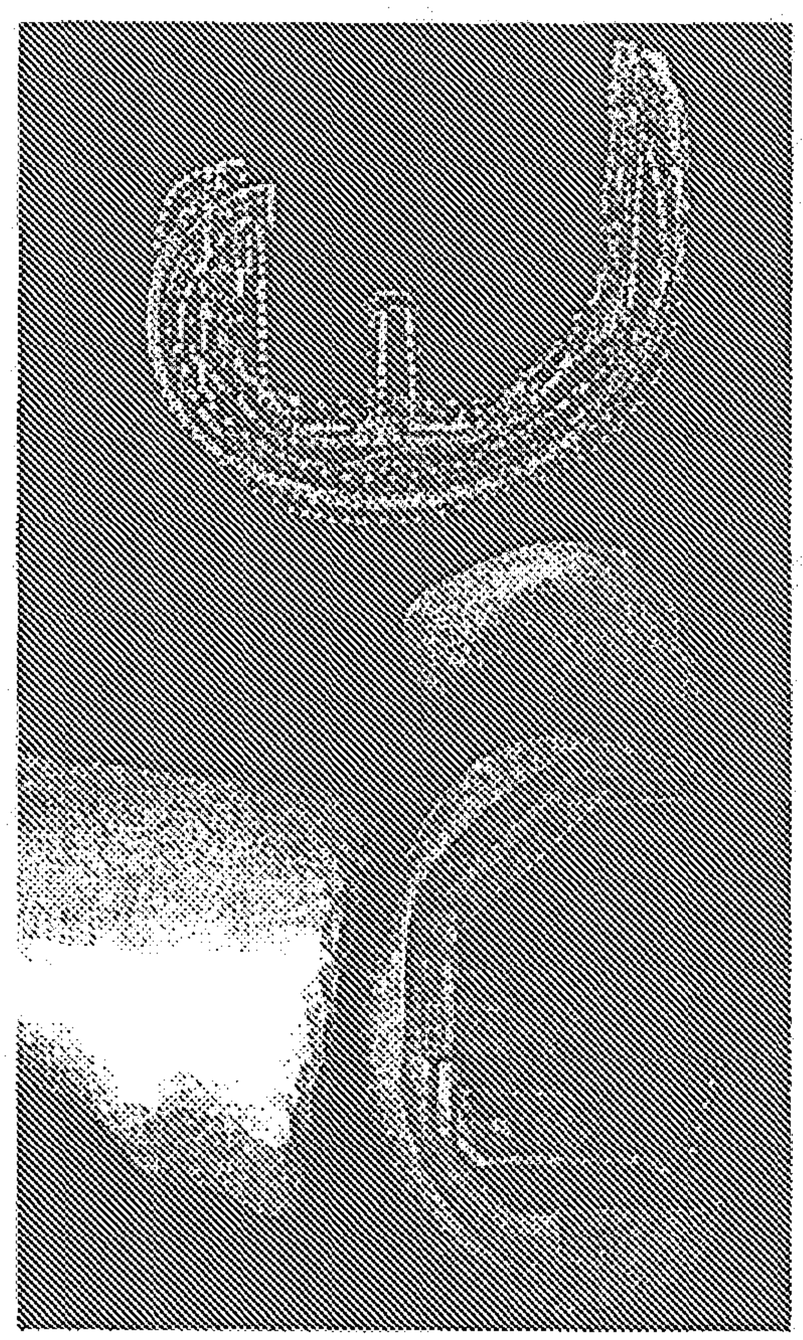

FIG. 57

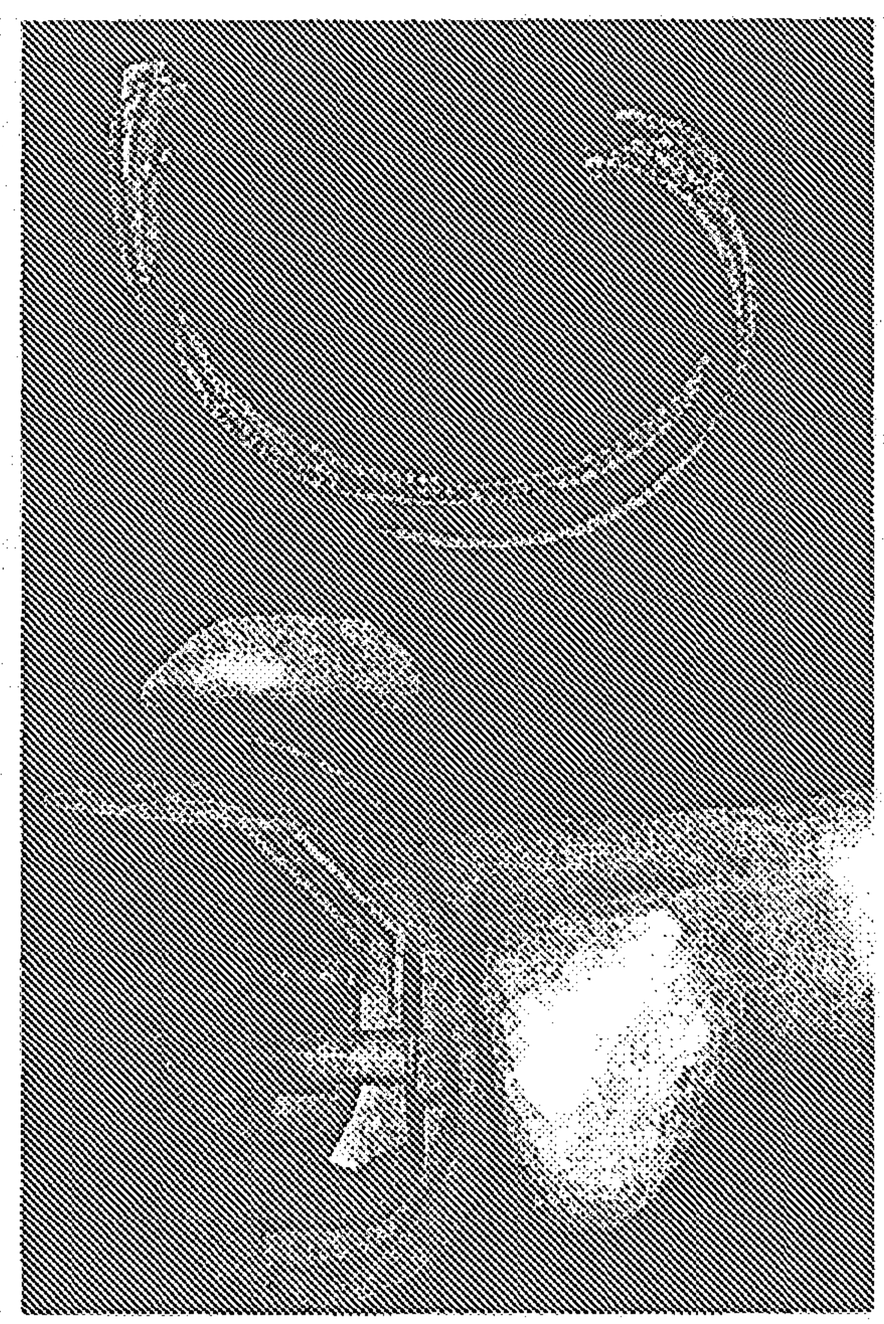

FIG. 58

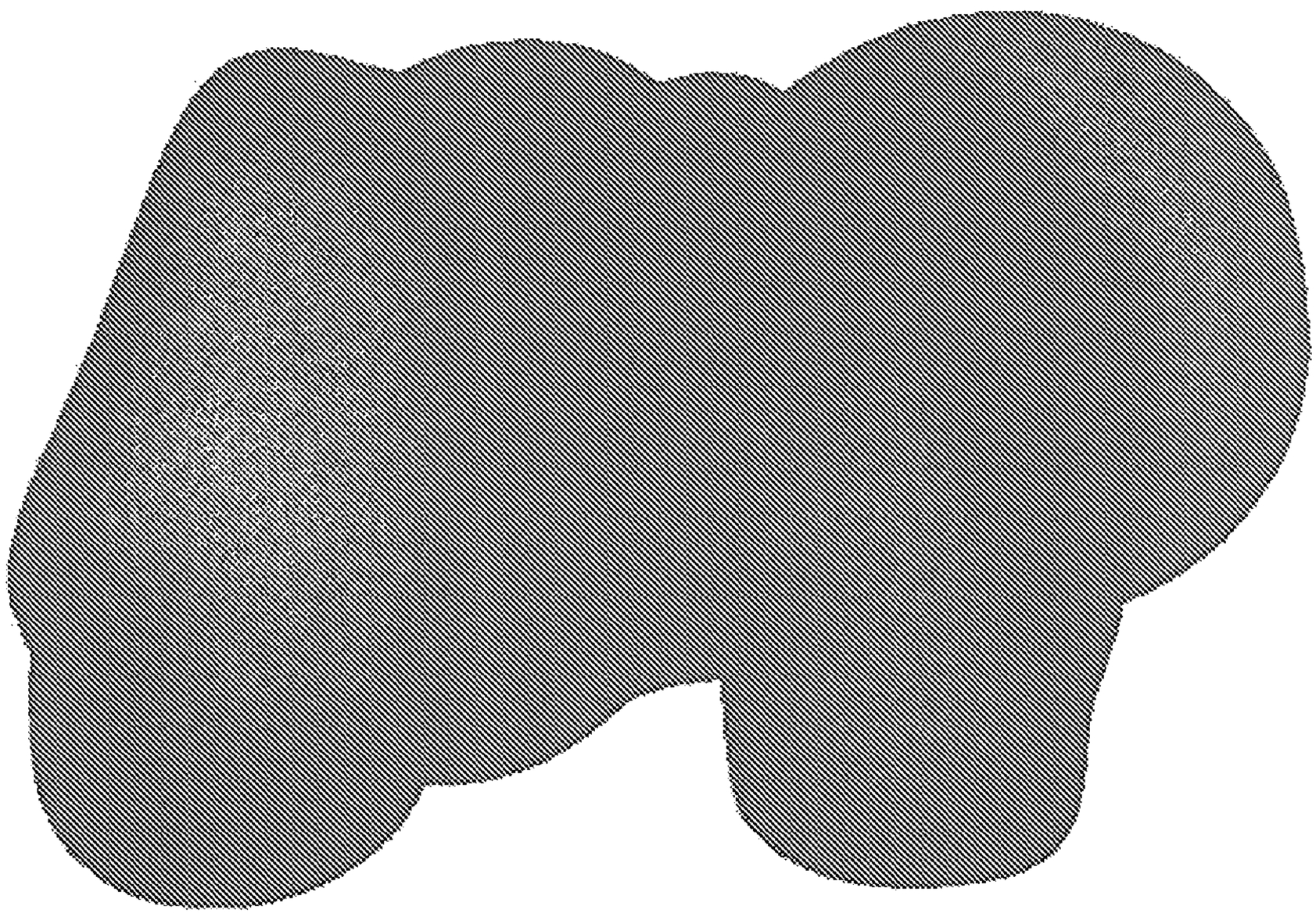

FIG. 59

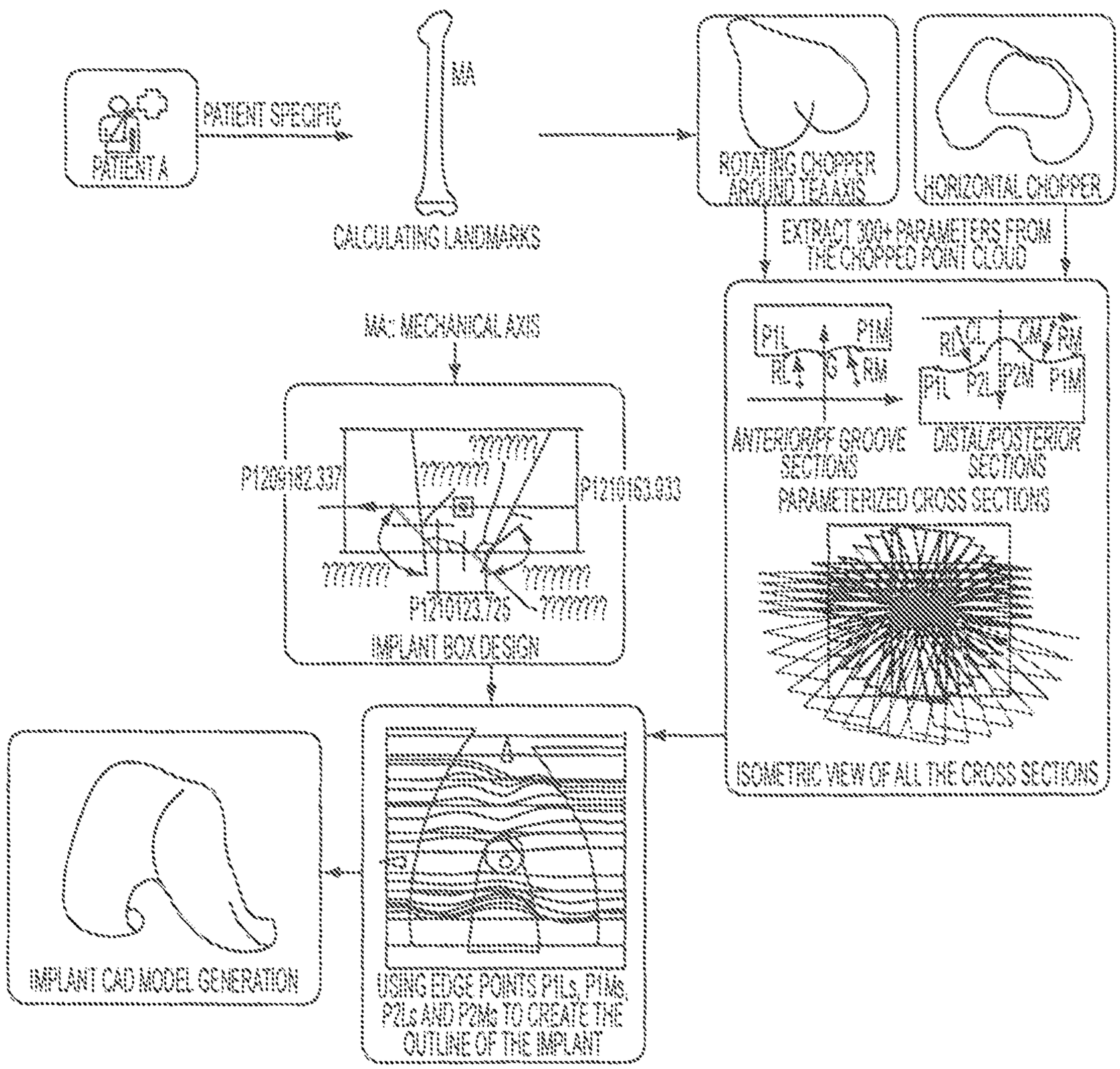
PATIENT A
PATIENT SPECIFIC
MA
CALCULATING LANDMARKS
ROTATING CHOPPER AROUND TEA AXIS
HORIZONTAL CHOPPER
EXTRACT 300+ PARAMETERS FROM THE CHOPPED POINT CLOUD
MA: MECHANICAL AXIS
P1209182.337
P1210163.933
P1210123.725
IMPLANT BOX DESIGN
P1L
P1M
RL
RM
ANTERIOR/F GROOVE SECTIONS
DISTAL/POSTERIOR SECTIONS
PARAMETERIZED CROSS SECTIONS
ISOMETRIC VIEW OF ALL THE CROSS SECTIONS
IMPLANT CAD MODEL GENERATION
USING EDGE POINTS P1Ls, P1Ms, P2Ls AND P2Ms TO CREATE THE OUTLINE OF THE IMPLANT

FIG. 60

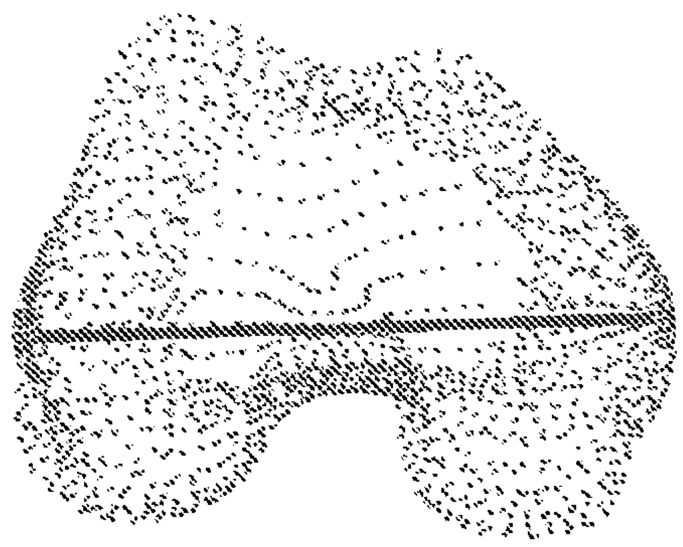

FIG. 61

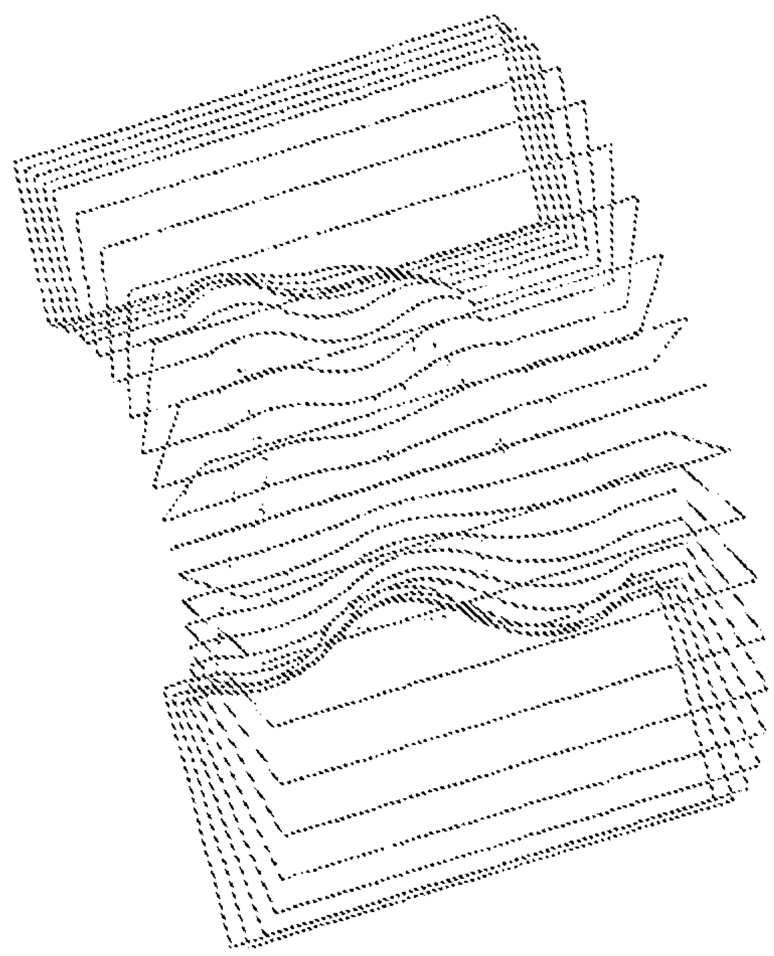

FIG. 62

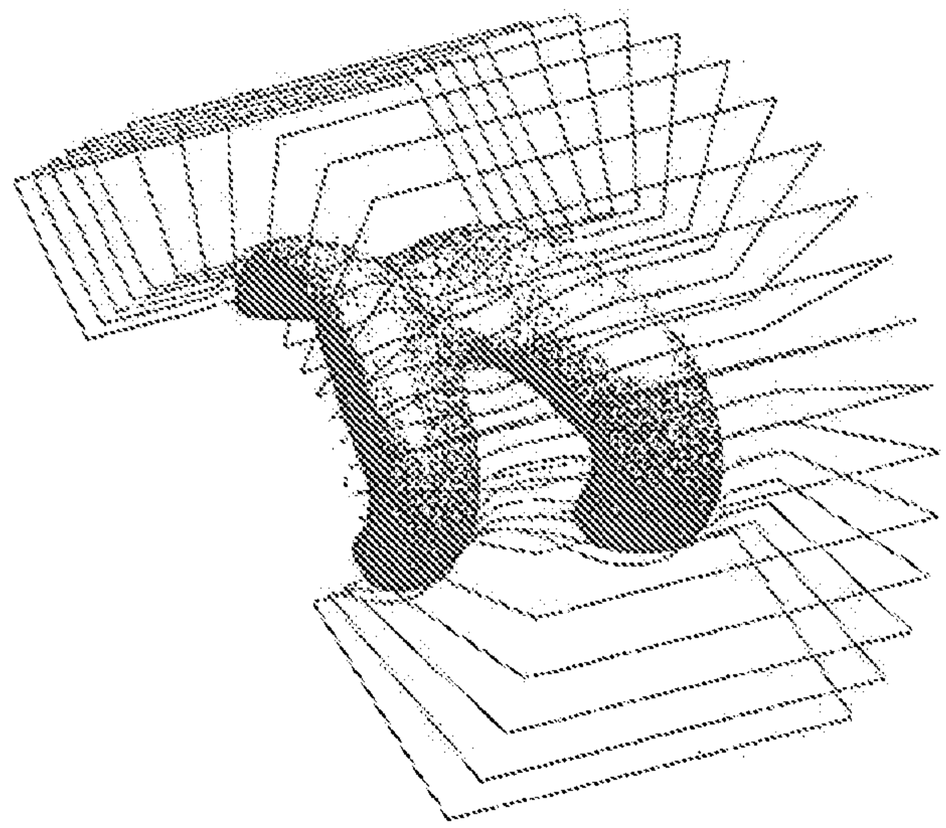

FIG. 63

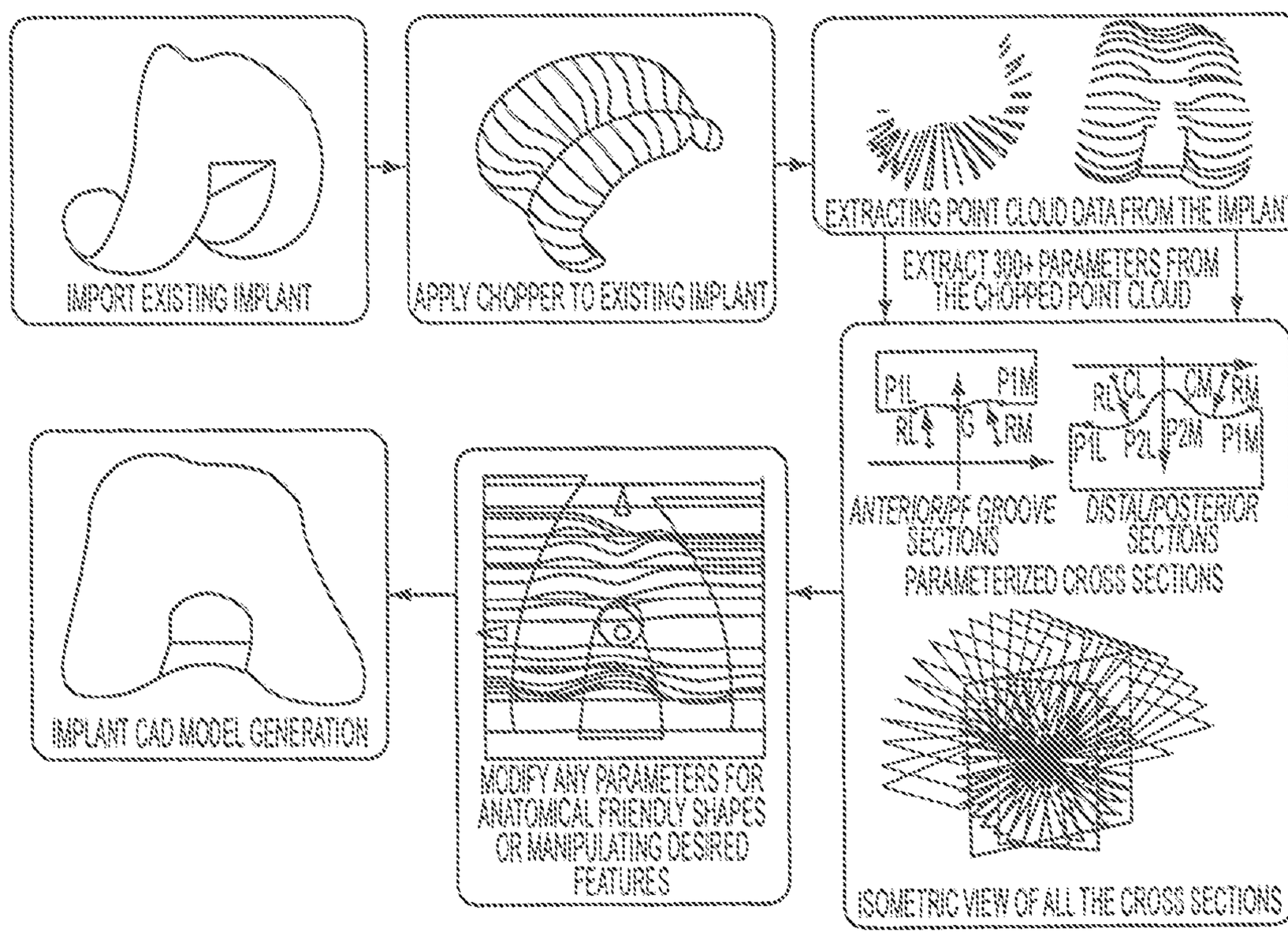
IMPORT EXISTING IMPLANT
APPLY CHOPPER TO EXISTING IMPLANT
EXTRACTING POINT CLOUD DATA FROM THE IMPLANT
EXTRACT 300+ PARAMETERS FROM THE CHOPPED POINT CLOUD
ANTERIOR/PF GROOVE SECTIONS
DISTAL/POSTERIOR SECTIONS
PARAMETERIZED CROSS SECTIONS
ISOMETRIC VIEW OF ALL THE CROSS SECTIONS
MODIFY ANY PARAMETERS FOR ANATOMICAL FRIENDLY SHAPES OR MANIPULATING DESIRED FEATURES
IMPLANT CAD MODEL GENERATION

FIG. 64

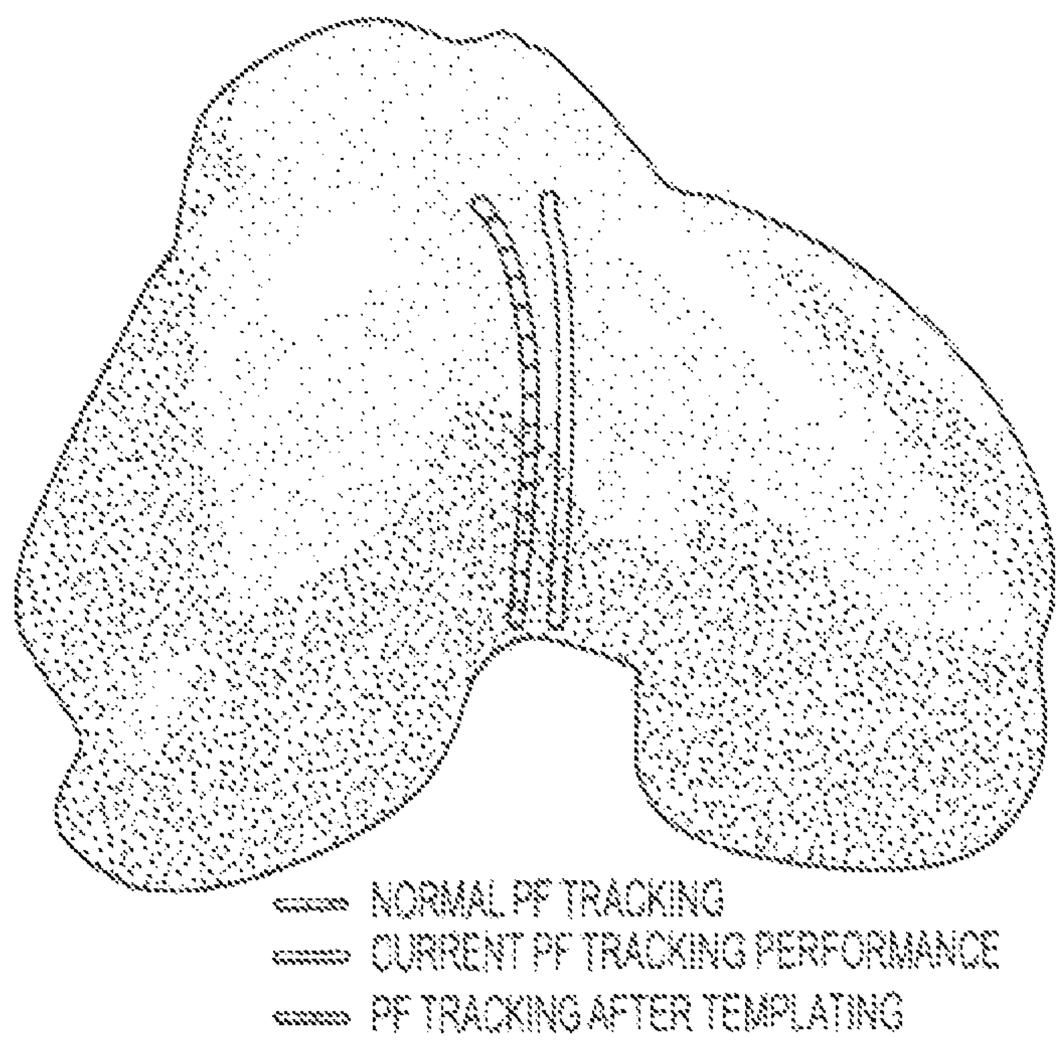
NORMAL PF TRACKING
CURRENT PF TRACKING PERFORMANCE
PF TRACKING AFTER TEMPLATING

FIG. 65

RX|ANTERIOR_GROOVE_THICKNESS=9
mm|bA|T7720
degrees|EcIK A|-04-90.8121524G772
degrees|EcIK |2-47.5157203217
degrees|EcIX |3-3.nA07561 2u4||
degrees|BOX |4-4U.5720257 0790
degrees|BOX |5-66.88v005y52224
mm|BOX_BOTTOM_ |21.7921617158
mm|BOX_BOTTOM_ P-23.3951453065
degrees|Box_CUI_CYSET_IMG=95|
mm|Box_TOF=40.5409325564
mm|D11.0|doc=20.3002
mm|CL110k=22.740
mm|C170OY=9.356
mm|CL120k=22.593
mm|CL120Y=10.E32
mm|CL130K=21.236
mm|CL130eY=18.210
mm|CL140OX=21.242
mm|CL140Y=20.53
mm|CL150Y=20.6.549
mm|CL150Y=21.591
mm|CL160Y=82.95308
mm|3170X=39.2436
mm|CH110k=74.597
mm|CH110k=3.813
mm|CM120k=22.371
mm|CM120k=5.503
mm|CH130X=15.311
mm|CH130Y=17.152
mm|CH140X=15.334
mm|CH140X=24.076
mm|CH150X=14.236
mm|CH150Y=26.768
bx|Odcox=15.07995
bx|Odcox=21.30343
mm|CK170X=17.50502
mm|CH170Y=26.55493
mm|CH170x=22.22124
mm|DIGITAL_CONDYLE_THICKNESS=12
mm|G110X=3.036
mm|G110Y=25.55
mm|G120X=2.065
mm|G120Y=25.519
mm|G130Y=2.3122
mm|G130Y=26.314
mm|G140X=2.202
mm|G140Y=30.413
mm|G150X=0.365
mm|G150Y=31.351
mm|G160X=0.22824
mm|G160Y=33.75265
mm|G170X=0.77320
mm|G170Y=35.279C1
mm|G180X=28.450
mm|G180Y=1.3
mm|G190Y=35.047
mm|GPeel=10.2107515592
mm|L5?R=11.8983721371
mm|L10R=16.85016
?7|L10kkR=13.9532579013
?7|L15kkR=1.5.0752120475
?7|L20R=36.17255
?7|L207?R=18.73800165?
?7|L30R=26.17143
?7|L40R=25.30243
?7|L50R=27.51294
?7|L60R=27.89532
mm|L70R=20.42643
?7|L80R=27.09035
?7|L90R=25.49022
?7|L100R=23.259
?7|L_?7=-{XL.3}
?7|edge_offset-2
mm|?7?23.40240 1207
mm|X10R=10.9037
mm|K15xR=20.3232035
mm|K15nxR=18.0D112332
mm|X20R=22.10722
mm|X207?R=18.8201946?
mm|X30R=22.D7517
mm|X40R=20.43797
mm|X50R=13.08763
mm|X60R=13.08763
mm|X70R=23.93811
mm|X80R=19.12239
mm|X90R=23.275
mm|M100R=28.8780173224?
mm|Medge_of?7?7=0.75
mm|ML=50
mm|MLshape_c=75
mm|X_?7?=3
mm|Xedge_offset-2
mm|P1L5ocX=25.513k
mm|P1L5ocY=41.013
mm|P1L10X=37.65339
mm|P1L10Y=22.9914
mm|P1L10ccX=23.8840477
mm|P1L10ccY=60.010553
mm|P1L15ccX=21.9398258
mm|P1L15ccY=21.0151523
mm|P1L20X=30.98102
mm|P1L20Y=24.42039
mm|P1L20exX=19.5442776
mm|P1L20exY=38.8525403 1053
mm|P1L30X=37.27778
mm|P1L30Y=38.8525403 1053
mm|P1L45X=38.8525403 1053
mm|P1L45Y=26.53279
mm|P1L50X=39.70393
mm|P1L50Y=26.83477
mm|P1L55X=39.78193
mm|P1L55Y=26.83477
mm|P1L70X=5V.31065
mm|P1L70Y=26.73074
mm|P1L80X=38.03985
mm|P1L80Y=26.8255
mm|P1L90X=32.79349
mm|P1L90Y=32.54121
mm|P1L100X=14.036
mm|P1L100Y=27.467
mm|P1L110X=34.085
mm|P1L110Y=28.275
mm|P1L120X=31.402
mm|P1L120Y=29.323
mm|P1L130X=30.115
mm|P1L130Y=31.491
mm|P1L140X=20.306
mm|P1L140Y=34.495
mm|P1L150X=28.075
mm|P1L150Y=37.183
mm|P1L160X=27.66182
mm|P1L160Y=39.96533
mm|P1L170X=27.24436
mm|P1L170Y=41.2602
mm|P1L180X=26.561
mm|P1L180Y=41.107
mm|P1L190X=20.4392440
mm|P1L190Y=20.825054963
mm|P1M10X=20.825054963
mm|P1M10Y=29.44504
mm|P1M10mX=19.0270662
mm|P1M10mY=31.627901
mm|P1M15xcX=18.04636962
mm|P1M15xcY=33737.8585
mm|P1M20X=34.66631
mm|P1M20Y=31.31968
mm|P1M20ceX=15.9363313
mm|P1M20ccY=10.964716
mm|P1M30X=34.8475537907
mm|P1M30Y=31.08687
mm|P1M40X=34.9552
mm|P1M40Y=32.49021
mm|P1M50X=36.12653
mm|P1M50Y=32.45436
mm|P1M60X=36.03524
mm|P1M60Y=32.39352
mm|P1M70X=34.1022712637?
mm|P1M70Y=32.1091
mm|P1M80X=34.0720
mm|P1M80Y=31.673
mm|P1M90X=36.5438
mm|P1M90Y=37.24329
mm|P1M100X=28.467
mm|P1M100Y=33.590
mm|P1M110X=28.661
mm|P1M110Y=33.402
mm|P1M120X=26.309
mm|P1M120Y=34.524
mm|P1M130X=24.576
mm|P1M130Y=34.579
mm|P1M140X=22.515
mm|P1M140Y=34.031
mm|P1M150X=21.576
mm|P1M150Y=34.353
mm|P1M160X=21.5035706500
mm|P1M160Y=32.5902657706
mm|P1M170X=27.33708
mm|P1M170Y=32.49441
mm|P1M180X=21.223
mm|P1M180Y=32.0339127319031
mm|P2L10X=15.031770823
mm|P2L10Y=22.3303494212
mm|P2L20Y=23.37838
mm|P2L30X=14.8076
mm|P2L30Y=23.3442514524
mm|P2L40X=14.02131
mm|P2L40Y=23.54878
mm|P2L50X=12.35306
mm|P2L50Y=23.00579
mm|P2L60X=18.09712
mm|P2L60Y=28.0627274011
mm|P2L70X=11.61419
mm|P2L70Y=22.81539
mm|P2L80X=23.0797040247
mm|P2L80Y=13.345042034
mm|P2L90X=8.94325
mm|P2L90Y=27.12024
mm|P2L100X=0.0234370214
mm|P2L100Y=23.0410265785
mm|P2M10X=10.55992
mm|P2M10X=24.34573
mm|P2M20X=10.64707
mm|P2M20X=26.7759163155

FIG. 66A

bmP2X30X=10.28670
bmP2X30Y=27.4173
bmP2X40X=10.31570
bmP2X40Y=27.98222
bmP2X50X=10.19352
bmP2X50Y=26.91203
bmP2X60X=10.22407
bmP2X60Y=26.91238
bmP2X70X=10.06613
bmP2X70Y=25.96405
bmP2X80Y=26.33407577
bmP2X90X=10.84039
bmP2X90Y=22.56546
bmP2X100X=3.042
bmP2X100Y=23.535
bmPPS_Pd=45
bmPOSTERIOR_CONDYLE_THICKNESS=3
bmSHEEP_CUT_DEPTH=30
bmTEA_AP=0
bmTEA_ST=0
bmTop_cut_height1=20
bmTop_cut_height2=60
bmTop_cut_width=70
bmV_Thick=9
bmback_clearance=32.0247144
bmc=0SCC/2
bmcondyle_offset=0.5
bmcondylesur_c=15
bmfont_clearance=23.611450
bmfrontal_shape_R=12.5
bmfrontalsur_c=1.5
bmpZ=120
bmpZX30X=10.05080
bmpZ=p2/2
p0=X_HT
p11=0_HT
bmp465=SHEEP_CUT_DEPTH
bmp466=SHEEP_CUT_DEPTH
bmp467=SHEEP_CUT_DEPTH
bmp471=PPS_Mid
bmp474=PPS_Mid
bmp475=PPS_Mid
bmp476=PPS_Mid
bmp477=PPS_Mid
bmp486=SHEEP_CUT_DEPTH
bmp490=PPS_Mid
bmp491=PPS_Mid
bmp502=SHEEP_CUT_DEPTH
bmp503=PPS_Pd
bmp504=PPS_Mid
bmp515=SHEEP_CUT_DEPTH
bmp516=PPS_Mid
bmp517=PPS_Mid
bmp528=SHEEP_CUT_DEPTH
bmp529=PPS_Mid
bmp530=PPS_Mid
bmp541=SHEEP_CUT_DEPTH
bmp542=PPS_Mid
bmp543=PPS_Mid
bmp554=SHEEP_CUT_DEPTH
bmp555=PPS_Mid
bmp556=PPS_Mid
bmp663=SHEEP_CUT_DEPTH
bmp667=SHEEP_CUT_DEPTH
bmp668=SHEEP_CUT_DEPTH
bmp669=SHEEP_CUT_DEPTH
bmp671=SHEEP_CUT_DEPTH
bmp674=PPS_Mid - 4
bmp674=(PPS_Mid-4)
bmp679=0
bmp680=50
p773=30.996
p774=619.4235378904
bmp850=SHEEP_CUT_DEPTH
bmp851=SHEEP_CUT_DEPTH
bmp852=SHEEP_CUT_DEPTH
bmp853=SHEEP_CUT_DEPTH
bmp854=PPS_Mid
bmp855=PPS_Mid
bmp864=PPS_Mid
bmp865=PPS_Mid
bmp867=14.87555
bmp900=PPS_Mid
bmp908=PPS_Mid
bmp909=PPS_Mid
bmp910=PPS_Mid
bmp921=PPS_Mid
bmp922=PPS_Mid
bmp926=PPS_Mid
bmp928=PPS_Mid
bmp931=PPS_Mid
bmp932=PPS_Mid
bmp933=PPS_Mid
bmp934=PPS_Mid
bmp939=PPS_Mid
bmp959=Top_cut_width*2
bmp960=ML shape_c
bmp969=ML shape_c
bmp1008=PPS_Mid
bmp1030=20.42202654963
bmp1031=17.89239418991
bmp1033=25.79509273746
bmp1038=27.55403532396
bmp1039=17.32085728682
bmp1040=ML shape_c
bmp1045=condyle_offset
bmp1060=PPS_Mid
bmp1065=PPS_Pd
bmp1066=SHEEP_CUT_DEPTH
bmp1073=PPS_Mid
bmp1074=PPS_Pd
bmp1075=SHEEP_CUT_DEPTH
bmp1084=PPS_Pd
bmp1085=PPS_Pd
bmp1086=SHEEP_CUT_DEPTH
bmp1091=PPS_Pd
bmp1092=PPS_Pd
bmp1093=SHEEP_CUT_DEPTH
bmp1094=0
bmp1100=FPS_Mid
bmp1101=FPS_Mid
bmp1109=5.845551609
p1110=0
p1112=0
bmp1114=15.50930975
bmp1115=FPS_Mid
bmp1116=FPS_Mid
bmp1118=10
p1152=0
p1154=0
p1156=0
bmp1160=41.61068494
bmp1162=68.96887890
bmp1163=0
bmp1164=25
bmp1169=12.5
bmp1181=6.5
bmp1184=6
bmp1192=5
bmp1194=7.5
bmp1198=16.8
bmp1200=16.5
bmp1202=0.5
bmp1212=FPS_Pd
bmp1213=FPS_Pd
bmp1214=condylesur_c
bmp1216=1.2521472285

FIG. 66B

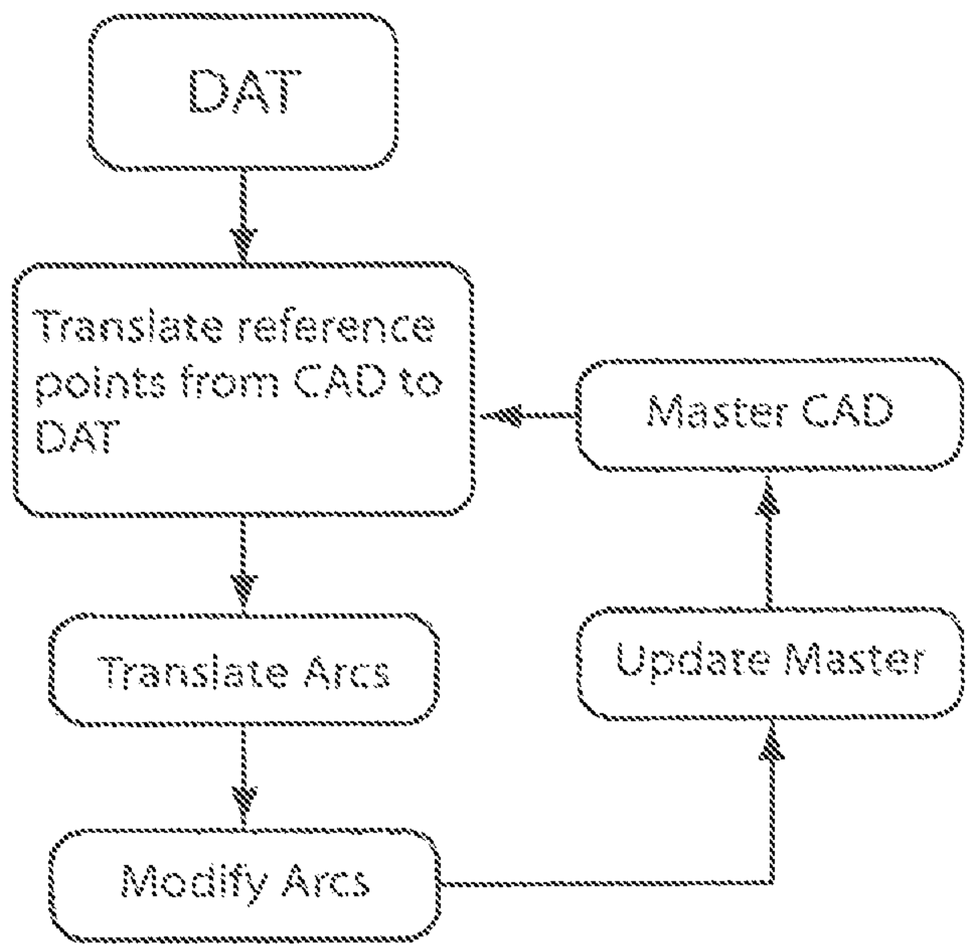
DAT
Translate reference points from CAD to DAT
Master CAD
Translate Arcs
Update Master
Modify Arcs

FIG. 67

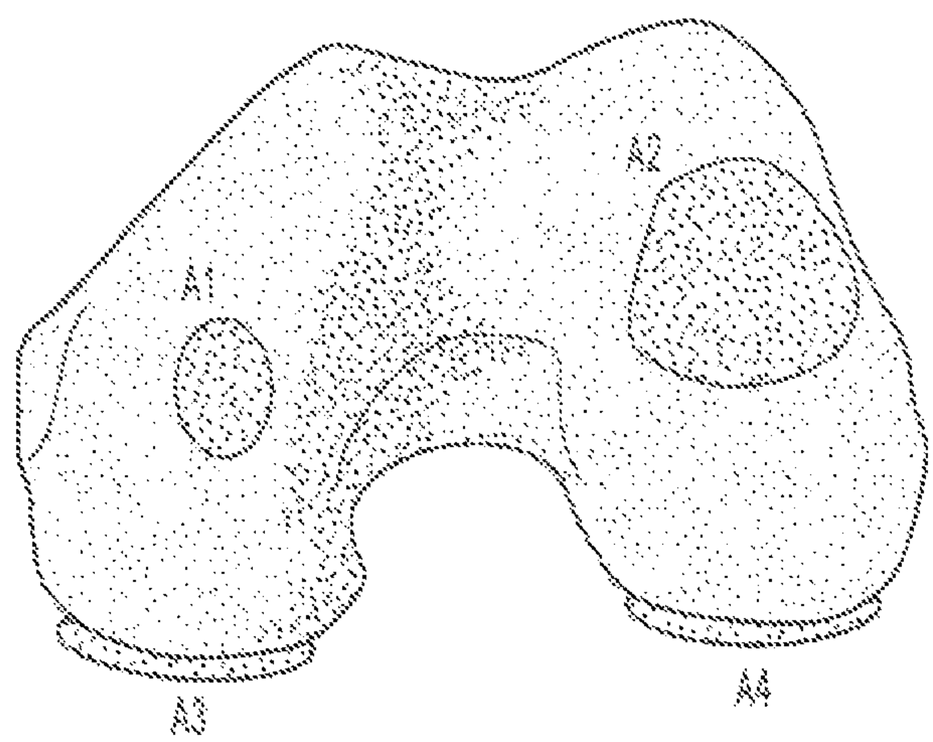
A1
A2
A3
A4

FIG. 68

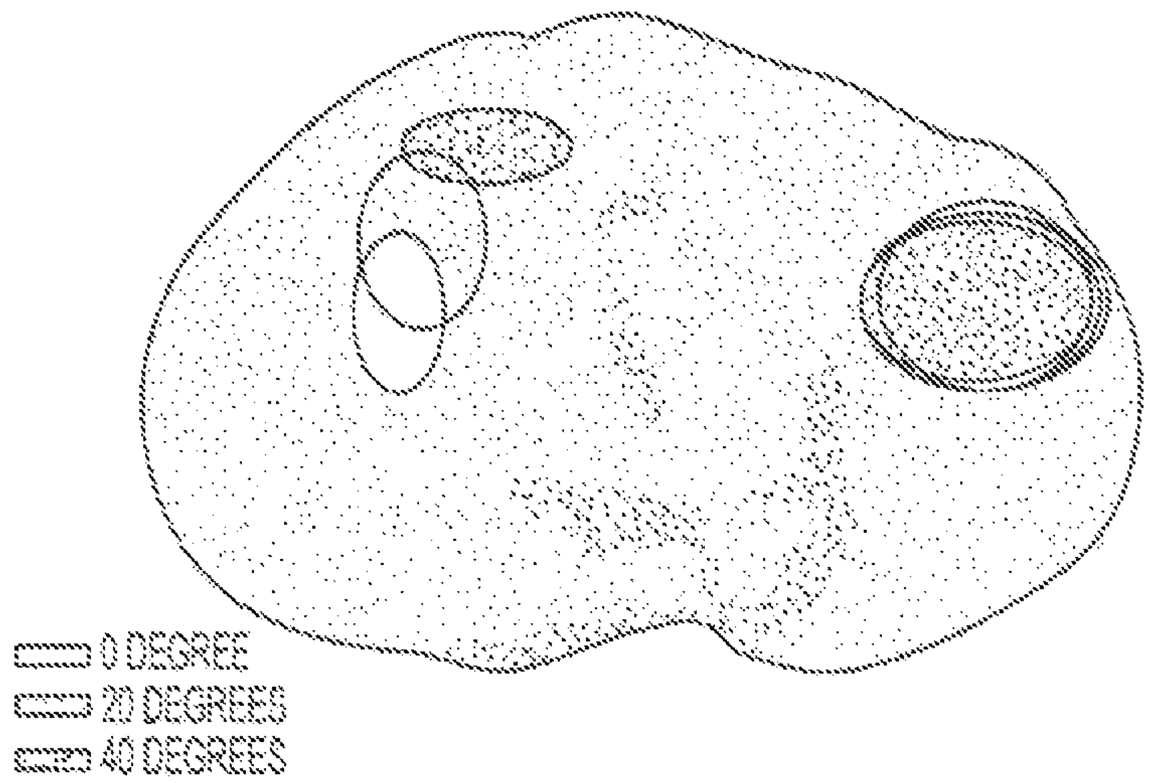
0 DEGREE
20 DEGREES
40 DEGREES

FIG. 69

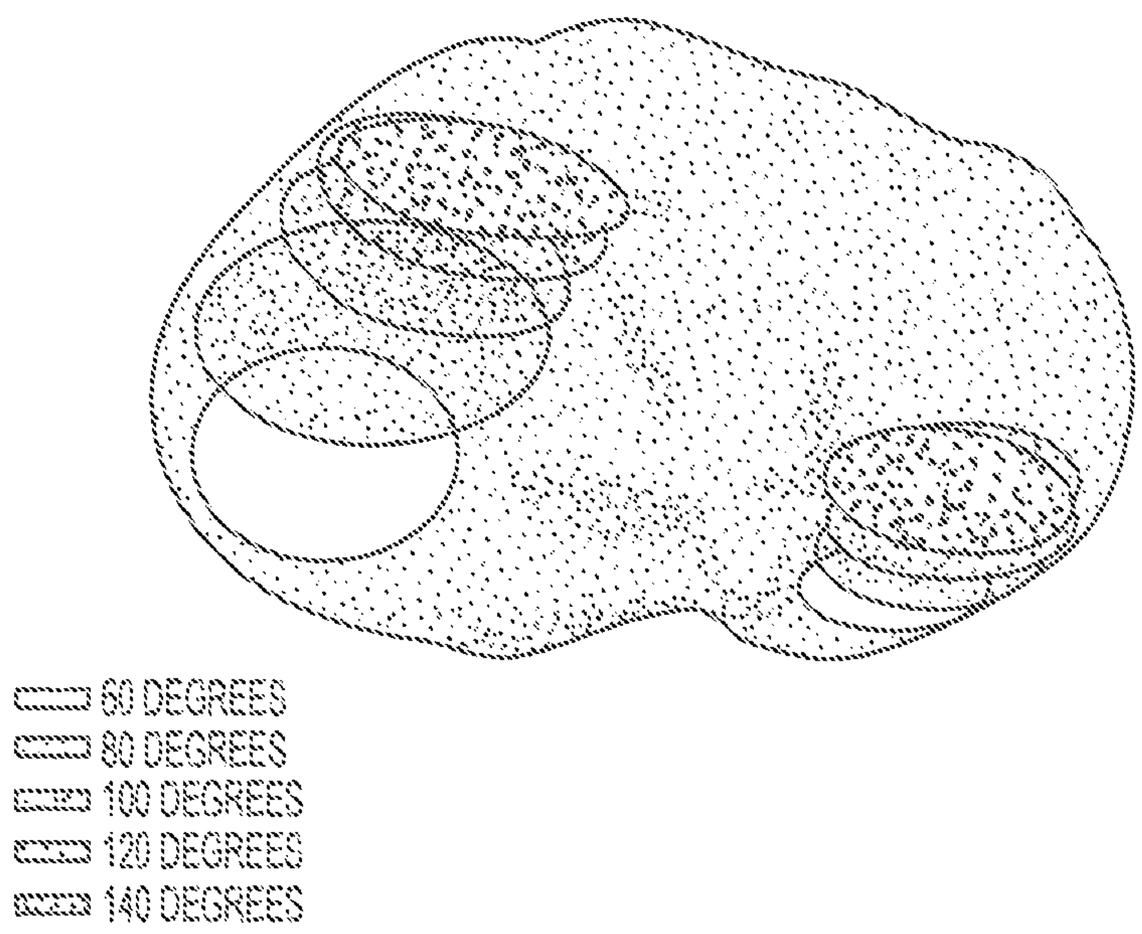
60 DEGREES
80 DEGREES
100 DEGREES
120 DEGREES
140 DEGREES

FIG. 70

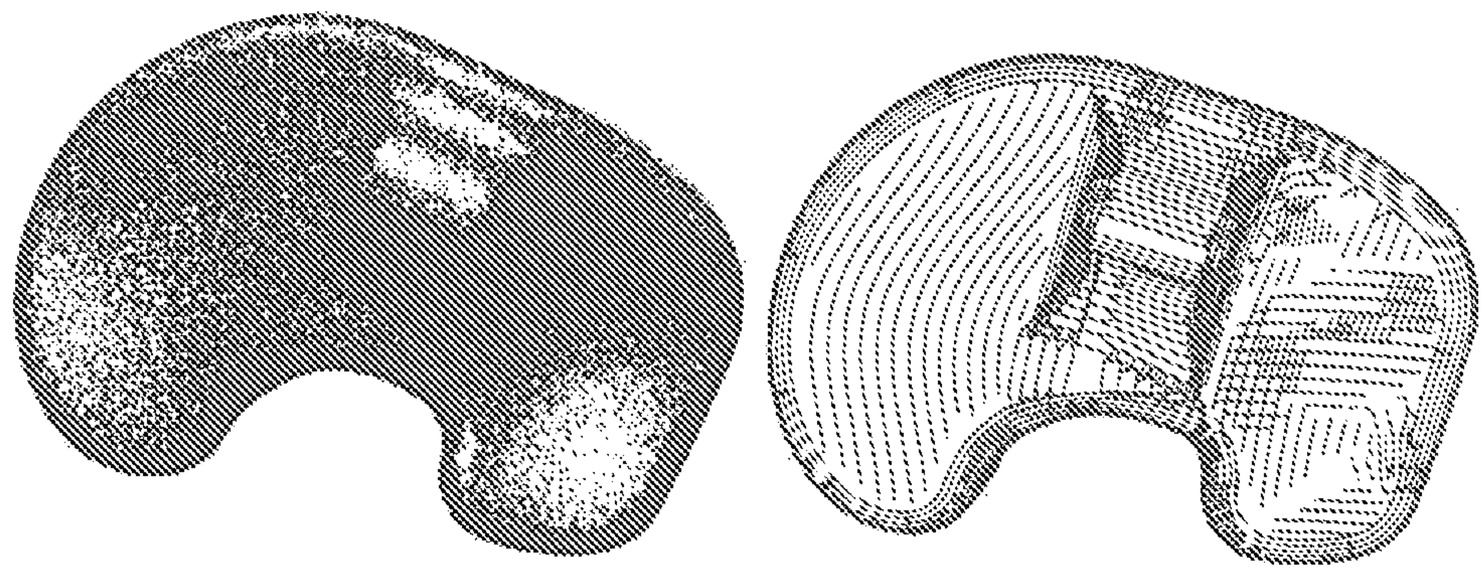

FIG. 71

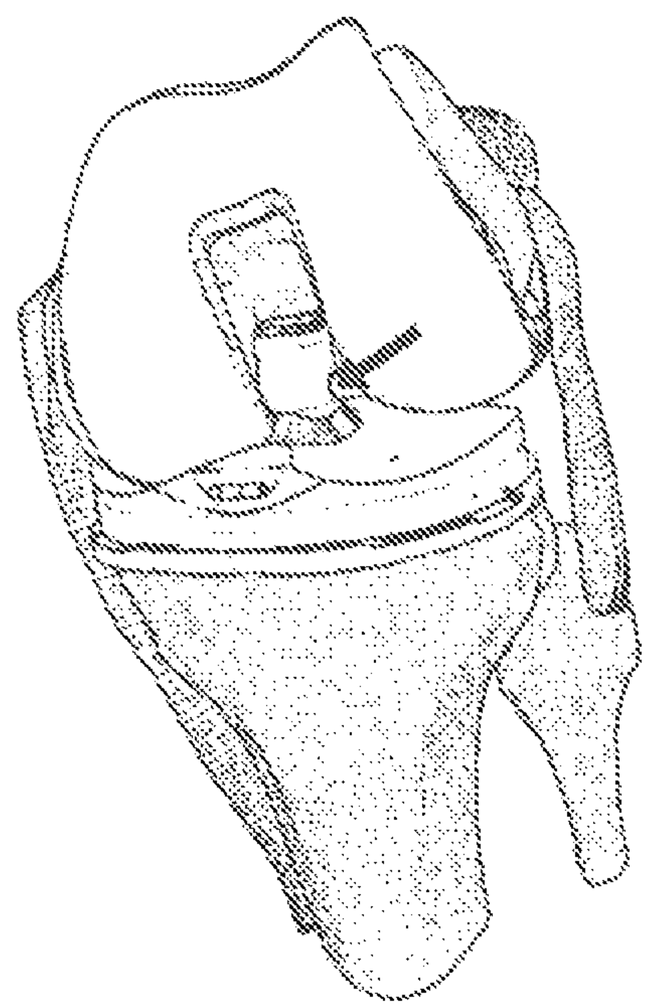

FIG. 72

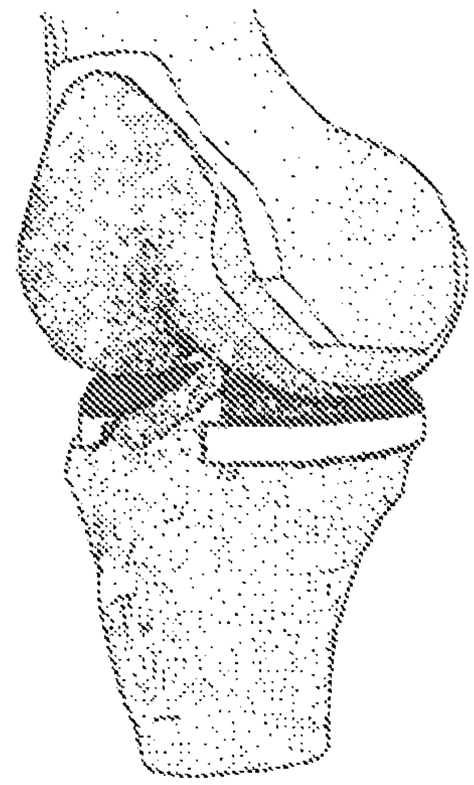

FIG. 73

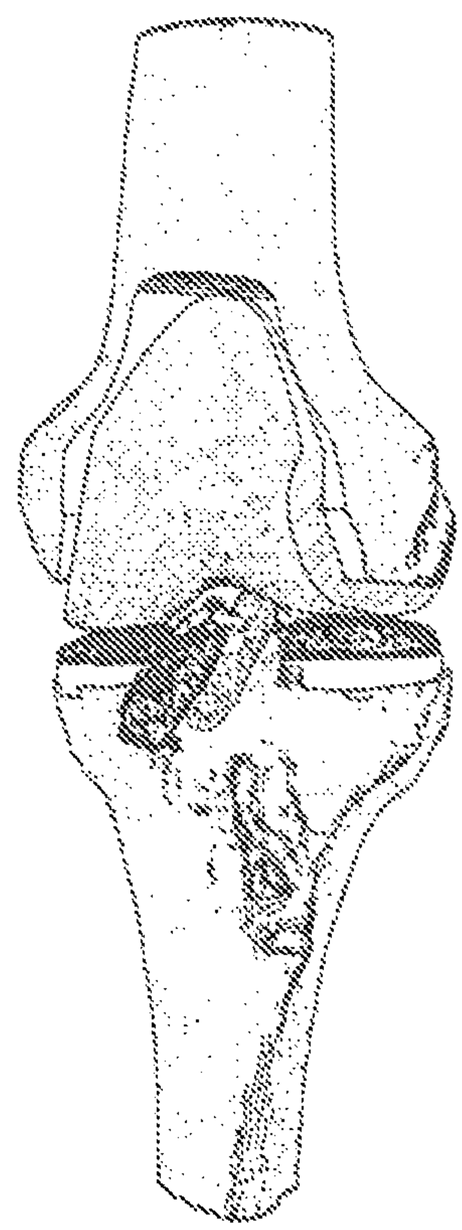

FIG. 74

		TEA	BML	APH	SMP	LAP	PA	GN	APA	AML	PML	DML	CTA
White	mean	5.71	7.61	5.13	5.59	6.59	98.42	0.78	6.10	3.83	5.40	5.54	6.07
	std	0.49	0.70	0.44	0.42	0.63	3.58	0.22	2.70	0.08	0.46	0.45	1.68
Black	mean	5.48	7.58	6.07	5.71	7.04	97.76	0.83	5.35	5.58	5.90	5.56	6.56
	std	0.47	0.77	0.35	0.29	0.86	3.36	0.19	4.19	0.52	0.52	0.51	1.78
Asian	mean	7.59	5.25	5.20	5.92	6.00	95.17	0.76	3.47	3.38	4.68	4.38	7.12
	std	0.40	1.08	0.47	0.33	0.85	9.59	0.47	2.53	0.47	0.65	0.65	2.65
White Vs Black	t-test	0.01	0.79	0.40	0.81	0.05	0.28	0.78	0.01	0.47	0.72	0.80	0.66
	Power test	355	13275	1105	13168	171	709	487	61	3175	637	14481	3577
White Vs Asian	t-test	0.01	0.01	0.01	0.01	0.01	0.01	0.64	0.01	0.01	0.01	0.01	0.07
	Power Test	4	7	9	7	5	107	1146	29	76	7	4	321
Black Vs Asian	t-test	0.01	0.01	0.01	0.01	0.01	0.11	0.43	0.01	0.01	0.01	0.01	0.75
	Power Test	7	8	9	5	5	164	704	13	72	30	5	896

TABLE 1

FIG. 75

		ML	AP	CW	TTA	LPH	LPW	MPH	MPW
White	Mean	7.81	5.73	1.32	82.96	4.85	3.26	5.13	3.08
	std	0.37	0.32	0.58	34.05	0.28	0.37	0.33	0.27
Black	Mean	7.88	5.73	1.44	79.29	5.03	3.22	5.15	3.14
	std	0.4	0.34	0.79	35.85	0.30	0.38	0.43	0.32
	t-test	0.41	0.96	0.4	0.63	0.05	0.64	0.75	0.34
	Power test	750	266814	758	2223	127	2425	5387	592

TABLE 2

FIG. 76

Flexion Angle	Length %
0	24.65
20	17.90
40	10.35
60	17.32
80	28.15
100	39.38
120	49.60
140	47.33

TABLE 3

FIG. 77

DEFORMABLE ARTICULATING TEMPLATES

CROSS REFERENCE TO RELATED APPLICATIONS

The present application is a divisional of U.S. patent application Ser. No. 13/203,012 filed Feb. 25, 2010, which is a national phase entry application of International PCT Patent Application No. PCT/US2010/25466 filed Aug. 24, 2011, which claims the benefit of U.S. Provisional Patent Application Ser. No. 61/208,509 filed Feb. 25, 2009 and U.S. Provisional Patent Application Ser. No. 61/222,560, filed Jul. 2, 2009, the disclosure of each of which is hereby incorporated herein by reference.

TECHNICAL

The present disclosure relates to orthopedic implants and, more specifically, to methods and devices utilized to design orthopedic implants and orthopedic jigs for use with joint replacement and revision procedures.

INTRODUCTION TO THE INVENTION

Of primary interest to the knee prosthetics industry is the analysis of the intrinsic shape differences of the knee joint between different ethnic populations for development of implantable orthopedic devices. The study presented is thus three-fold: by developing a novel automatic feature detection algorithm, a set of automated measurements can be defined based on highly morphometric variant regions, which then allows for a statistical framework when analyzing different populations' knee joint differences.

Ethnic differences in lower limb morphology focuses on the differences between Asian and Western populations because this variation is of great import in implant design. For example, Chinese femora are more anteriorly bowed and externally rotated with smaller intermedullary canals and smaller distal condyles than Caucasian femora. Likewise, Caucasian femora are larger than Japanese femora in terms of length and distal condyle dimensions. Ethnic differences in proximal femur bone mineral density (BMD) and hip axis length also exists between American Blacks and Whites. The combined effects of higher BMD, shorter hip axis length, and shorter intertrochanteric width may explain the lower prevalence of osteoporotic fractures in Black women compared to their White counterparts. Similarly, elderly Asian and Black men have been found to have thicker cortices and higher BMD than White and Hispanic men, which may contribute to greater bone strength in these ethnic groups. In general, Blacks have thicker bone cortices, narrower endosteal diameters, and greater BMD than Whites. Interestingly, though, these traits are most pronounced in African Blacks compared to American Blacks.

The following analysis considers metric and geometric morphometric variation in the lower limb of modern American Blacks, Whites and East Asians. Three-dimensional statistical bone atlases are used in order to facilitate rapid and accurate data collection in the form of automated measurements, as well as measurements used in biomedical studies and some newly-devised measurements. The shape analysis is conducted with a statistical treatment combining Principal Components Analysis (PCA) and Multiple Discriminant Analysis; metric analysis is performed using t-tests, power tests, and linear discriminant analysis in the Implant Design and Analysis Suite (see co-pending U.S. patent application Ser. No. 12/673,640, entitled, IMPLANT DESIGN ANALYSIS SUITE, the disclosure of which is incorporated herein by reference) system. The results of these analyses add to the existing knowledge of morphological variation in the knee joint and provide useful information that can be extracted for knee prosthesis design as will be outlined in the remainder of this disclosure.

The innovativeness of the instant approach derives, in part, from the use of Computed Tomography (CT) scans for data collection combined with the computational power and precision offered by statistical bone atlases. An exemplary data set that comprises 943 male and female individuals (81.5% American White, 9% American Black and 9.5% East Asians, where the overall male/female ratio 65/35%) was scanned using CT scans. Only normal femora and tibia were included in this study; femora or tibia with severe osteophytes and other abnormalities were specifically excluded. Only one femur and tibia was chosen from each individual, with no preference taken to either right or left side.

The bones were CT scanned using 0.625 mm×0.625 mm×0.625 mm cubic voxels. The result is high resolution, three dimensional radiographs in the form of DICOM image slices. This stacked image data was then segmented and surface models were generated. This process has been found to be reliable with negligible inter- and intra-observer error. These models were then added to the ethnicity-specific statistical bone atlases.

Briefly, a bone atlas is an average mold, or template mesh, that captures the primary shape variation of a bone and allows for the comparison of global shape differences between groups or populations. Bone atlases were developed initially for automatic medical image segmentation; however, it can be used as a way to digitally recreate a bone and conduct statistical shape analyses. In addition, bone atlases have proven useful in biological anthropology as a means of studying sexual dimorphism and for reconstructing hominid fossils and making shape comparisons among fossil species.

For the ethnicity difference analysis, a previously developed technique for creating a statistical representation of bone shape was employed in a novel manner. Three separate statistical atlases of femora were compiled with one atlas containing only American White femora, one atlas containing only American Black femora, and one atlas containing only East Asian femora. Likewise, three separate atlases were created for the tibia and divided in the same manner (i.e., American White, Black tibiae and East Asians). The processes of creating these statistical atlases and adding bones to the atlases are outlined hereafter.

First, all of the bone models in the dataset were compared, and a bone model with average shape characteristics was selected to act as a template mesh. The points in the template mesh were then matched to corresponding points in all of the other training models. This ensures that all of the bones have the same number of vertices and the same triangular connectivity. Next, a series of registration and warping techniques was used to select corresponding points on all the other bone models in the training set. This process of picking point correspondences on new models to be added to the atlas is 'non-trivial'. The matching algorithm described hereafter uses several well-known techniques of computer vision, as well as a novel contribution for final surface alignment.

During the first step in the matching algorithm, the centroids of the template mesh and the new mesh were aligned, and the template mesh was pre-scaled to match the bounding box dimensions of the new mesh. Second, a rigid

alignment of the template mesh to the new mesh was performed using a standard vertex-to-vertex Iterative Closest Point (ICP) algorithm. Third, after rigid alignment, a general affine transformation was performed without iteration. This method was applied to align the template mesh to the new mesh using 12 degrees of freedom (including rotations, translations, scaling, and shear). After the affine transformation step, the template and new model have reached the limits of linear transformation, but local portions of the models still remain significantly distant. Since the goal of final surface-to-surface matching is to create new points on the surface of the new model that will have similar local spatial characteristics as the template model, a novel non-linear iterative warping approach was developed to reduce misalignment.

Referring to FIG. **1**, to achieve point correspondence, an iterative algorithm is used where the closest vertex-to-vertex correspondences are found from the template to the new model as before, but now the correspondences from the new model to the template model are also found. Using both of these point correspondences, points on the template mesh are moved toward locations on the new mesh using a non-symmetric weighting of the vectors of correspondence. Next, a subroutine consisting of an iterative smoothing algorithm is applied to the now-deformed template mesh. This smoothing algorithm seeks to average the size of adjacent triangles on the template mesh, thereby eliminating discontinuities. At the beginning of the warping algorithm, the smoothing algorithm uses the actual areas of the surrounding triangles to dictate the smoothing vector applied to each point, which aids in effectively removing outlying points with large triangles. Consequently, at the beginning of the process, the template mesh makes large steps, and larger smoothing is required. Toward the end of the process, however, the smoothing vector is normalized by the total area of the surrounding triangles, which allows for greater expansion of the template mesh into areas of high curvature. After this procedure has been completed on all the femora and tibiae in their respective atlases, the atlases are ready for morphological shape analyses and automated metric comparisons.

An innovative statistical treatment was used to analyze global shape differences between the two groups. This method utilizes the power of (linear and nonlinear) PCA both as a means of variable reduction and as a global shape descriptor. This method is designed to find points of high discrimination between different gender and/or different ethnic groups when normalized against the first principal component (PC), which is considered primarily to scale. This procedure highlights areas on models that would be highly discriminating without the use of any other information. The landmarks identified by this algorithm provide adequate discrimination without the use of any other landmarks between ethnic groups. This feature finder algorithm is used to examine femoral and tibial shape differences independent of the size differences between American Whites, Blacks and East Asians.

A wide array of comparisons was made using specific measurements at defined landmarks on the ethnicity-specific statistical atlases. These landmarks were chosen based on surgical importance, clinical relevance, and historical measurements. Since the atlas consists of homologous points on each femur or tibia model, it provides ample information for automating this process. Also, each bone model in the atlas is aligned to the same coordinate frame. A total of 99 femur and 23 tibia measurements, angles, and indices were calculated. Furthermore, for purposes of brevity, only the most significant metric properties are discussed in the results section. Unless otherwise specified, the measurements outlined below represent three dimensional (3D) Euclidean distances between pairs of landmarks, and angles are measured as 3D rotations between vectors. In some instances these measurements were projected onto a plane for comparison with previous work in the field. A subset of these measurements is shown in FIGS. **2-4**. The landmarks that define the measurement endpoints are first computed and then defined relative to surgical and anatomical axes.

Presented are novel methods to ascertain ethnic differences on the distal femur and proximal tibia on a global scale, to discover regions that were likely to offer discriminating information, and to measure relevant surgical and anatomical features to aid implanted prosthesis design. Different studies have tried to identify ethnical differences of the femur and tibia using measurement techniques that lacked accuracy or precision. Unfortunately, these methods have been unable to find features of smaller consequence.

The ordered series of methods used pursuant to the instant disclosure evidenced significant global differences among sex and race, which subsequently allowed for isolation of regions likely to be highly different using the feature finder method, and finally allowed for the coding of algorithms to locate and measure surgically relevant anatomic features with a high degree of accuracy and repeatability. Bones with different scales were considered to have the possibility of shape changes dependent on size. In this way, correlations between measured variables and size were removed in order to expose demonstrable shape differences inherent to the ethnicities.

The inventor has used the foregoing analysis to determine that American Blacks have longer, straighter femora with narrower knees than American Whites. In addition, this analysis revealed differences in the dimensions and orientation of the lateral condyle that result in overall shape differences in the distal femur: American Blacks have a trapezoidal-shaped knee, and American Whites have a more square-shaped knee. For each group, the differences in the distal femur are echoed in the adjacent tibia, whereby American Blacks have a longer lateral tibial condyle. The mean medial-lateral length of the tibial plateau is slightly longer in Blacks than in Whites, but this difference was not overly significant given the sample size. However, American Blacks do have significantly longer and more robust tibiae. In this study, major shape difference was found between East Asian population and both American whites and American blacks.

It is not clear to what extent genetic differences contribute to lower limb morphology, admixed individuals present a challenge. Indeed, blood type data indicates that since their arrival in the United States, American Blacks have become more similar to American Whites and more divergent from their ancestral West African population.

Although racial differences in lower limb morphology are apparent and register statistically significant, there may be more statistical noise in the American Black sample versus the American White sample. This noise may be a result of the combined effects of genetic admixture since their arrival in the United States, as well as relaxed selection in a more temperate environment. Nonetheless, as discussed earlier, the effects of admixture have not erased the distinctive morphological differences between these subgroups of the American population.

In order, to understand normal knee joint kinematics, one must first understand the anatomy of the articulating surfaces of the knee joint. The knee joint is the articulation of

the two largest bones in the human lower extremity, the tibia and the femur. The articular surfaces at the knee joint consists of the curved surfaces that form the lateral and medial condyles of the distal portion of the femur and are in contact with the lateral and medial tibial plateaus of the proximal portion of the tibia.

The femoral condyles blend into an anterior groove, the trochlea, which is the articulation for the patella or kneecap. The tibial plateaus are separated by an intercondylar eminence, which serves as an attachment point for the anterior cruciate ligament and the menisci. The tibial plateaus are also asymmetric, with the lateral plateau the smaller of the two. Anatomical studies of the femorotibial articulation have shown that the medial compartment has greater contact area than the lateral compartment.

The fibula is attached to the tibia's lateral side by a dense membrane along its length and at the ends by cartilaginous joints supported by ligaments. The connection of the bones permits very little relative movement. The proximal tibiofibular joint is below the level of the tibio-femoral articulation, while the distal ends of the two bones form the proximal end of the ankle joint.

In the normal knee, posterior femoral rollback during an increasing flexion routinely occurs. Greater amounts of posterior femoral rollback have been observed during activities requiring greater magnitudes of flexion such as a deep knee bend maneuver. Posterior rollback is substantially greater at the lateral femorotibial articulation than medially, therefore creating a medial pivot type of axial rotational pattern in which the tibia internally rotates relative to the femur as flexion increases. Numerous kinematic evaluations have found a similar pattern and magnitude of posterior femoral rollback during deep flexion activities. This differs somewhat from axial rotational patterns observed after total knee arthroplasty (TKA), which showed lower magnitudes of axial rotation and occasional pathologic rotational patterns such as lateral pivot rotation and reverse screw-home rotation (tibia externally rotating relative to the femur with increasing flexion).

Also, the anterior translation of the femur on the tibia observed after TKA has numerous potential negative consequences. First, anterior femoral translation results in a more anterior axis of flexion, lessening maximum knee flexion. Second, the quadriceps moment arm is decreased, resulting in reduced quadriceps efficiency. Third, anterior sliding of the femoral component on the tibial polyethylene (PE) surface risks accelerated PE wear.

A primary objective of TKA should be to reproduce the kinematics of a normal knee. At present, this objective is largely overlooked. Numerous in vivo, weightbearing, and fluoroscopic analyses have shown that normal knee kinematics are difficult to obtain after TKA using existing orthopedic implants. Multiple kinematic abnormalities (reduced posterior femoral rollback, paradoxical anterior femoral translation, reverse axial rotational patterns, and femoral condylar lift-off) are commonly present. Understanding these kinematic variances assisted in design of better TKA implants, which work toward reducing and eliminating these kinematic abnormalities or at least accommodating them without creating adverse conditions that limit implant performance or longevity. Most of the knee implants are off-the shelve-knee systems, which are designed for average motion—not patient specific kinematics. Accordingly, TKA motion and kinematics of the knee that are indistinguishable from a normal knee should utilize customization for each patient. Currently, customization is a difficult task, but the instant disclosure addresses this customization, in part, by offering a deformable articulating template (DAT) methodology described hereafter.

For purposes of the instant disclosure, radius of curvature is the radius of a circle having a circumferential curvature that approximates the curvature of a rounded object. For example, the radius of curvature is infinite for a straight line, while the radius of decreases from infinity as the curvature increases. As can be seen in FIG. **5**, the radius of curvature for the smaller circle is less than the radius of curvature for the larger circle because the curvature of the smaller circle is greater than the curvature of the larger circle. Simply put, the smaller the radius of curvature, the larger the curvature.

Referring to FIGS. **6** and **7**, the inventor has found that one may map and simulate the curvature of the natural knee condyles by applying two or more radii of curvature along the camming surfaces from anterior to posterior. In particular, it has been found that for the Caucasian population, five distinct radii of curvature (identified as r1-r5) closely track the curvature of the camming surfaces of the condyles from anterior to posterior. Moreover, it has been found that asymmetry in the radii of the curvature of the condyles is responsible for imposing an internal rotation of the tibia with respect to the femur during flexion. Beyond 20° of flexion, sliding motion begins on both condyles.

Extension of the knee joint produces a coupled external rotation of the tibia with respect to the femur; this rotation has been described as the "screw-home" movement of the knee. This screw-home movement is due to the existence of a larger area of bearing surface on the medial condyle than on the lateral condyle. When the whole articular surface of the lateral condyle has been used up, the femur rotates around the tibial spine until the joint is screwed home or close packed in extension. As the knee joint flexes and extends, this rotation causes the tibial motion on the femur to assume a spiral or helicoid form that results from the anatomical configuration of the medial femoral condyle. As the tibia slides on the femur from the fully extended position, it descends and ascends the curves of the medial femoral condyle and simultaneously rotates externally. This motion is reversed as the tibia moves back into the fully flexed position. The screw-home mechanism gives more stability to the knee in any position than would be possible if the femorotibial joint was a pure hinge joint.

Referring to FIG. **8**, the meniscal cartilages (menisci) between the femoral condyles and the tibial articular surfaces are two crescentic fibrocartilage structures that serve to deepen the articular surfaces of the tibia for reception of the femoral condyles. On cross-section, the menisci have a wedge-like appearance. The menisci perform several important functions, including (1) load transmission across the joint, (2) enhancement of articular conformity, (3) distribution of the synovial fluid across the articular surface, and (4) prevention of bone impingement during joint motion. When the menisci are present, the load-bearing area for each condyle approximates 6 cm^2, but this surface area decreases to approximately 2 cm^2 when the menisci are damaged or severely degraded. Therefore, when the effective area of load bearing is increased, the stress transferred to the cartilages is reduced and vice versa.

Referencing FIGS. **9** and **10**, in the normal knee joint, the anterior cruciate ligament (ACL) and the posterior cruciate ligament (PCL) are intrinsic, lying inside the joint in the intercondylar space. These ligaments control the anterior-postrior and axial rotational motion in the joint. The anterior cruciate ligament provides the primary restraint for anterior movement of the tibia relative to the femur while the

posterior cruciate ligament offers the primary restraint to posterior movement of the tibia, accounting for over 90% of the total resistance to this movement. FIG. **10** shows the change in length of the ACL and PCL during different flexion angles of the knee joint. A detailed description of the effect of ACL and PCL constraints on the design of posterior stabilized knee implants will be discussed in more detail hereafter.

The morphologic shape of the distal femur should dictate the shape, orientation, and kinematics of the prosthetic replacement used for TKA. Traditional prosthetic designs incorporate symmetric femoral condyles with a centered trochlear groove. Traditional surgical techniques center the femoral component to the distal femur and position it relative to variable bone landmarks. However, documented failure patterns and kinematic studies demonstrate how traditional design and surgical techniques reflect a poor understanding of distal femoral morphology and knee joint kinematics, in addition to a disregard for the patella and its tracking of the distal femur.

The trochlea is designed to guide and hold the patella. Patella tracking is influenced by many different factors: the geometry of the trochlear groove, the geometry of the posterior side of the patella, soft tissue extensor mechanism and the orientation of the tibia. The normal movement of the patella on the femur during flexion is a vertical displacement along the central groove of the femoral patellar surface down the intercondylar notch. The geometry of the trochlear groove and the posterior side of the patella constrains patella tracking, particularly at high flexion angles. The patella is held centrally by the conformity of the facets with the sulcus of the femur and by the patellofemoral ligaments. These ligaments represent a conformation of the capsule into thickened structures on the medial and lateral side of the patella. These ligaments are located superiorly and inferiorly on either side, and extend from the anterior surface of the patella posteriorly to the side of each femoral condyle. These ligaments also constrain the motion of the patella, but can be overruled by the sulcus constraints or by external forces. In a normal knee it is acceptable to presume that the tracking of the patella will be very similar to the orientation of the trochlea. As a result, the orientation of the trochlear groove of a knee prosthesis should be similar to the orientation of the natural trochlea to reproduce this natural patella track.

In sum, the knee joint is an example of very well balanced system. A slight change within this system, affects the whole system. Changes within the patella-femoral joint can have considerable long term effects, as the transmitted forces within this part of the knee joint are relatively high. TKA easily induces changes within the patella-femoral joint. At present, the simulated trochlear groove orientation of TKA components does not conform to the natural trochlear orientation. Accordingly, the groove orientation of fiture femoral components should incorporate a trochlear groove that simulates the natural orientation of the trochlear groove of a natural femur.

BRIEF DESCRIPTION OF THE DRAWINGS

FIG. **1** is a flow chart outlining the process of atlas creation.

FIG. **2** is a screen shot and associated image showing automatic calculation of landmarks using the IDAS software.

FIG. **3** is a distal end view of a femur showing the axes, landmarks, and measurements taken.

FIG. **4** is a frontal view of the femur of FIG. **3**, showing certain axes, landmarks, and measurements taken.

FIG. **5** is an exemplary diagram showing how curvature on the surface of a bone may be approximated using circles having different radii.

FIG. **6** is a profile view of the lateral condyle of a human knee joint having five radii of curvature applied to approximate the curvature of the camming surfaces from anterior to posterior.

FIG. **7** is a profile view of the medial condyle of a human knee joint having five radii of curvature applied to approximate the curvature of the camming surfaces from anterior to posterior.

FIG. **8** is a plan view of the proximal end of a human tibia that includes cartilage forming a portion of a human knee joint.

FIG. **9** is a frontal view of a knee joint showing the anterior cruciate ligament and posterior cruciate ligament during partial knee flexion.

FIG. **10** includes a series of frontal views of a knee joint at various degrees of knee flexion showing the position of the anterior cruciate ligament and the posterior cruciate ligament.

FIG. **11** is an overall schematic of an exemplary process for designing an orthopedic implant that is customized for a patient or comprises one of a series of templates for general populations.

FIG. **12** is a bottom view of several electronic 3D distal femur models generated from medical imaging equipment that correspond to actual natural femurs from human patients.

FIG. **13** is an electronic model of a human knee joint, including cartilage and ligaments, based upon medical imaging equipment data of an actual human knee joint, with the joint shown in the flexed position.

FIG. **14** is an electronic model of a human knee joint, including cartilage and ligaments, based upon medical imaging equipment data of an actual human knee joint, with the joint shown proximate full extension.

FIG. **15** is a series of 2D vertical slice representations of a knee joint showing the interaction between the tibia, femur, and patella proximate full extension.

FIG. **16** is a 3D representation of the 2D slices of FIG. **15** in addition to other vertical slices to show where the slices are taken and the relative positions of the tibia, femur, and patella proximate full extension.

FIG. **17** is a distal view of the femur showing furthest anterior, distal and posterior points along the medial and lateral camming paths.

FIG. **18** is a compilation of views of the medial and lateral condyles of a distal femur having a path approximating the most outward portion of the camming surface of each condyle throughout the range of motion of each condyle.

FIG. **19** is an elevated posterior view of a 3D representation showing a tibia and patella relative to the path of the outward most portion of the camming surface of each condyle for an exemplary distal femur, as well as the inner most surface of the trochlear groove associated with the distal femur.

FIG. **20** is a lateral profile view of a knee joint showing the tibia and patella of FIG. **18**, as well as the camming paths and trochlear groove path, in addition to showing the distal femur in phantom.

FIG. **21** is an exemplary chart representing measurements of radii of curvature for a series of distal femurs for both human males and females, as well as where the measurements were taken.

FIG. **22** is a lateral profile view of a knee joint showing the tibia and patella relative to the positions and size of corresponding radii of curvature for the outermost camming surface paths of the lateral and medial condyles.

FIG. **23** is a frontal view showing a common differences between the shape of a distal femur among Asians, American Whites, and American Blacks.

FIG. **24** is a profile view showing a common differences between the shape of a medial femoral condyle among Asians, American Whites, and American Blacks.

FIG. **25** is a profile view showing a common differences between the shape of a lateral femoral condyle among Asians, American Whites, and American Blacks.

FIG. **26** is an exemplary profile cross-section of an exemplary lateral condyle prosthetic showing how the measurements of c1-c4 translate into the curvature of a prosthetic device fabricated in accordance with the instant disclosure.

FIG. **27** is a 3D representation showing the outermost camming surface paths of the lateral and medial condyles for an exemplary distal femur, as well as the innermost path of the trochlear groove, in addition to the arcuate profiling of the lateral and medial condyles and the trochlear groove.

FIG. **28** is the 3D representation of FIG. **22** overlaid onto a 3D bone model of a natural femur.

FIG. **29** is a magnified view of FIG. **23** showing the distal portion of the femur and the overlaid 3D representation.

FIG. **30** is a perspective view of a distal portion of a femur including an exemplary 3D representation of the surface.

FIG. **31** is the mathematical representation of the curvature displayed in FIG. **24**.

FIG. **32**A is a graphical image plotting the ratio of the medial and lateral condyles to one another for 0-30 degrees.

FIG. **32**B is a graphical image plotting the ratio of the medial and lateral condyles to one another for 40-70 degrees.

FIG. **32**C is a graphical image plotting the ratio of the medial and lateral condyles to one another for 80-110 degrees.

FIG. **32**D is a graphical image plotting the ratio of the medial and lateral condyles to one another for 120-150 degrees.

FIG. **33** is a proximal end of a tibia showing the axes, landmarks, and measurements taken in accordance with the instant disclosure.

FIG. **34**A is an end view of a distal femur showing the trochlear path of a typical Asian.

FIG. **34**B is an end view of a distal femur showing the trochlear path of a typical American White.

FIG. **34**C is an end view of a distal femur showing the trochlear path of a typical American Black.

FIG. **35** is a composite view showing the trochlear paths for a typical Asian, American White, and American Black.

FIG. **36** is a composite profile view showing the shape of trochlear paths for a typical Asian, American White, and American Black.

FIG. **37** is a distal view of a femur showing areas of maximum difference between an Asian and an American White.

FIG. **38** is a distal view of a femur showing areas of maximum difference between an American White and an American Black.

FIG. **39** is a elevated perspective view of a tibia showing areas of maximum difference between an American White and an American Black.

FIG. **40** is a proximal view of a tibia showing areas of maximum difference between an Asian and an American White.

FIG. **41** is a diagram showing an exemplary process for restoring deformed or missing anatomy using C1/C2 ratio in accordance with the instant disclosure.

FIG. **42** is an exemplary plot of AP height versus ML width.

FIG. **43** is a plot for determining the optimum number of clusters using Dunn's Index and modified Dunn's Index.

FIG. **44** is an alternative Dunn's Index Equation (ADI).

FIG. **45** is a collection of views depicting an exemplary approximation of a tibial plateau using a series of contours normal to the principal axes of the medial and lateral plateaus.

FIG. **46** is an exemplary plot of AP height versus ML width.

FIG. **47** is a perspective view of an exemplary polyethylene implant.

FIG. **48** is a series of perspective views of an exemplary implant.

FIG. **49** is a perspective view of an exemplary implant.

FIG. **50** is a cross sectional view of an exemplary implant.

FIG. **51** is a perspective view of an exemplary implant.

FIG. **52** is an anterior view of exemplary femoral and tibial components fabricated to correspond to the anatomical shape of the patient's knee for a cruciate retaining implant.

FIG. **53** is a cross-sectional view taken across the lateral condyle and condyle receiver for exemplary femoral and tibial components fabricated to correspond to the anatomical shape of the patient's knee for a cruciate retaining implant.

FIG. **54** is a cross-sectional view taken across the medial condyle and condyle receiver for exemplary femoral and tibial components fabricated to correspond to the anatomical shape of the patient's knee for a cruciate retaining implant.

FIG. **55** is a comparison showing the difference between the anatomical implants and existing functional implants.

FIG. **56** is a comparison showing the difference in the restoration of the correct ratio between the medial and lateral anterior portions of the knee.

FIGS. **57** and **58** show the profiles of many functional implants.

FIG. **59** is an exemplary shaded map showing the variation between African American and Caucasian populations, where less shading corresponds to greater differences, whereas more shading corresponds to less differences.

FIG. **60** is an exemplary flow diagram for generating a patient specific implant from the 3D bone model.

FIG. **61** is a depiction of the point cloud used to represent the surface of patient's bone and used to calculate bone cross sectional contours.

FIG. **62** is a depiction of updating parameterized implant constraints with the patient specific contours at an early stage of creation of a patient specific implant.

FIG. **63** is a depiction showing sweeping contours to generate smooth articulating implant surfaces that are patient-specific in accordance with the instant disclosure.

FIG. **64** is an exemplary process flow diagram for updating existing legacy implant systems with anatomical friendly templates.

FIG. **65** is a depiction of an updated existing legacy implant system that incorporates a more anatomically accurate patellar groove.

FIGS. **66**A and **66**B are exemplary listings of parameters used to describe an exemplary femoral component designed in accordance with the instant disclosure.

FIG. **67** is an exemplary flow chart describing a process of automatically updating the template parameters and generating an implant CAD.

FIG. **68** is a distal femur shown with corresponding contact areas that are highlighted.

FIG. **69** is a proximal tibia shown with corresponding contact areas that are highlighted for between 0-40 degrees of knee flexion.

FIG. **70** is a proximal tibia shown with corresponding contact areas that are highlighted for between 60-140 degrees of knee flexion.

FIG. **71** are overhead views of a tibia tray insert having been modified or redesigned to simulate or approximate normal knee kinematics.

FIG. **72** is a conventional PS knee implant having limited axial rotation.

FIG. **73** is an elevated perspective view of an exemplary knee prosthesis designed in accordance with the instant disclosure that provides for retention of the anterior cruciate ligament.

FIG. **74** is a frontal view of an exemplary knee prosthesis designed in accordance with the instant disclosure for use after an anterior cruciate ligament revision surgical procedure.

FIG. **75** (Table 1) lists important femur measurements means, standard deviations, t-tests, and power test results for typical Asians, typical American Whites, and typical American Blacks.

FIG. **76** (Table 2) lists important tibia measurements—means, standard deviations, t-tests, and power test results for typical Asians, typical American Whites, and typical American Blacks.

FIG. **77** (Table 3) lists percentage length change in anterior cruciate ligament and posterior cruciate ligament with respect to knee flexion angle.

DETAILED DESCRIPTION OF EXEMPLARY EMBODIMENTS

The exemplary embodiments of the present invention are described and illustrated below to encompass methods and devices for designing prosthetic knee implants and, more specifically, to devices and methods for designing knee implants that more closely track the biomechanics of the natural knee and the resulting implants themselves. Of course, it will be apparent to those of ordinary skill in the art that the preferred embodiments discussed below are exemplary in nature and may be reconfigured without departing from the scope and spirit of the present invention. However, for clarity and precision, the exemplary embodiments as discussed below may include optional steps, methods, and features that one of ordinary skill should recognize as not being a requisite to fall within the scope of the present invention.

The following are definitions that relate to axes, landmarks, and measurements with respect to the distal femur (see FIGS. **2**-**4**). These definitions also govern the proper construction of these terms as used in the instant disclosure.

Transepicondylar Axis (TEA)—This measurement is known in the anthropological literature as biepicondylar breadth. To compute the clinical transepicondylar axis (TEA), rough sets of vertices were manually defined on an average femur on the most lateral prominence of the lateral epicondyle and the most medial prominence of the medial epicondyle. This step was only performed once, since vertices in the atlas femora are homologous. Using these rough sets of points, a search region of 10 mm radius was defined from the centroid of the rough sets of vertices on both the lateral and medial sides. Defining the vector from each of these centroids then gives a rough direction for the TEA. A pair of points was selected by maximizing the distance in this rough direction; these selected points form the endpoints of the TEA measurement (see FIG. **2**).

Distal Anatomical Axis—The distal anatomical axis was defined by locating the shaft centroids at the distal one-third and distal one-fifth of the overall femur length.

Central AP Axis (CAP)—Using the distal anatomical axis and the TEA, a mutually perpendicular axis was defined with termini at the posterior aspect of the intercondylar notch and the most anterior portion of the intercondylar groove. The length of this axis is recorded as CAP (FIG. **3**). This axis is similar to 'height of intercondylar notch'.

Femoral Saddle Point—A landmark located at the most distal extension of the intercondylar groove.

Knee Center (K)—Using the two endpoints of the CAP measurement and the femoral saddle point, a plane is defined which bisects the femur into medial and lateral sides. The intersection of this plane with the TEA is the knee center, which forms the distal endpoint of the mechanical axis (MA) of the femur. The proximal endpoint of the MA is the center of the femoral head (see proximal femur measurements below).

AP Direction—Using the MA and the TEA, a mutually perpendicular vector with its origin at the knee center is used to define the antero-posterior (AP) direction, resulting in a direction similar to Whiteside's line.

Anterior Medio-lateral Width (AML) and Posterior Medio-lateral Width (PML)—The AP direction was used to locate four landmarks: the most anterior and posterior points on the medial and lateral condyles of the distal femur. Connecting the two most anterior points gives a measurement of anterior medio-lateral width (AML) along the trochlear line, while connecting the two most posterior points gives a measure of posterior medio-lateral width (PML) measured along the posterior condylar axis (PCA) (see FIG. **2**).

AP Length of Medial and Lateral Condyles (LAP and MAP)—Connecting the pairs of lateral and medial vertices defined above, respectively, gives the AP length of the lateral condyle (LAP) and medial condyle (MAP) (see FIG. **3**).

Posterior Plane—A unique plane containing the endpoints of the PML measurement, which is also parallel to the MA, was used to define the posterior plane.

Overall AP Length—The minimum distance between the prominences of the lateral anterior condyle and the posterior plane (see FIG. **3**).

AP Angle—The angle of the AML vector relative to the posterior plane (see FIG. **3**).

Distal Medial-lateral Length (DML)—The most distal aspects of the medial and lateral condyles were recorded using MA as a reference direction. The distance between these two landmarks was denoted as DML.

Posterior Angle (PA)—The angle between the vector connecting the DML length and the mean axis of the femur (see FIG. **4**).

Condylar Twist Angle (CTA)—The angle between the TEA and PCA.

Patellar Groove Height (GH)—Calculated between the posterior aspect of the intercondylar notch and the midpoint between the two DML axis points (see FIG. **4**).

Femoral Shaft Curvature (SC)—The radius of curvature of the femoral mean axis.

End of definitional section

Referring to FIG. **11**, a schematic overview of the exemplary knee design process **100** includes obtaining one or

more electronic three dimensional (3D) bone representations **102** that are stored in an electronic database. For purposes of designing a total knee implant, in the case of total knee arthroplasty, that will replace the distal portion of the femur, the proximal portion of the tibia, the cartilage therebetween, and at least a portion of the patella, it is useful to have 3D bone representations of the distal femur, the proximal tibia, and the patella, as well as 3D jig representations utilized to prepare the femur, tibia, and patella for accepting TKA orthopedic components. To generate these 3D bone representations and 3D jig representations, a patient or cadaver may undergo a CT scan, a series of X-rays, an MRI, and/or ultrasound imaging. The images of the bones and soft tissues from these tests, and possibly interpolated aspects of bone or soft tissue, are utilized to construct one or more 3D bone representations and one or more 3D jig representations.

The images from the foregoing tests are loaded into a computer for data analysis. As is known to those skilled in the art, an MRI creates a series of 2D "slices" of the relevant portion of the human anatomy. These 2D slices may then be segmented and stacked upon one another to create a 3D model or representation of the human anatomy. To the extent MRI is used to construct the slices, the precision of the 3D model depends in part upon how "thick" the slices are from the MRI. An analogous process is utilized for CT scans, X-rays, and ultrasounds where the 2D images are taken from distinct points and utilized to construct a 3D model of the anatomical feature in question, for exemplary purposes only this anatomical feature in question is described in the context of a human knee joint.

This same process for taking 2D images and using these images to create a 3D model is applicable to generating any 3D model of a human joint or bone(s). This same process may be applied to a living or dead human being in order to generate a plurality of bone or joint models for further analysis. It should also be understood that these same 2D images are useful to construct 3D models of cartilage that may be selectively interposed between bones, in exemplary form the femur and tibia, to more accurately depict the anatomy of each human feature (bone, joint, etc.). As will be discussed hereafter, the 3D models of the cartilage may be useful in constructing the 3D jig models.

Referring to FIG. **12**, a series of 3D distal femoral representations are shown. As will be discussed in more detail hereafter, the exemplary knee design process **100** may be utilized to design and construct a customized knee implant that is unique to the anatomy of each patient. In addition, the exemplary knee design process **100** may be utilized to design and construct one or more generic implants that may be utilized to approximate the anatomies of larger populations where customization costs are not commercially feasible or preferable.

Referring back to FIG. **11**, after one or more bones have been modeled so that 3D representations, in electronic form, have been generated, the 3D representations are stored in a database **104** that correlates additional data with the 3D representations. In exemplary form, the database **104** also includes data specific to each 3D representation in order to classify the representation including, without limitation, age, gender, race, and height of the human from which the bones, joint, etc., were scanned. At the same time, each 3D representation may include a grade or evaluation as to the condition of the bone, joint, etc. In exemplary form, when a 3D depiction of a knee joint (at least the proximal tibia and distal femur) is saved in the database **104**, classifications for cartilage wear, bone degeneration, and osteophyte growth can be identified.

Referring to FIGS. **13** and **14**, subsequent to the generation of each individual bone model, the exemplary process **100** includes generation of a 3D model of the knee joint **300**. This 3D model **300** of the knee joint includes orienting the distal femur **302**, proximal tibia **304**, and patella **306** as each would be when the joint was in full extension. Thereafter, computer software is operative to reposition the bones of the 3D model to create a virtual range of motion for the knee joint through full flexion. At the same time, the 3D models **300** may include cartilage (not shown) that interposes the bones **302**, **304**, **306** to represent the natural cartilage that cooperates with the proximal end of the tibia **304** to form medial and lateral condyle receivers.

Referencing FIGS. **15** and **16**, the 3D joint model **300** is useful to generate 2D contact profiles or "slices" showing how the orientation of each slice changes as knee joint is taken through its range of motion. In particular, these 2D representations are useful in understanding that a prosthetic implant, just like a natural knee, can be thought of as a series of slices that combine and work together to form the entire joint. As a result, by evaluating and understanding the geometry of each slice, specific contours may be seen that will be unique to each patient or may be generalized over a more encompassing population. It should be noted that the 3D joint model **300** may incorporate different topographies depending upon ethnicity, gender, and/or age. These differing topographies result in differing slices.

Referring to FIGS. **17-20**, after each 3D model **300** has been generated and saved, a series of radii of curvature measurements are taken for both the medial and lateral condyles **308**, **310** associated with each 3D model. In exemplary form, a distal femoral 3D model includes corresponding medial and lateral condyles **308**, **310** separated by a trochlear groove **312**. Each lateral and medial condyle **308**, **310** includes a camming surface having points along the camming surface that are farthest away from the center of the bone as the femur rotates through its range of motion. In order to calculate medial profile, a plane defined by the medial anterior point (most anterior point in medial condyle), the medial distal point (most distal point on medial condyle) and the medial posterior point (most posterior point in medial condyle) is intersected with the distal femora this results in contour that corresponds to the most protruding points on medial condyle surface, the same method is used to calculate the lateral profile as shown in FIGS. **17**, **19** and **20**. These 3D paths are then converted to a single best-fit path within one plane for each condyle.

For the sulcus profile calculation, a set of contours is extracted by intersecting the distal femur with a series of planes rotating around the transepicondylar axis with a 10 degree increment. The lowest points on these contours are then used to define the sulcus points as shown in FIG. **19**.

A similar procedure is utilized to generate a set of points along a 3D path of the trochlear groove using the points along the surface that are closest to the center of the bone as the femur rotates through its range of motion. These closest points (i.e., lowest portion of the trough) are shown in FIGS. **19** and **20**. This 3D path is then converted to a single best-fit path within one plane (as shown in FIGS. **19** and **20**).

Referring to FIGS. **21** and **22**, the inventors of the present invention have found that the shape of the 2D paths for both the medial and lateral condyle bearing surfaces, as well as the 2D path for the trochlear groove, are important in attempting to design a prosthetic femoral component that closely resembles the natural shape of the distal femur. In order to generate specific sizing and curvature measurements for generation of the femoral component, the inven-

tors have found that application of four radii of curvature to each femoral condyle accurately resembles the curvature of the natural femur condyles.

Referencing FIGS. **23-25**, FIG. **23** is a composite view of the lateral and medial femoral condyles for the Whites, Blacks, and Asians, whereas FIG. **24** shows the medial profile for a medial femoral condyle for Whites, Blacks, and Asians, and FIG. **25** shows the lateral profile for a lateral femoral condyle for Whites, Blacks, and Asians.

Referring back to FIGS. **6** and **21**, as well as FIG. **26**, each path for the outermost medial condyle camming surface and the outermost lateral condyle camming surface is segmented into four zones. It has been identified by the inventors that the curvature of each of these zones can be approximated by the curvature of a circle. In other words, each zone has a curvature that approximates the constant arc of a circle. For example, the first zone has a radius of curvature, identified as c1. Simply put, this c1 value is the radius of a circle that most closely approximates the curvature of this portion of the camming surface 2D path, which is the most posterior portion of the path. The second zone, immediately adjacent to the first zone, has a radius of curvature of c2. Again, this c2 value is the radius of a circle that most closely approximates the curvature of this second zone. The third zone follows the second zone and also includes a radius of curvature, c3. Finally, the fourth zone, which approximates the contour of the anterior portion of each of the respective condyles, has a radius of curvature of c4.

In the circumstances where a series of knee joints are electronically modeled from X-rays, CT scans, MRIs, etc., a comparison may be carried out to discern how the radii of curvature vary within each zone and across all zones. The chart in FIG. **21** is derived from actual 3D bone models derived from human X-rays, CT scans, MRIs, and/or ultrasounds. This chart includes mean radii of curvature in metric units (in centimeters) for each zone based upon gender. In addition to giving the mean radius of curvature for each zone, the table also represents the standard deviation for each zone to provide a quick comparison between the zones for the lateral and medial condyles.

Referring back to FIGS. **22** and **26**, a profile view of a human knee joint removes the distal portion of the femur and replaces it with circles corresponding to the radii of curvature for each of the four zones (c1-c4) for both the medial and lateral condyles. This figure provides a representative view of what radii of curvature represent in terms of are and the relative sizes of the circles in relation to the adjacent anatomical features of the distal femur. As will be discussed hereafter, these circles are relevant in attempting to approximate the curvature of a native distal femur in a prosthetic implant. The locations of the centers of the circles may be used inside an exemplary model. They may be calculated using linear square fitting of a circle in each set of curve points, which gives radii and centers of best approximating circles for the curves.

Referring to FIGS. **27-32**, as discussed above, 3D paths are created that track the outermost camming points throughout the range of motion for both the medial and lateral condyles, as well as the innermost points throughout the range of motion of the trochlear groove. Each outermost camming path is utilized in conjunction with the path for the trochlear groove to mathematically map the topography of both condyles and the trochlear groove. Curvature of the medial, lateral and sulcus profiles are then calculated by finding best number of circles passing that accurately approximate the curve as shown in FIG. **27**. To capture the curvature of the condylar surface, the curves produced earlier by intersecting the femur with the planes around TEA are trimmed around the medial, lateral and sulcus profiles, the circle of curvature of each of these trimmed contours are then calculated as shown in FIG. **27**.

Each outermost condyle camming path, in addition to the trochlear groove trough path, is divided into variable degree increments along the range of motion of the distal femur as it rotates with respect to the tibia. In the images provided, ten degree increments were used, although other increments are within the scope of the disclosure (e.g., 5-15 degree increments may be employed in some exemplary embodiments). The length of each path is divided into ten degree increments, with a curve being applied at the boundary of each increment. A separate medial-lateral curve is applied to the widthwise portion (medial to lateral) of each condyle and the trochlear groove at each ten degree increment. The arch of each separate medial-lateral curve is chosen to most closely approximate the medial-lateral curvature at each point along the respective paths. Thereafter, a radius of curvature is determined for each medial-lateral curve.

Referring to FIG. **33**, the following landmarks and measurements were identified automatically for the distal femur:

1) Intercondylar Eminence Points—The two highest projecting points on the medial and lateral intercondylar eminences.
2) Eminence Midpoint—The midpoint between the lateral and medial intercondylar eminence points.
3) Tibial Tuberosity—The most anteriorly protruding point on the tibial tuberosity.
4) ML—Maximum width of the tibia plateau in the medial-lateral direction.
5) AP—Length of the tibial plateau in the anterior-posterior (AP) direction and passing through the midpoint of the tibial intercondylar eminence (i.e. eminence midpoint).
6) Eminence Width (EW)—Distance between medial and lateral intercondylar eminence points.
7) Tibial Twist Angle (TTA)—Angle between the AP direction and a line connecting the intercondylar eminence midpoint and tibial tuberosity.
8) Lateral Plateau Height (LPH)—Length of the lateral tibial plateau in the AP direction.
9) Lateral Plateau Width (LPW)—Length of the lateral tibial plateau in the ML direction.
10) Medial Plateau Height (MPH)—Length of the medial tibial plateau in the AP direction.
11) Medial Plateau Width (MPW)—Length of the medial tibial plateau in the ML direction.
12) Eminence ML Ratio (EMLR)—Ratio of MPW (i.e. medial plateau width) over ML.
13) Maximum Length—Length of the tibia from the medial malleolus to the intercondylar eminence.

Referring to FIGS. **34**A-**36**, it can be seen that the trochlear groove for different ethnicities has a different shape and path. FIG. **34**A represents the trochlear groove path for a typical Asian, while FIG. **34**B represents the trochlear groove path for a typical American White, while FIG. **34**C represents the trochlear groove path for a typical American Black. In addition, FIG. **35** provides a composite view of the trochlear groove path for a typical Asian, a typical American White, and a typical American Black. Finally, FIG. **36** provides a profile view showing how the shape of the trochlear groove also varies among Asians, American Whites, and American Blacks. The results from the feature finder shape analysis tool, as described above,

highlight shape differences in the femoral shaft, lateral condyle, and greater trochanter, in addition to the distal femur.

Referring to Table 1 and FIGS. **37-40**, the results from the t-tests and power tests for the automated measurements. In American Blacks, the lateral condyle has higher AP height ($p<0.01$) whereas the medial condyle height wasn't significant, thereby creating a more trapezoidal-shaped knee as opposed to the more square-shaped knee in American Whites which resulted in larger AP condyle angle in American blacks. On the other hand, our analysis performed on the distal femur of the East Asian population identified a distinct pattern in the AP and ML where the AP and ML measurements are smaller in the East Asian population as compared to both the Caucasian and African American populations ($p<0.01$). In general, the Asian population exhibits a more trapezoidal shape than the Caucasian and African American populations ($p<0.01$). In addition, the East Asian population also has a narrower anterior width ($p<0.01$).

Analyzing the curvature of both lateral and medial profiles it has been found that they can be accurately approximated by four distinct radii of curvature for American black and American white and three distinct radii for East Asians (see FIG. **6**). These four radii were found to be consistent between both ethnicities (American Black and American White), however the value of these radii were different in each ethnicity as shown in FIGS. **23-25**.

The feature finder results for the tibia indicate that ethnic shape differences between American white and American black are not as significant at the medial and lateral plateau areas as opposed to more shape differences around tibial tuberocity area. Besides minor differences in the proximal anterior tibia, the only area that registered significant was the tip of the medial malleolus (see FIGS. **39** and **40**). However, a major shape difference was found between East Asian population and both American White and American Black (FIGS. **23-35**). The results from the t-tests and power test underscore these findings, as well. The most significant variables are those related to scale, including maximum length, measures of shaft robusticity, and several measurements of the tibial plateau. In short, American Black tibiae are longer with a more robust shaft and slightly larger tibial plateau.

Table 2 shows the automated measurements for the tibia with lateral plateau height as the most significant measurement ($p<0.05$) which correlates to the significant difference in the lateral femoral condyle height.

Referring back to FIG. **31**, the radii of curvature for the medial-lateral curves are determined for both the medial condyle and the lateral condyle at each ten degree increment, from posterior to anterior. The first column is structured in ten degree increments along each outwardmost camming surface path for both the medial and the lateral condyles. The second and third columns refer to the radius of curvature for the medial and lateral condyles at the respective angle increments. The final two columns are ratios corresponding to the curvature of the medial-lateral radius of curvature divided by the radius of curvature for the respective camming surface paths. In other words, the ratio has a numerator that is the radius of curvature from side to side of each condyle, and a denominator that is the radius of curvature for the zone (which is the same number for a zone) along the path of the outermost camming surface of each condyle. This ratio is then plotted for each zone, for various planes taken at specific angles with respect to the mechanical axis (MA).

Referring to FIG. **41**, the ratio of C1/C2 (see FIG. **29**) can be used to restore deformed anatomy to generate a smooth articulating surface of patient specific implant. The process may begin by calculating lateral and medial profile and the curves for the condylar surface for the patient as outlined in the previous point, these contours are then evaluated to verify that the curvature of each sectional curve is within the normal anatomical range. Deformed sections are then highlighted and C1/C2 ratios are calculated for the anatomical correct sections, these sections are then used to interpolate the ratio for the deformed section, upon completion of this process a smooth implant articulating curvature that mimics the patient correct anatomy is generated.

The results are utilized to approximate the radii of curvature along the condyles, C2, when abnormalities exist within the bone. A relationship between ratios of C1 and C2 for the medial and lateral condyles has been identified and can be used calculated the radius of curvature for a specific location along either condyle, C2.

Using the radii of curvature for the outermost camming surface paths for the medial and lateral condyles, as well as the mapping of the curvature for the medial-lateral arcs, a novel prosthetic implant may be fabricated that is patient specific. At each degree increment, a smooth curve is generated using the radii of curvature and three points along the medial condyle, trochlear groove, and lateral condyle (see FIG. **29**). The articular surface of the implant is then approximated using a sweep surface of these smooth curves.

Referring to FIGS. **41** and **26**, four distinct radii of curvature have been identified for the outermost camming surface of the lateral and medial condyles.

Referring to FIG. **42-44**, six cutting box sizes were identified by analyzing the aspect ratio between the anterior-posterior height and ML Width. The AP height is defined as the distance between the sizing point and most posterior point on the femur while the ML width is defined as the size of the femur in the medial lateral dimension. This aspect ratio are then calculated for all population this ratio along with and not limited to features highlighted in table I are then used as a multidimensional feature vector to cluster the population, best number of clusters are determined using both Dunn's Index and alternative Dunn's Index (see FIGS. **43** and **44**) which are used to identify of how compact and well separated the clusters are. In exemplary form, twelve clusters were found that best represent the American White population which are divided into six clusters for males and six for females)

Referring to FIG. **45**, the tibial plateau is approximated using a series of contours normal to the principal axis of the medial and lateral plateau. These contours are used to parameterize the surface of the polyethylene for the tibial implant.

Referring to FIG. **46**, six tibial plate sizes were identified by measuring the length of the tibial surface in the anterior-posterior direction and measuring the tibia length in the medial-lateral direction. The ratio between these two measurements was then clustered using fuzzy c-means to identify six sizes the best fit the population.

Referring to FIG. **47-51**, the polyethylene reflects the anatomical shape of the tibial plateau for a cruciate retaining implant (see FIG. **47**) and for a bi-cruciate implant (see FIGS. **48-51**). The polyethylene can also be modular and may include medial and lateral polyethylene inserts which preserve the tibial eminence. A connector is used (FIG. **39**) to ensure the accurate placement of the inserts. Once

secured, the connector is removed leaving only the medial and lateral polyethylene inserts and tibial trays in place (FIG. **51**).

Referring to FIGS. **52-54**, the femoral and tibial components of the implant corresponding to the anatomical shape of the knee showing the curvature matching between the two components radii.

Referring to FIGS. **55-58**, a comparison shows the difference between the anatomical implants and existing functional implants. FIG. **55** shows the difference in the restoration of the correct ratio between the medial and lateral anterior portions of the knee. Existing functional implant (blue) does not properly restore this ratio causing more tension along the quadriceps which can alter the motion of the knee and can cause sublaxation of the patella. FIGS. **56-58** show the curvature of the medial and lateral profiles for the anatomical implant as compared to existing functional implants. FIG. **56** illustrates a direct comparison to a typical implant, whereas FIGS. **57** and **58** shows the profiles of many functional implants.

Referring to FIG. **59**, the color map shows the variation between African American and Caucasian populations. The brighter colors show higher differences than darker colors. Little variation exists on the distal end of the femur although the lateral condyle does show slight differences.

An exemplary process of selecting a template that best fit patient anatomy can be described as following. A patient knee will first be imaged and a 3D surface of the patient femur and tibia will be generated. The femoral bone is then analyzed to calculate the medial and lateral camming paths. Medial and lateral sagital curves are then calculated. Anterior posterior size and medial lateral size of the femur are also calculated. The curvature of the camming paths along with the sagital curves, AP size and/or medial lateral width may be used to locate the best template that fit the patient. For patients where implant template doesn't fit their anatomy, a custom implant is generated as shown by the right branch of FIG. **11**.

Referring to FIG. **60**, an exemplary process for generating a patient specific implant from any imaging modality includes generating three dimensional patient specific models, these models are then added to the foregoing discussed (DAT) statistical atlas to achieve point correspondence and normalization, upon completion of this process relevant surgical landmarks are automatically calculated (TEA, MA, PCA, . . . etc).

Referencing FIGS. **61-63**, a rotating plane around the TEA is then used to calculate bone cross sectional contours (see FIG. **61**) and another set of contours normal to the MA are then calculated (see FIG. **62**). These two sets of contours are then used to update the constraints of the parameterized implant template automatically, upon updating of these constraints, the implant articulating surface is then swept to generate a smooth continuous surface (see FIG. **63**). Measurements of the anterior-posterior height and medial-lateral width from the patient's bone are also used to update a template cutting box. This box is then combined with the smooth articulating surface to generate a patient specific implant CAD model. This implant 3D CAD model is then evaluated against the 3D model of the patient specific bone to verify the placement and a simulation of range of motion is performed with the 3D implant model and the 3D bone model. Upon completion of the verification process, the 3D implant model is output from a computer to a manufacturing facility in order to manufacture the implant. In exemplary form, the computer output of the 3D implant model may be in the form of G-code for a CNC machine.

Referring to FIG. **64**, an exemplary flow chart outlines how implant templates generated from the clusters that best fit the population can also be used to update existing legacy systems to ensure conformity with the patient's anatomical trends. This process involves importing a CAD model of an existing implant system and transforming it to same parameterization space as the anatomical templates. This process includes generating a set of three dimensional contours around the implant mid axis. These contours are used to generate a set of constraints in same manner as the anatomical templates. Once the implant is parameterized just as are the templates, the templates parameter values are used to update the parameterized implant features. These parameterized implant features include, but are not limited to, patellar groove curvature, condylar curvature, AP height, and ML width.

FIG. **65** shows how anatomical friendly templates can be used to update existing implant families to create an implant that mimics an anatomical patellar groove.

Referring to FIGS. **66**A-**66**B and **67**, an exemplary parametric femoral CAD model consists of 300+ parameters. The CAD model is defined by cross sections around the TEA axis at 10 degrees increment. The parameters define specific points and curvatures of each cross section. The patella-femoral section of the implant is defined by three points from the medial, lateral, and groove curvatures along with 3 radii, as has been previously discussed. As for the condylar cross sections, the medial side and lateral side are defined by two points and a single radius. Shaping information is inherent within the cross-sections in order to create a full implant CAD model automatically.

Referring to FIG. **68-70**, in order to design a functional implant that best mimics the normal knee motion, the full range of the femur relative to the tibia should be completely characterized. To achieve this goal, a set of anatomical areas are localized on the femur and projected on the tibia during the full range of motion. First, the most distal area on the medial side of the femur was localized, which is the area of contact between the femur and tibia in case of full extension (A**1**) (see FIG. **69**). The second area is the most distal area of the lateral condyle (A**2**), while the third area is the most posterior area of the medial condyle (A**3**) and the fourth area is the most posterior area of the lateral condyle (A**4**) (see FIG. **70**). During the full range of motion, each of the areas on the femur was projected on the tibia to characterize the motion of these areas relative to the tibial plateau surface. A distinct motion pattern is observed on the medial side where area A**1** moves anteriorly until 40 degrees flexion and then disengages from any contact with the tibia surface. At the same time after 40 degrees, the area A**3** starts to move anteriorly while performing axial rotation tracking. On the lateral side, the area A**2** moves anteriorly with less magnitude compared to A**1** until 40 degrees flexion, where it disengages in a similar fashion as A**1**. At the same time, area A**4** comes in contact with and moves anteriorly in a smaller area compared to area A**3**.

Referring to FIGS. **68-72**, in order to achieve the normal motion pattern with a functional PS implant, the design of both the femoral implant curvature and the polyethylene component should be modified to provide a more natural motion. In addition, modifying the cam location on the polyethylene component provides constraint for the femur motion and allows for more axial rotation (see FIG. **71**). None of the existing functional implants is operative to provide the same axial rotation as is observed in the normal knee. When a PS implant (see, e.g., FIG. **72**) was implanted and thereafter X-ray fluoroscopy studies were carried out to

observe the location of the femoral component relative to the cam, it was observed that the cam position intruded into the femoral implant, thereby implying that the cam location does not allow for sufficient axial rotation. In order to improve the axial rotation of the implant joint, the cam position was modified to tilt laterally according to the loci on the medial side. This modification allowed for a better range of axial rotation, which more closely approximated the normal range of motion of a natural knee joint.

As seen in FIGS. **69** and **70**, the lateral side of the tibia has two distinct loci. The lateral curvatures of the PS polyethylene in FIG. **71** are designed to accommodate such unique conditions. During the flexion from 0 to 40 degrees, the anterior portion of the polyethylene component is defined by four sets of curvatures. This geometry also angles to prevent excessive anterior sliding of the femoral component during these flexion angles. The posterior portion of the polyethylene component is also defined by four sets of curvatures, which engage the lateral condyle from 60 to 140 degrees of flexion. This portion is designed to be flatter to provide smoother motion and prevent impingements. The medial side has one set of curvature that is shaped as a deep dish for the rolling motion during the 60 to 140 degrees of flexion. A second set of curvatures introduce a unique track that first follow the loci from 60 to 120 degrees of flexion and blends into the loci from 0 to 40 degrees of flexion, which allows for a smooth transition between the two loci tracks.

Referring to FIGS. **73-74** and Table 3, in order to design anatomically friendly bicruicate, ACL, and PCL implants, the location of the PCL and the ACL should be studied as the knee joint is taken through its range of motion. A statistical atlas was utilized to localize and propagate the location of insertions of the ACL and the PCL across an entire population. Both the ACL and PCL were deformed by taking the knee joint through a range of motion in order to map the change in shape and length of the ligament during range of motion. Table 3 highlights the differences in length of the ACL and the PCL as percentage of the ACL length. Using this data, an implant may be designed to accommodate retention of either the PCL or the ACL or both the ACL and PCL.

Following from the above description and invention summaries, it should be apparent to those of ordinary skill in the art that, while the methods and apparatuses herein described constitute exemplary embodiments of the present invention, the invention contained herein is not limited to this precise embodiment and that changes may be made to such embodiments without departing from the scope of the invention as defined by the claims. Additionally, it is to be understood that the invention is defined by the claims and it is not intended that any limitations or elements describing the exemplary embodiments set forth herein are to be incorporated into the interpretation of any claim element unless such limitation or element is explicitly stated. Likewise, it is to be understood that it is not necessary to meet any or all of the identified advantages or objects of the invention disclosed herein in order to fall within the scope of any claims, since the invention is defined by the claims and since inherent and/or unforeseen advantages of the present invention may exist even though they may not have been explicitly discussed herein.

What is claimed is:

1. A prosthetic implant comprising:

a human joint component implant unique to a patient to replace a natural anatomical portion of the patient, the human joint component implant imitating size and curvature features of the natural anatomical portion;

wherein the human joint component implant incorporates a camming surface fabricated by associating a plurality of radii of curvature approximating a plurality of radii of curvature of the natural anatomical portion.

2. The prosthetic implant of claim **1**, wherein:

the human joint component is a femoral component of a knee joint;

the femoral component includes a medial condyle having the camming surface; and

the camming surface includes an anterior-to-distal-to-posterior surface incorporating at least three radii of curvature obliquely angled to a medial-lateral direction of the femoral component.

3. The prosthetic implant of claim **1**, wherein:

the human joint component is a femoral component of a knee joint;

the femoral component includes a lateral condyle having the camming surface; and

the camming surface includes an anterior-to-distal-to-posterior surface incorporating at least three radii or curvature obliquely angled to a medial-lateral direction of the femoral component.

4. The prosthetic implant of claim **1**, wherein:

the human joint component is a femoral component of a knee joint;

the femoral component includes a lateral condyle and a medial condyle, where each condyle includes its own camming surface;

the camming surface for the lateral condyle includes an anterior-to-distal-to-posterior surface incorporating at least three radii of curvature obliquely angled to a medial-lateral direction of the femoral component; and

the camming surface for the medial condyle includes an anterior-to-distal-to-posterior surface incorporating at least three radii of curvature obliquely angled to the medial-lateral direction of the femoral component;

wherein the at least three radii of curvature for the lateral condyle arc not identical to the at least three radii of curvature fur the medial condyle.

5. The prosthetic implant of claim **4**, wherein:

the femoral component includes a trochlear groove surface; and

the trochlear groove surface includes an anterior-to-distal surface incorporating at least two radii of curvature obtusely angled to a medial-lateral direction of the femoral component.

6. The prosthetic implant of claim **4**, wherein:

the femoral component includes a trochlear groove surface; and

the trochlear groove surface includes a medial-to-lateral surface incorporating at least two radii of curvature parallel to a medial-lateral direction of the femoral component.

7. The prosthetic implant of claim **1**, wherein:

the human joint component is a femoral component of a knee joint;

the femoral component includes a medial condyle having the camming surface; and

the camming surface includes a medial-to-lateral surface incorporating at least three radii of curvature generally parallel to a medial-lateral direction of the femoral component.

8. The prosthetic implant of claim **1**, wherein:

the human joint component is a femoral component of a knee joint;

the femoral component includes a lateral condyle having the camming surface; and

the camming surface includes a medial-to-lateral surface incorporating at least three radii of curvature generally parallel to a medial-lateral direction of the femoral component.

9. The prosthetic implant of claim **1**, wherein:

the human joint component is a femoral component of a knee joint;

the: femoral component includes a lateral condyle and a medial condyle, where each condyle includes its own camming surface;

the camming surface for the lateral condyle includes a medial-to-lateral surface incorporating at least three radii of curvature generally parallel to a medial-lateral direction of the femoral component; and

the camming surface for the medial condyle includes a medial-to-lateral surface incorporating at least three radii of curvature generally parallel to a medial-lateral direction of the femoral component;

wherein the at least three radii of curvature for the lateral condyle are not identical to the at least three radii of curvature for the medial condyle.

10. The prosthetic implant of claim **1**, wherein:

the human joint component is a femoral component of a knee joint;

the femoral component includes a trochlear groove surface; and

the trochlear groove surface includes an anterior-to-distal surface incorporating at least two radii of curvature obtusely angled to a medial-lateral direction of the femoral component.

11. The prosthetic implant of claim **1**, wherein:

the human joint component is a femoral component of a knee joint;

the femoral component includes a trochlear groove surface: and

the trochlear groove surface includes a medial-to-lateral surface incorporating at least two radii of curvature parallel to a medial-lateral direction of the femoral component.

12. The prosthetic implant of claim **1**, wherein:

the human joint component is a femoral component of a knee joint; and

the camming surface is a shell of a femur formed by generating profiles/points by sweeping the human joint component every ten degrees, generating a curve from the profiles/points, and matching at least four of the radii of curvature to the curve.

* * * * *